Microfluidics with Nanoscale Additive Manufacturing: Devices and Applications

BY

Yang Lin

B.S., Beijing Information Science and Technology University, China, 2012
M.S., Beijing Information Science and Technology University, China, 2015

THESIS

Submitted as partial fulfillment of the requirements
for the degree of Doctor of Philosophy in Mechanical Engineering
in the Graduate College of the
University of Illinois at Chicago, 2019

Chicago, Illinois

Defense Committee:

Prof. Jie Xu, Chair and Advisor
Prof. Xiaonan Lu, The University of British Columbia
Prof. David Eddington, Richard & Loan Hill Department of Bioengineering
Prof. Ran Zhou, Purdue University Northwest
Prof. Erica Jung

To my beloved wife Can,

my lovely son,

my loving parents and grandparents,

all my sincere friends,

and Doraemon the gadget cat from the future.

Acknowledgements

First, I would like to express my most sincere gratitude to my advisor, Prof. Jie Xu, who has provided unconditionally endless support not only in my study and research, but also in my life. I still remember four years ago when I was desperate, it is Prof. Xu lent a hand to me and offered me an opportunity to pursue a doctoral degree abroad, rather than getting a mediocre job. Compared to his kindness and generosity, any thank you words are pale and powerless. Throughout these years at UIC, he has always been a beacon of light in my doctoral study, and I have learned a lot from him, the way he performs teaching and research, the strategies of lab and student management, and even his life styles to balance work and family.

My sincere gratitude also goes to Prof. Xiaonan Lu, from the University of British Columbia, Canada, for his valuable advices and suggestions on my research, especially when biochemistry is involved. I would also like to thank the rest of my dissertation committee members, Prof. David Eddington, Prof. Ran Zhou, and Prof. Erica Jung, for their invaluable advice and help with my thesis work in various aspects. In addition, I would acknowledge Prof. Gabriela Caraveo Piso from Northwestern University for her support in cell trapping and analysis.

I am also grateful to all my lab mates and collaborators for their support and suggestions, especially Dmitry Gritsenko, Yuan Gao, Mengren Wu, Weiqi Zhao, and Alireza Ahmadianyazdi. Lastly, I would like to express my sincere gratitude to all the graduate, undergraduate, visiting, and high school students I have supervised, for their valuable work. Without all the selfless help and fruitful discussions from them, this dissertation would only be a dream.

Contribution of Authors

Chapter 1 generally introduces the fundamentals of microfluidics and additive manufacturing, along with the motivation and outline of this dissertation. Chapter 2 further provides the basics of microfluidics, fabrication methods of microfluidics, and fundamentals of two-photon polymerization technology, in which part of the content has been reprinted with permission from Lin, Y., & Xu, J. (2018). *Microstructures Fabricated by Two-Photon Polymerization and Their Remote Manipulation Techniques: Toward 3D Printing of Micromachines*. **Advanced Optical Materials**, 6(8), 1701359. Copyright (2018) by John Wiley & Sons. DOI: https://doi.org/10.1002/adom.201701359; and another part of the content has been reprinted with permission from Lin, Y., Gao, C., Gritsenko, D., Zhou, R., & Xu, J. (2018). *Soft lithography based on photolithography and two-photon polymerization*. **Microfluidics and Nanofluidics**, 22 (9), 97. Copyright (2018) by Springer Nature. DOI: https://doi.org/10.1007/s10404-018-2118-5. As these two chapters only encompass basic introductions of the dissertation, I have contributed to all the work related, along with the advises and proofreading from Prof. Jie Xu.

Chapter 3 has been primarily reprinted with permission from Lin, Y., Gao, C., Gritsenko, D., Zhou, R., & Xu, J. (2018). *Soft lithography based on photolithography and two-photon polymerization*. **Microfluidics and Nanofluidics**, 22 (9), 97. Copyright (2018) by Springer Nature. DOI: https://doi.org/10.1007/s10404-018-2118-5. For this study, I have made the primary contribution in experimental design, argumentation, verification, analysis as well as the manuscript writing and submission. Can Gao has contributed to the experimental performing and analysis. Dmitry Gritsenko has

provided suggestions on experiments and proofread the manuscript. Prof. Ran Zhou and Prof. Jie Xu have verified the feasibility of the methods and provided advises on parameter adjustments, along with manuscript proofreading.

Chapter 4 has been primarily reprinted with permission from Lin, Y., Zhou, R., & Xu, J. (2018). *Superhydrophobic surfaces based on fractal and hierarchical microstructures using two - photon polymerization: toward flexible superhydrophobic films*. **Advanced Materials Interfaces**, 5(21), 1801126. Copyright (2018) by John Wiley & Sons. DOI: https://doi.org/10.1002/admi.201801126. I have made the primary contribution in experimental design, argumentation, verification, analysis as well as the manuscript writing and proofreading. Prof. Ran Zhou and Prof. Jie Xu have verified the feasibility of the methods and provided advises on the designs and fabrication of microstructures, along with final analyses and manuscript proofreading. Prof. Sushant Anand and Hassan Bararnia have also provided the assistance with contact angle measurements.

Chapter 5 has been reprinted with permission from Lin, Y., Gao, C., Gao, Y., Wu, M., Yazdi, A. A., & Xu, J. (2019). *Acoustofluidic micromixer on lab-on-a-foil devices*. **Sensors and Actuators B: Chemical**, 287, 312-319. Copyright (2019) by Elsevier. DOI: https://doi.org/10.1016/j.snb.2019.02.050. For this work, I have made the primary contribution in experimental design, argumentation, verification, analysis as well as the manuscript writing and manuscript proofreading. Can Gao has contributed to the experimental performing and analysis. Yuan Gao and Mengren Wu have provided assistance in experimental performing, analysis and manuscript proofreading. Alireza Ahmadian Yazdi has proofread the manuscript and

provided suggestions. Prof. Jie Xu has verified the feasibility of the methods and provided advises on the actuation of acoustic waves, microstructure design and fabrication, data analyses, along with manuscript proofreading.

Chapter 6 has been reprinted with permission from Lin, Y., Gao, Y., Wu, M., Zhou, R., Chung, D., Caraveo, G., & Xu, J. (2019). *Acoustofluidic stick-and-play micropump built on foil for single-cell trapping*. **Lab on a Chip**. Copyright (2019) by Royal Society of Chemistry. DOI: https://doi.org/10.1039/c9lc00484j. For this work, I have made the primary contribution in experimental design, argumentation, verification, analysis as well as the manuscript writing and manuscript proofreading. Yuan Gao and Mengren Wu have provided assistance in experimental performing, analysis and manuscript proofreading. Daayun Chung has assisted in the preparation of biological samples. Prof. Gabriela Caraveo has provided suggestions on yeast trapping and proofread the corresponding content. Prof. Ran Zhou and Prof. Jie Xu have verified the feasibility of the methods and provided advises on microstructure design and fabrication, data analyses, along with manuscript proofreading.

Chapter 7 has provided conclusions of this dissertation, along with the prospects of microfluidics with nanoscale additive manufacturing technologies. For this chapter, I have contributed to all the work related, along with the advises and proofreading from Prof. Jie Xu.

Table of Contents

List of Tables

List of Figures

List of Abbreviations

ALD	Atomic Layer Deposition
AM	Additive Manufacturing
AOM	Acousto-Optic Modulator
BHF	Buffered Hydrofluoric Acid
CAD	Computer-aided Design
DI	Deionized
DOMES	Defended Oscillating Membrane Equipped Structures
DRIE	Deep Reactive ion Etching
DUV	Deep Ultraviolet
EBM	Electron Beam Melting
EUV	Extreme Ultraviolet
FDM	Fused Deposition Modeling
FESEM	Field Emission Scanning Electron Microscope
HMDSO	Hexamethyldisiloxane
IDT	Interdigital Transducer
IPA	Isopropyl Alcohol
ITO	Indium Tin Oxide
LCAT	Lateral Cavity Acoustic Transducers
LENS	Laser Engineered Net Shaping
LIGA	Lithography, Electroplating, and Molding
LOC	Lab on a Chip
LOM	Laminated Object Manufacturing
μCP	Microcontact Printing
MEMS	Microelectromechanical Systems
MIMIC	Micromolding in Capillary
micro-SLA	Microstereolithography
μTAS	Micro Total Analysis Systems

μTM	Microtransfer Molding
Ni	Nickle
Pe	Peclet Number
PECVD	Plasma Enhanced Chemical Vapor Deposition
PET	Polyethylene Terephthalate
PDMS	Polydimethylsiloxane
PGMEA	Propylene Glycol Methyl Ether Acetate
Re	Reynolds Number
REM	Replica Molding
RIE	Reactive Ion Etching
RMI	Relative Mixing Index
ROI	Regions of Interest
SAMIM	Solvent-Assisted Micromolding
SAW	Surface Acoustic Wave
SEM	Scanning Electron Microscopy
SLA	Stereolithography
SLS	Selective Laser Sintering
STL	Standard Tessellation Language
Ti	Titanium
2D	Two-dimensional
3D	Three-dimensional
TPP	Two-photon Polymerization
UV	Ultraviolet

Nomenclature

$\partial\Omega$	Surface of the Given Region
α	Isobaric Thermal Expansion Coefficient
β	Viscosity Ratio of Fluids
γ	Specific Heat Capacity Ratio
ε_f	Scaling Factor
θ	Azimuthal Angle
κ	Isentropic Compressibility
κ_0	Compressibility of Fluid
κ_w	Wave Number
μ	Dynamic Viscosity
ρ	Density of fluids
σ	Surface Tension
φ	Contact Angle
ω	Angular Frequency
Δp	Pressure Difference
Ω	Given Region
a	Radius of the Membrane
da	Area Element on Surface
$\mathbf{f}$	Body Forces
f_1	Pre-factor 1
f_2	Pre-factor 2
h	Distance between plates
i	Index of the Pixel
n	Index
$\boldsymbol{n}$	Surface Normal
p	Pressure
r	Radial Distance

$\boldsymbol{r}$	Position Vector of the Given Region
s	Entropy
t	Time
$\boldsymbol{u}$	Velocity of the Particle
$\mathbf{v}$	Convection Velocity
v_0	Velocity Amplitude
v_x	Velocity Profile
w_D	Classical Solution for the Displacement Equation
w	Width
A_1	Arbitrary Constant
B_1	Arbitrary Constant
C_p	Specific Heat Capacity
D	Diffusion Coefficient
D_f	Fractal Dimension
D_s	Fractal Dimension of Sierpinski Tetrahedron
D_{th}	Thermal Diffusivity
F_{drag}	Stokes Drag
F_{rad}	Secondary Radiation Force
G_{hyd}	Hydraulic Conductance
$\langle I \rangle$	Average of Pixel Intensities in the Measuring Region
I_i	Local Intensity of the i-th Pixel After Mixing
I_n	Modified Bessel Function
I_{oi}	Local Intensity of the i-th Pixel Before Mixing
$\mathbf{J}$	Mass Current Density
J_n	Type One Bessel Function
L	Length
L_0	Dimensions of the Microchannels
M	Total Mass
N	Number of Pixels in the Measuring Region

N_f	Number of the parts forming fractal objects
Q	Flow Rate
R	Radius of Microchannel
R_0	Radius of the Spherical Object
R_{hyd}	Hydraulic Resistance
T	Temperature
T_0	Constant Temperature of the Walls
$\boldsymbol{V}$	Given Vector Field
V_0	Flow Velocity Relative to the Object
W	Displacement of a Thin Clamped Circular Membrane

Summary

Over the past years, additive manufacturing technologies have emerged as a powerful tool in the field of microfluidic engineering, owing to their powerful capabilities in fabrication of 3D microstructures for diverse functions. However, most of the current applications in microfluidics only adopt these technologies to create simple microchannels rather than functional components, since the resolution of conventional additive manufacturing techniques usually fall within the range of tens to hundreds of micrometers. Herein, this dissertation has centered on the use of a specific additive manufacturing technique that possesses extremely high resolution, the two-photon polymerization technique, for different applications in microfluidics.

Given the fact that two-photon polymerization builds objects through a voxel-by-voxel manner, the time of fabrication could be significantly long, therefore it is more suitable to create only the essential parts at regions of interest (ROI) in a microfluidic device, instead of creating the whole device. More specifically, based on this criterium, we have contributed to several applications of microfluidics, including novel fabrication method for soft lithography, superhydrophobic foil with hierarchical structures, acoustofluidic micromixer and micropump, as well as the cell traps.

First of all, a novel hybrid fabrication method based on photolithography and two-photon polymerization has been developed to create master moulds in soft lithography. As a result, this proposed method prevents the huge time expenses from printing the entire parts using two-photon polymerization, along with taking

advantages of conventional photolithography.

Afterwards, we have investigated the capabilities of two-photon polymerization in the control of surface wetting by creating fractal Sierpinski tetrahedron and hierarchical pyramid microstructures on glass slides and flexible plastic films. Since different microstructures can be built at different regions, the proposed method could be applied for a controllable management of surface wetting.

Based on the experience of creating microstructures on flexible foils, we have developed a novel acoustofluidic micromixer by means of embedding the created microstructures in flexible devices made of off-the-shelf materials such as plastic films and double-sided tapes. The mixing effect is generated from 3D printed microstructures, through which the acoustically oscillated air-liquid interfaces are connected to the ambient air, thus preventing the oscillation of these interfaces from dissolution and compression.

Extending the capabilities of the embedded microstructures proposed, we have also developed an acoustofluidic micropump on the foils. A maximal flow rate of 420 nL/min can be obtained when the driving voltage was set to 4 Vpp. To further investigate the pumping abilities of the proposed micropump, it has been utilized to drive flows for single-cell trapping.

Despite the successful development and implementation of devices in several applications, the work has been not comprehensive enough. This is because the field is still at its beginning stage, and encompasses numerous uncovered matters and possibilities. Therefore, fundamental studies on topics such as

photopolymerization, hydrophobicity, post treatments, acoustofluidics, and others, have to be done in the next stage to further improve the performance of two-photon polymerization in these applications and expand its capabilities in other fields. On the other hand, two-photon polymerization is still not a widely accessible technique, since it requires expensive fabrication systems and long fabrication time. Therefore, future works should empathize on further improvements in critical aspects such as the speed and cost of fabrication. Nevertheless, we truly believe the proposed devices and applications in this dissertation have manifested the capabilities of two-photon polymerization in microfluidics and other fields, and will serve as an important example and the foundation for future developments in microfluidics and nanoscale additive manufacturing technologies.

Chapter 1

Motivation and Overview

The past few decades have witnessed a great success of microfluidics and additive manufacturing due to their remarkable capabilities of solving problems in diverse areas. In this chapter, a brief introduction on these two fields is presented, along with the motivation and goal of this dissertation: using one of the most powerful and promising nanoscale additive manufacturing technologies, two-photon polymerization, to explore a variety of applications in microfluidics, including novel fabrication approach in soft lithography, controllable surface hydrophobicity, as well as revolutionary microfluidic components such as micromixer, micropump, cell traps in micro systems. In-depth reviews on these two topics are delivered by references (Bruus 2008; Folch 2016; Gibson et al. 2014; Gravesen et al. 1993; Tabeling 2005; Whitesides 2006; Wong and Hernandez 2012; Yazdi et al. 2016), and interested readers are encouraged to refer to them for a deeper and more comprehensive scope.

1.1 Microfluidics

Microfluidics is a technology involving the manipulation and control of small amounts of fluids (microliters to picoliters) in tiny channels (tens of nanometers to hundreds of micrometers wide, Figure 1.1). Herein, it is also called the Lab on a Chip

(LOC) technology (Whitesides 2006). Microfluidics has attracted ever-increasing attentions over the decades, and currently plays a pivotal role in diverse areas such as physics, chemistry, biomedicine, and environmental monitoring (Folch 2016).

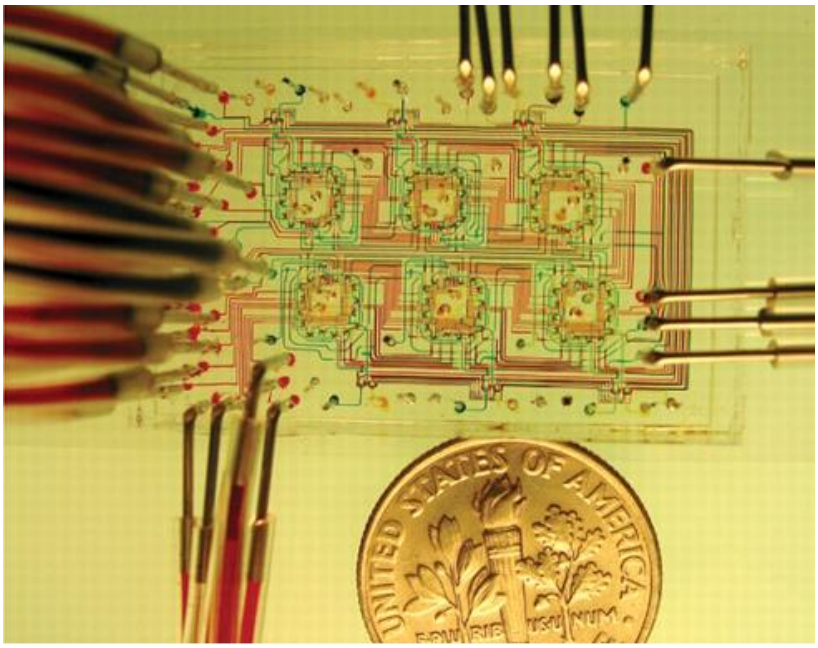

Figure 1.1 Photo of a microfluidic chip used to study microbial growth. Reproduced with permission from reference (Balagaddé et al. 2005).

Similar to the miniaturization of electronics, the future of microfluidics lies in integrating the majority of laboratory functionalities into a small chip (Tabeling 2005). This approach offers striking advantages that are difficult to achieve in a laboratory scale. To be more specific, only small quantities of samples and reagents are usually required in a microfluidic process (Folch 2016). Certain biological fluids such as sweats (Koh et al. 2016), tears (Versura et al. 2012), and salivas (Herr et al. 2007), which have long been overlooked because of their limited quantities, have now become important clinical samples in diagnoses and other microfluidics-based applications in public healthcare; Furthermore, such low consumption of samples

and reagents also gives rise to shorter reaction time due to short diffusion distances (Folch 2016). Thanks to this benefit, microfluidics has made bioanalyses less invasive and affordable, especially for countries and regions without professional point-of-care centers.

Compared to bulky equipment used in the laboratory, microfluidic devices also have small footprints that allow for fabricating large numbers of devices simultaneously, thus they are considered to be more affordable than their bulky counterparts. More importantly, small footprints do not compromise their performances in terms of the sensitivity and specificity. For example, they have exhibited competitive performances for determining heavy metal ions in waters (Lin et al. 2016a). Furthermore, the substrates of microfluidics are no longer limited to silicon and glass slides, the earliest materials used in a few decades ago, a variety of options such as plastics, foils, and papers have been investigated till now (Lin et al. 2019a). Compared to silicon and glass, these materials provides unique advantages such as cost-effectiveness, ease of fabrication, flexibility, biocompatibility, disposability and others (Focke et al. 2010; Lin et al. 2019a; Lin et al. 2019b; Lin et al. 2016b; Lin and Xu 2017).

Last but not the least, systems involving complex functions can be realized by integrating multiple microfluidic devices into a system. For example, chips aiming at different functions such as cell coculture, protein detection, and analysis of drug metabolites can be integrated together for investigating tumor-endothelial cell interaction (Lin et al. 2017).

1.2 Additive Manufacturing

On the other hand, additive manufacturing (AM) technology, also known as the 3D printing technology, has revolutionized the way how microfluidic devices are fabricated (Au et al. 2016), and become an important tool in various applications (Yazdi et al. 2016). Compared to other traditional fabrication methods, AM technology directly builds three-dimensional (3D) objects according to digital models created using computer-aided design (CAD) software (Ngo et al. 2018). Therefore, microstructures with complicated geometries involving spirals, helixes, and curved surfaces, which previously largely constrained the abilities of microfluidic engineers in design and fabrication processes, have now become possible to build (Ambrosi et al. 2016).

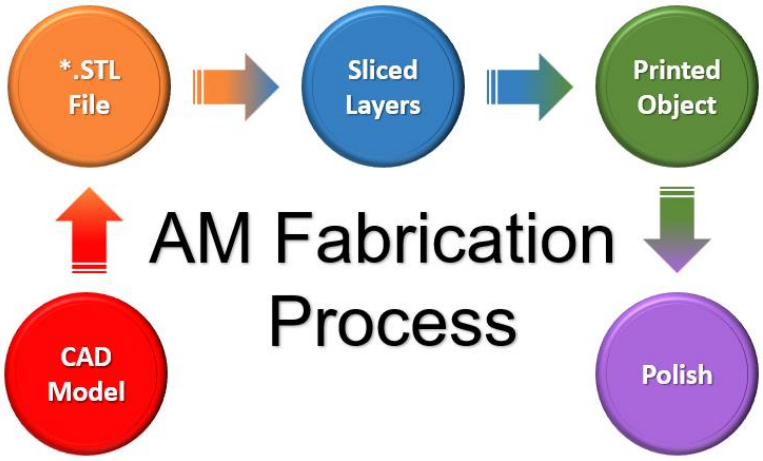

Figure 1.2 Schematic illustration of a typical AM fabrication process.

In a typical AM fabrication process (Figure 1.2), a digital CAD model with desired geometry is first created using CAD software, and then converted into Standard Tessellation Language (STL) format. After that, the STL-format file should be transferred to a slicing software, by which numerous thin layers with controlled

thickness are generated. Based on these sliced layers, the AM systems (3D printers) produce the final parts in a layer-by-layer manner until all layers are completely built. Finally, the stacked products may undergo polishing processes or other post-treatments to enhance qualities for different purposes.

Currently, great strides have been made in this field and countless AM technologies have been developed and improved using various mechanisms (Wong and Hernandez 2012), including fused deposition modeling (FDM) (He et al. 2016), stereolithography (SLA) (Waheed et al. 2016), selective laser sintering (SLS) (Fina et al. 2017), laser engineered net shaping (LENS) (Niu et al. 2015), laminated object manufacturing (LOM) (Luong et al. 2018), electron beam melting (EBM) (Körner 2016), and others (Gibson et al. 2014; Ngo et al. 2018; Wong and Hernandez 2012). Among these technologies, FDM and SLA have been widely adopted in the field of microfluidics due to favorable cost-effectiveness and ease of operation (Gaal et al. 2017; Kanai and Tsuchiya 2016). The examples of microfluidic devices fabricated using these two technologies are shown in Figure 1.3.

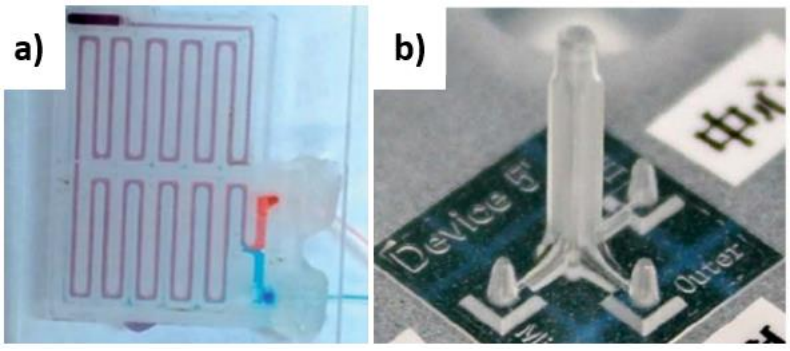

Figure 1.3 Examples of 3D printed microfluidic devices: a) Photo of a FDM-printed microfluidic chip for the analyses of nitrite, total proteins, and nitric oxide. Reproduced with permission from reference (Bressan et al. 2019). b) Photo of a SLA-

printed microfluidic chip for producing monodisperse double emulsions. Reproduced with permission from reference (Kanai and Tsuchiya 2016).

1.3 Motivation

As aforementioned, microfluidics deals with fluids in microchannels with widths ranging from tens of nanometers to hundreds of micrometers. However, most of the AM technologies developed hitherto only have a resolution in the range of micrometers (Yazdi et al. 2016). Therefore, current 3D printed microfluidic devices rarely contain microchannels and microstructures with high resolution and complex designs, thus limiting the development of AM technologies in microfluidic field. Fortunately, two-photon polymerization (TPP), one of the AM technologies working at microscale (Lin and Xu 2018), has made the fabrication of these microstructures possible.

Unlike single-photon polymerization used in the conventional SLA method, TPP capitalizes on simultaneous absorption of two photons by photosensitive materials. This process gives rise to a nonlinear absorption mechanism, in which only the materials near focal point can be polymerized and the others remain unpolymerized (Lin and Xu 2018). The polymerized part is termed as a voxel, and the final products are built in a voxel-by-voxel manner instead of the layer-by-layer approach used in conventional SLA approach. Hence, the resolution of TPP depends on the size of the voxel. Since the size of a voxel usually falls into a range of hundreds of nanometers to one micrometer (Baldacchini 2015), TPP has been considered as an AM technology working at nanoscale.

Nevertheless, it is also because of such extremely high resolution, the

fabrication time required in a TPP process is usually quite long, making such technology not attractive in the fabrication of microfluidic devices. Fortunately, given the fact that only certain regions in microfluidic devices, also known as the regions of interest, require complicated microstructures with complex geometries, in this dissertation, we focus on the use of TPP to fabricate important components for diverse microfluidic applications such as mixing, pumping and filtration, while the remaining parts in the systems are fabricated through standard methods. In addition, since TPP currently is still not a widespread technology and require expensive fabricating systems, off-the-shelf materials such as plastic films and tapes are also adopted to build the main devices. By this approach, we believe that the cost for a unit device could be reduced and become more affordable.

1.4 Dissertation Overview

This dissertation presents our research findings on using TPP technology for creating microfluidic devices in various applications. Specifically, Chapter 2 gives an in-depth introduction of the basics of microfluidics, current microfabrication methods in microfluidics, and the fundamentals of TPP technology. Chapter 3 presents a novel fabrication method to fabricate high resolution 3D master moulds for soft lithography, a widely used method for building microfluidic chips. This method combines conventional photolithography and TPP for creating the main structures and microstructures in the regions of interest, respectively. Chapter 4 describes a novel approach to create superhydrophobic films using TPP. Basically, fractal and hierarchical microstructures are printed on desired areas on the surfaces, thus giving rise to controllable wettability of the surfaces in different regions. Based

on such success experience of creating microstructures on plastic films, we further built a rapid and homogeneous micromixer and a programmable micropump on plastic films, which are actuated using acoustic energy. Corresponding research findings are presented in Chapter 5 and Chapter 6, respectively. Lastly, Chapter 7 summarizes all the work presented in this dissertation and discusses the future directions of microfluidics based on AM technologies.

Chapter 2

Microfluidics and two-photon polymerization

This chapter introduces the basics of microfluidics, fabrication methods of microfluidics, and fundamentals of two-photon polymerization technology. Part of the content in this chapter has been reprinted with permission from Lin, Y., & Xu, J. (2018). *Microstructures Fabricated by Two-Photon Polymerization and Their Remote Manipulation Techniques: Toward 3D Printing of Micromachines*. **Advanced Optical Materials**, 6(8), 1701359. Copyright (2018) by John Wiley & Sons. DOI: https://doi.org/10.1002/adom.201701359. Part of the content in this chapter has been reprinted with permission from Lin, Y., Gao, C., Gritsenko, D., Zhou, R., & Xu, J. (2018). *Soft lithography based on photolithography and two-photon polymerization*. **Microfluidics and Nanofluidics**, 22 (9), 97. Copyright (2018) by Springer Nature. DOI: https://doi.org/10.1007/s10404-018-2118-5.

2.1 Basics of microfluidics

Like bulk fluids flowing in piping systems, flows in microchannels also follow the rules of fundamental fluid dynamics, yet the principles governing their behaviors are totally different (Tabeling 2005). When it comes to the microscale condition, volume forces such as gravity and inertial forces that play critical roles in our daily life, become less significant when compared with viscous forces and surface tensions, which are usually neglected in our common sense. For example, mixing

two fluids in microfluidic devices is no longer as easy as mixing coffee and milk in our morning cups, since laminar flows are dominated rather than turbulent flows. Hence, innovative passive or active micromixers are very common in microfluidic applications (Huang et al. 2013; Lin et al. 2019a). In this section, we will introduce the governing equations and essential dimensionless numbers of microfluidics, flow profiles and hydraulic resistance in microchannels, as well as the Stokes drag on suspended substances.

2.1.1 Governing equations

The governing equations for microfluidics in general stem from the fundamental equations describing the rates of changes in mass, momentum and energy (Bruus 2008), which could be represented using Gauss's theorem:

$$\int_{\Omega} d\boldsymbol{r}\ \boldsymbol{\nabla}\cdot\boldsymbol{V} = \int_{\partial\Omega} da\ \boldsymbol{n}\cdot\boldsymbol{V}, \tag{2.1}$$

where $\boldsymbol{V}(\boldsymbol{r})$ is a given vector field in a given region Ω with a position vector $\boldsymbol{r}$ and a surface $\partial\Omega$; da is an area element on this surface with a surface normal $\boldsymbol{n}$.

In the case of a compressible fluid (the fluid with varied density ρ), the total mass can be represented using a volume integral over ρ,

$$M(\Omega,t) = \int_{\Omega} d\boldsymbol{r}\ \rho(\boldsymbol{r},t) \tag{2.2}$$

Here, the time derivative of the mass can be represented as follows:

$$\partial_t M(\Omega,t) = \partial_t \int_{\Omega} d\boldsymbol{r}\ \rho(\boldsymbol{r},t) = \int_{\Omega} d\boldsymbol{r}\ \partial_t\rho(\boldsymbol{r},t). \tag{2.3}$$

In addition, the mass current density $\mathbf{J}$ is defined as:

$$\boldsymbol{V} = \mathbf{J}(\boldsymbol{r}, t) = \rho(\boldsymbol{r}, t)\mathbf{v}(\boldsymbol{r}, t), \tag{2.4}$$

where $\mathbf{v}(\boldsymbol{r}, t)$ is the convection velocity.

Thus, we are able to obtain Equation 2.5 based on Equation 2.1:

$$\partial_t M(\Omega, t) = -\int_{\partial\Omega} da\, \boldsymbol{n} \cdot \big(\rho(\boldsymbol{r}, t)\mathbf{v}(\boldsymbol{r}, t)\big) = -\int_{\Omega}\ d\boldsymbol{r}\, \boldsymbol{\nabla} \cdot \big(\rho(\boldsymbol{r}, t)\mathbf{v}(\boldsymbol{r}, t)\big), \tag{2.5}$$

in which the minus sign means that the mass inside the region Ω diminishes when $\mathbf{v}(\boldsymbol{r}, t)$ is pointing outward.

By comparison of the Equation 2.3 and Equation 2.5, we could immediately obtain the continuity equation:

$$\partial_t \rho(\boldsymbol{r}, t) = -\boldsymbol{\nabla} \cdot \big(\rho(\boldsymbol{r}, t)\mathbf{v}(\boldsymbol{r}, t)\big). \tag{2.6}$$

As most fluids used in microfluidics are incompressible solutions, thus the continuity equation becomes:

$$\boldsymbol{\nabla} \cdot \mathbf{v} = 0. \tag{2.7}$$

The second governing equation used in microfluidics deals with momentum fluxes and force densities, corresponding to the rate of change in momentum originating from convection of momentum, pressure forces, viscous forces and body forces. The derived equation is the famous Navier-Stokes equation, one of the most commonly used equation in fluid mechanics. Interested readers are encouraged to refer to reference (Bruus 2008) for detailed derivation process. The equation is represented as follows:

$$\rho\left(\frac{\partial \mathbf{v}}{\partial t} + \mathbf{v} \cdot \boldsymbol{\nabla}\mathbf{v}\right) = -\boldsymbol{\nabla} p + \mu\boldsymbol{\nabla}^2\mathbf{v} + \mathbf{f}, \tag{2.8}$$

where p is the pressure, and μ is the dynamic viscosity, $\mathbf{f}$ denotes the body forces.

In a typical microfluidic configuration, inertial forces are usually relatively small compared to viscous forces, thus the nonlinear term in Navier-Stokes equation becomes negligible, and the flow is often called the Stokes flow or creeping flow (Bruus 2008). Here, the equation can be rewritten as:

$$\rho \frac{\partial \mathbf{v}}{\partial t} = -\boldsymbol{\nabla} p + \mu \boldsymbol{\nabla}^2 \mathbf{v} + \mathbf{f}. \tag{2.9}$$

The third and the last governing equation used in microfluidics is the energy equation. However, as this dissertation does not involve any energy-related topics, the equation is not discussed here. Interested readers could refer to the reference (Bruus 2008) for more details.

2.1.2 Dimensionless numbers

In fluid mechanics, dimensionless numbers have widely been adopted to reduce the complexity of problems and predict the behaviors of fluids. When it comes to microscale or mesoscale conditions, Reynolds number (Re) is often applied to determine whether viscosity or inertia dominates the systems. The expression for Re is quantitatively defined as the ratio of product of density of fluids ρ, average flow velocity v, and dimensions of the microchannels L_0 over the viscosity of the fluids μ:

$$Re = \frac{\rho \mathrm{v} L_0}{\mu}. \tag{2.10}$$

The Re in a microfluidic system is usually much smaller than 100, in a range from 0.01 to 10.0 (Lee et al. 2016). Therefore, the flows are completely laminar.

Waters and oils that flows smoothly at macroscale start to behave like honey-peanut butters. More importantly, conventional mixing and pumping methods become unsuitable. In Chapter 5 and 6, we will present the novel micromixer and micropump based on the oscillation of air-liquid interfaces upon acoustic actuation (Lin et al. 2019a; Lin et al. 2019b).

Another dimensionless number often used in microfluidics is the Peclet number (Pe). It relates the performances of two phenomena, the advection and the diffusion. Advection is the transport of substances by the fluids, while diffusion is the movement of substances from regions with higher concentration to regions with lower concentration. The expression of Pe is defined as follows:

$$Pe = \frac{\mathrm{v}L_0}{D}, \tag{2.11}$$

where D is the diffusion coefficient.

2.1.3 Poiseuille-flow and flow profiles

Although Navier-Stokes equation is notoriously difficult to solve in most cases, analytical solutions have already been developed in several special but important cases. In particular, Poiseuille-flow problems are very common in microfluidics, and it has been solved analytically based on a number of assumptions describing pressure-induced steady-state flows in an infinitely long, and translation-invariant channel (Bruus 2008; Tabeling 2005).

To solve the governing equations analytically, boundary conditions are indispensable to determine the constants that remain unknown in the final solutions. An important boundary condition in fluid mechanics is the so-called no-

slip boundary condition. This condition assumes that the parts of fluids collide with walls have the same velocity of the walls, which stems from the momentum relaxation between the molecules of the walls and the outmost molecules of the fluids (Bruus 2008), or the hypothesis that the forces of attraction between the wall molecules and fluid molecules are greater than that between fluid molecules.

Poiseuille flows are also called the Hagen-Poiseuille flows, which represent the basic fluid behaviors in microfluidics since most of the flows in relevant applications are driven by pressure differences between two ends of the microchannels. In this section, we will present the flow profiles and the flow rates of Poiseuille flows in various microchannels with different geometries.

1) Infinite parallel-plate channel

In a case that the aspect ratio of a rectangular microchannel is very large, the microchannel is often approximately considered as an infinite parallel-plate configuration, as shown in Figure 2.1.

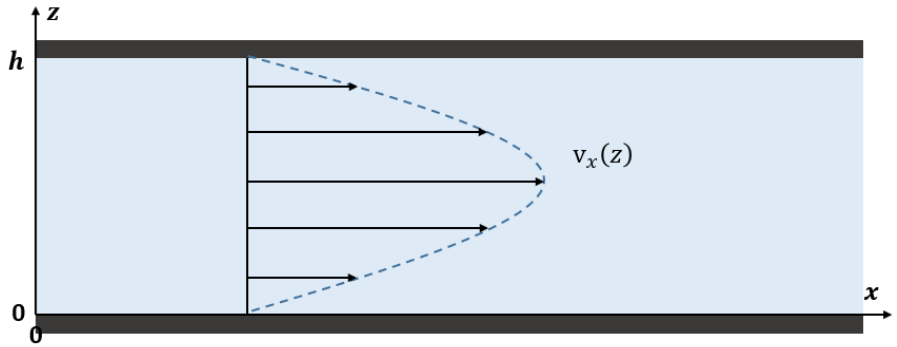

Figure 2.1 Sketch of an infinite parallel-plate configuration in the x and z plane, with a distance of h between two plates.

In this case, the velocity profile $v_x(z)$ is parabolic, and can be expressed as:

$$\mathrm{v}_x(z) = \frac{\Delta p}{2\mu L}(h - z)z, \tag{2.12}$$

where Δp is the pressure difference over a length of L, and h is the distance between two plates.

The flow rate Q through a width of w is calculated to be (Bruus 2008):

$$Q = \frac{h^3 w}{12\mu L}\Delta p. \tag{2.13}$$

2) Rectangular cross-section microchannel

Another common shape used in microfluidics is the rectangular shape, due to the fact that photolithography, reactive ion etching (RIE), and other similar microfabrication techniques usually result in microchannels with rectangular cross-section (Lin et al. 2018; Queste et al. 2010).

The velocity profile $\mathrm{v}_x(y, z)$ for a rectangular cross-section microchannel can be expressed as:

$$\mathrm{v}_x(y, z) = \frac{4h^2\Delta p}{\pi^3 \mu L}\sum_{n,odd}^{\infty}\frac{1}{n^3}\left[1 - \frac{\cosh\left(n\pi\frac{y}{h}\right)}{\cosh\left(n\pi\frac{w}{2h}\right)}\right]\sin\left(n\pi\frac{z}{h}\right). \tag{2.14}$$

The flow rate Q through a width of w is:

$$Q = \frac{h^3 w\Delta p}{12\mu L}\left[1 - \frac{192}{\pi^5}\frac{31}{32}\varsigma(5)\frac{h}{w}\right], \tag{2.15}$$

where

$$\varsigma(x) \equiv \sum_{n=1}^{\infty}\frac{1}{n^x}. \tag{2.16}$$

When $h < w$, an approximate formula can be applied:

$$Q = \frac{h^3 w \Delta p}{12 \mu L}\left[1 - 0.630\frac{h}{w}\right]. \quad (2.17)$$

3) Circular cross-section microchannel

In circular cross-section microchannels with radius R such as tubing and needles, the velocity profile $\mathrm{v}_x(r, \phi)$ in a cylindrical coordinate system (x, r, ϕ) can be expressed as:

$$\mathrm{v}_x(r, \phi) = \frac{\Delta p}{4 \mu L}(R^2 - r^2). \quad (2.18)$$

The flow rate Q through the microchannel is:

$$Q = \frac{\pi}{8}\frac{R^4}{\mu L}\Delta p. \quad (2.19)$$

2.1.4 Hydraulic resistance

As shown in section 2.1.3, the flow rate Q can be expressed as the product of a coefficient and the pressure difference Δp:

$$Q = G_{\mathrm{hyd}}\Delta p. \quad (2.20)$$

Here, the coefficient G_{hyd} is called the hydraulic conductance, and if we rewrite the equation as:

$$\Delta p = \frac{1}{G_{\mathrm{hyd}}} Q = R_{\mathrm{hyd}} Q, \quad (2.21)$$

we obtain another coefficient R_{hyd}, which is called the hydraulic resistance.

Similar to the Ohm's law, hydraulic resistance relates the flow rate (like the electrical current) with pressure difference (like the electrical potential drop) along microchannels (like the wires). A list of hydraulic resistance expressions for

conventionally used straight microchannels is shown in Table 2.1 (Bruus 2008).

Table 2.1 Hydraulic resistance expressions for straight microchannels with different cross-section shapes

Cross-section shape	Expression
Circle (radius: R)	$\frac{8}{\pi}\mu L\frac{1}{R^4}$
Ellipse (major axis: a; minor axis: b)	$\frac{4}{\pi}\mu L\frac{1+(b/a)^2}{(b/a)^3}\frac{1}{a^4}$
Equilateral triangle (side length: a)	$\frac{320}{\sqrt{3}}\mu L\frac{1}{a^4}$
Two plates (width: w; distance: h)	$12\mu L\frac{1}{h^3 w}$
Rectangular (width: w; height: h)	$\frac{12\mu L}{1-0.63(h/w)}\frac{1}{h^3 w}$

2.1.5 Stokes drag

Not only does the microfluidics deal with pure fluids, but it also involves the manipulation of suspended objects in fluids, such as magnetic beads, biological cells and fluorescent markers (Lin et al. 2019b; Zhou and Wang 2016). Therefore, it is necessary to understand the forces exerted on these objects. The frictional force due to the viscosity of fluids is called the Stokes drag F_{drag}, and it is expressed as follows:

$$F_{\mathrm{drag}} = 6\pi\mu R_0 V_0, \tag{2.22}$$

where R_0 is the radius of the spherical object, and V_0 is the flow velocity relative to the object.

2.2 Fabrication methods in microfluidics

At present, numerous fabrication technologies, including photolithography, electron beam lithography, chemical vapor deposition and others, have been investigated and applied for creating microfluidic devices (Abgrall and Gue 2007; Folch 2016; Ren et al. 2013). In this section, several widely used microfabrication technologies of microfluidic engineering will be briefly presented.

2.2.1 Photolithography

Photolithography or the so-called optical lithography patterns a thin film of photoresist on substrates via selective exposure through a photomask. This technology is usually the starting point of other microfabrication technologies (Kim et al. 2008). For instance, the microstructures created using photolithography can be used as a mould in micromolding processes (Han et al. 2018). At present, various photoresists have been developed for photolithography, yet in microfluidics, SU-8 outshines the others due to its capabilities in creating vertical and tall structures with high aspect ratios (Lee et al. 2015), as well as advantages such as good optical properties, biocompatibility and chemical inertness (Narayan et al. 2018). It is a type of negative photoresists, which become insoluble when exposed to the light; on the contrary, positive photoresists become soluble when exposed (Folch 2016).

The procedure of a typical photolithography process be divided into the following steps as shown in the steps 1-3 in Figure 2.2: first, the substrates should be thoroughly cleaned to avoid unstable attachments, which may distort the spreading of photoresist during spin-coating processes. By adjusting the spinning

speed, the thickness of the coated films can be controlled. After removing the edge beads and performing a softbake process, the film is loaded in a mask aligner, and exposed to UV light through a photomask. It is worth noting that at this stage, some photoresists only undergo the activation process rather than the final polymerization. For example, the cross-linking of SU-8 only occurs if the temperature is raised to desired temperature (del Campo and Greiner 2007). Herein, additional baking process should be performed. Finally, the uncured parts of the film are dissolved in the solvent to form final microstructures.

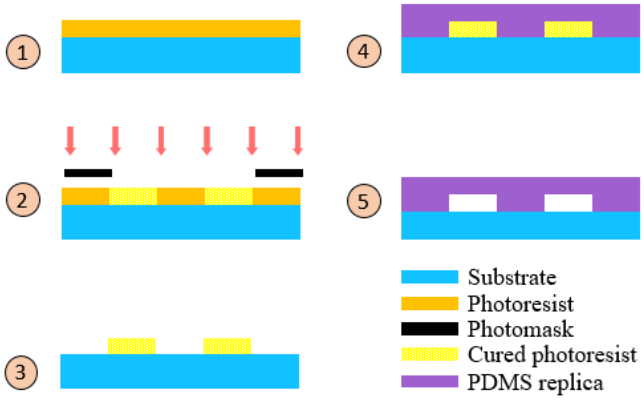

Figure 2.2 Schematic illustration of a typical process in photolithography (step 1-3) and soft lithography (step 4-5).

Although photolithography possesses favorable advantages such as high resolution (less than 1 μm), high aspect ratio, and good reproducibility, it is not impeccable. Photolithography requires clean room, expensive mask aligner and photosensitive materials. 3D microstructures are usually produced by stacking multiple layers of photoresists. Herein, coating, exposure, and polymerization of the photoresists should be operated several times, thus inevitably increasing the fabrication cost for a single device.

2.2.2 Soft lithography and micromolding

Soft lithography is another important technique in microelectromechanical systems (MEMS) and Micro Total Analysis Systems (μTAS, or lab on a chip) nowadays (Rogers and Nuzzo 2005), as evidenced by numerous examples in micro- and nano-fabrication (Qin et al. 2010), electronics (Jeon et al. 1998), chemistry (Pang et al. 2003), biology (Kane et al. 1999), pharmaceutics (Whitesides et al. 2001), and microfluidics (Kim et al. 2008). Compared to other microfabrication techniques (*e.g.*, photolithography and electron-beam lithography), soft lithography possesses several unique advantages (Xia and Whitesides 1998). For instance, it is more cost-effective and requires neither expertise nor sophisticated equipment (Folch 2016). It is suitable for not only planar, but also non-planar surfaces, hence the structures with different heights are no longer obstacles (Kane et al. 1999). Besides, soft-lithography also provides a very good resolution (~35 nm), which is competitive even when compared with electron-beam lithography (~15 nm) (Waldner 2013; Xia and Whitesides 1998).

At present, several techniques that are classified as soft lithography have been developed, including microcontact printing (μCP) (Filipponi et al. 2016), replica molding (REM) (Carugo et al. 2016), microtransfer molding (μTM) (Yang et al. 2000), solvent-assisted micromolding (SAMIM) (King et al. 1997), micromolding in capillary (MIMIC) (Kim et al. 1995), decal transfer lithography (Childs and Nuzzo 2002), nanoskiving (Xu et al. 2008), and so on. The schematic illustration of fabrication processes for several common methods is shown in Figure 2.3.

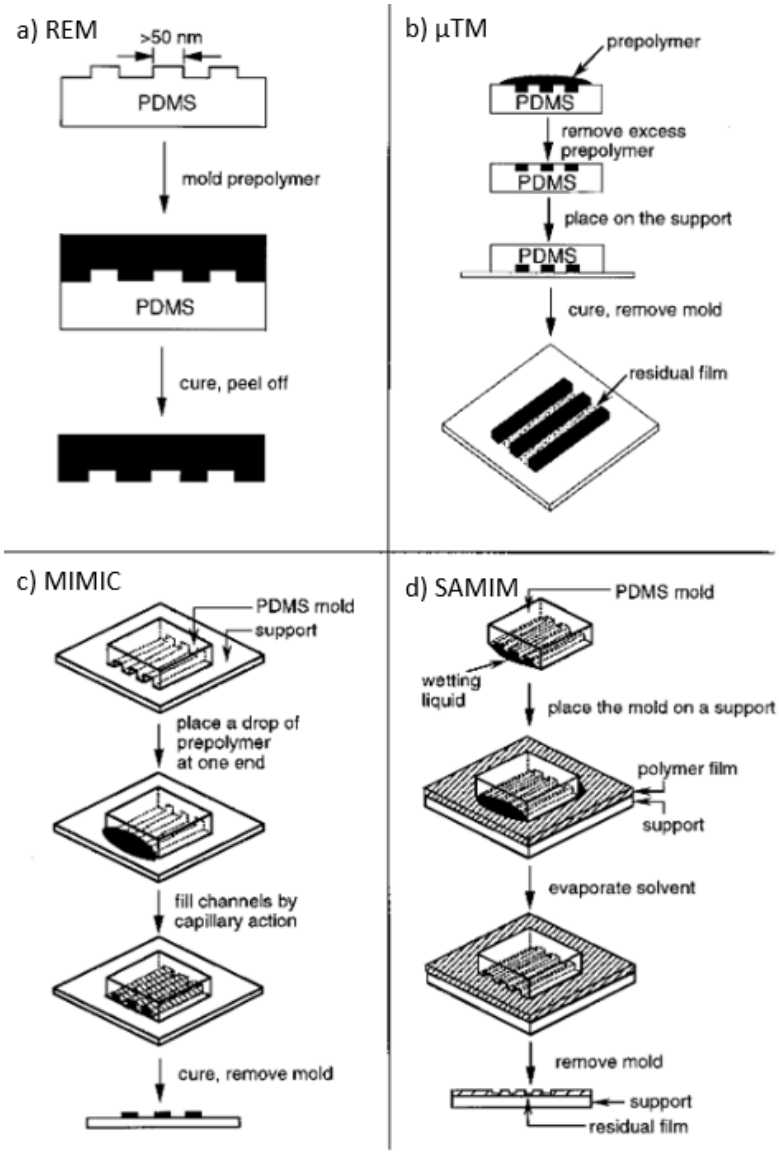

Figure 2.3 Schematic illustration of the fabrication processes for a) REM, b) μTM, c) MIMIMC, and d) SAMIM. Reproduced with permission from reference (Xia and Whitesides 1998).

Among them, REM has been widely used in microfluidics, with elastomer polydimethylsiloxane (PDMS) as the key component to imprint patterned relief structures on the surfaces of master moulds (Folch 2016). Specifically, microstructures are first fabricated on substrates, then the mixture of PDMS

precursors is poured onto the substrate, followed by baking using a hotplate or an oven to induce cross-linking of the monomers. As the contact between PDMS precursors and the moulds is conformal, the reversed pattern of the microstructures from substrates is imprinted to PDMS after separation. Finally, the replica can be bonded to another substrate (*e.g.*, glass slide) to create enclosed microchannels for further applications (Shin et al. 2003), as shown in the steps 4-5 in Figure 2.2.

It is worth mentioning that PDMS possesses many superior advantages, which are quite attractive for microfluidic applications. To name a few, it has a great optical transparency (Schneider et al. 2009), gas permeability (Merkel et al. 2000), biocompatibility (Borenstein et al. 2010), and chemical inertness (Zhu et al. 2017). Hence, it has been widely used in biomedicine-related microfluidics over the past decades. Additionally, PDMS is soft and elastic, hereby it is also an ideal candidate for microscale valves and actuators (Choi et al. 2010). Although intrinsic hydrophobicity may be unfavourable for the introduction of aqueous solutions into channels, this shortcoming can be easily addressed via oxygen plasma (Tan et al. 2010). Last but not least, PDMS-based devices are relatively cheaper than the counterparts made via glass or silicon because of the ease of fabrication and multiple castings of a master mould.

Apart from PDMS and soft lithography, other micromolding techniques that use polymers have also been investigated for microfluidics. Among them, injection molding and hot embossing are the two most widely used approaches. The polymers used in injection molding can be thermoset and thermoplastic polymers, while those used in hot embossing usually fall into thermoplastic type (Folch 2016).

Thermoset polymer is a type of polymers, in which monomers are cross-linked upon the curing reactions; while thermoplastic polymer can be molded into desired shapes once the temperature is set to be higher than its glass transition temperature.

2.2.3 Micromachining

Micromachining includes bulk micromachining, surface micromachining and other technologies such as LIGA (Lithography, Electroplating, and Molding) and deep reactive ion etching (DRIE) (Ehrfeld and Schmidt 1998; Steigert et al. 2007; Yazdi et al. 2016). Generally speaking, bulk micromachining creates microstructures inside the materials, while surface micromachining adds microstructures on the surfaces with the help of sacrificial photoresist layers.

In a typical bulk micromachining process, silicon wafers are selectively etched after an initial photolithography step (Fang et al. 2015). The etching can be performed by means of wet etching (using chemical solutions such as buffered hydrofluoric acid, BHF) or dry etch (using bombardment of ions, usually the plasma of reactive gases). On the other hand, surface micromachining starts with the deposition of new layers on the surfaces of substrates. Afterwards, patterning and selective etching are performed to create microstructures in these layers (French and Sarro 1998). Conventionally, sacrificial layers are adopted to build complex microstructures such as a suspended cantilever. Similarly, the etching process can be a wet or dry etching, depending on different conditions involving material properties, requirement of isotropy or anisotropy, and rates of etching.

Another well-known micromachining approach used in microfluidics is the lift-off technique (Bohl et al. 2005). Basically, this technique starts with creating a

photoresist pattern on top of the silicon wafers, after which the deposition of desired materials is performed in two ways, the blanket deposition (deposit on the entire surface) or selective growth (deposit on selected areas). Finally, photoresist and the coated materials on it are removed together upon the development in solvents.

Other technologies such as laser cutting (Nie et al. 2013), milling and xurography that can be used to cut microchannels are also considered as the micromachining (Folch 2016; Lin et al. 2019a). For example, inexpensive CO_2 laser has been adopted to cut thin plastic films, and xurography uses a desktop plotter to cut double-sided tapes. These simple approaches have received increasing attentions over the past few years and opened new possibilities to fabricate cost-effective and reliable microfluidic devices.

2.2.4 Additive Manufacturing

Generally speaking, fabrication methods described above deal with two types of materials, the elastic polymers and the rigid materials such as silicon and glass. Micromolding and direct machining are often used to fabricate polymer structures, while rigid substrates usually undergo photolithography and micromachining (Mitra and Chakraborty 2016). However, neither of these methods is able to create 3D microstructures with complex geometries efficiently. Although soft lithography is able to imprint real 3D microstructures, it is challenging to produce structures with high aspect ratios (Folch 2016).

Fortunately, recent advances in AM technologies have revolutionized the way how 3D microstructures are fabricated. Owing to the capabilities of converting arbitrary designs into 3D objects, AM technologies have been adopted to fabricate

real 3D microfluidic devices over the past years. Compared to other microfabrication techniques, these approaches are mostly automated without tedious operations and low fault tolerance (Figure 2.4).

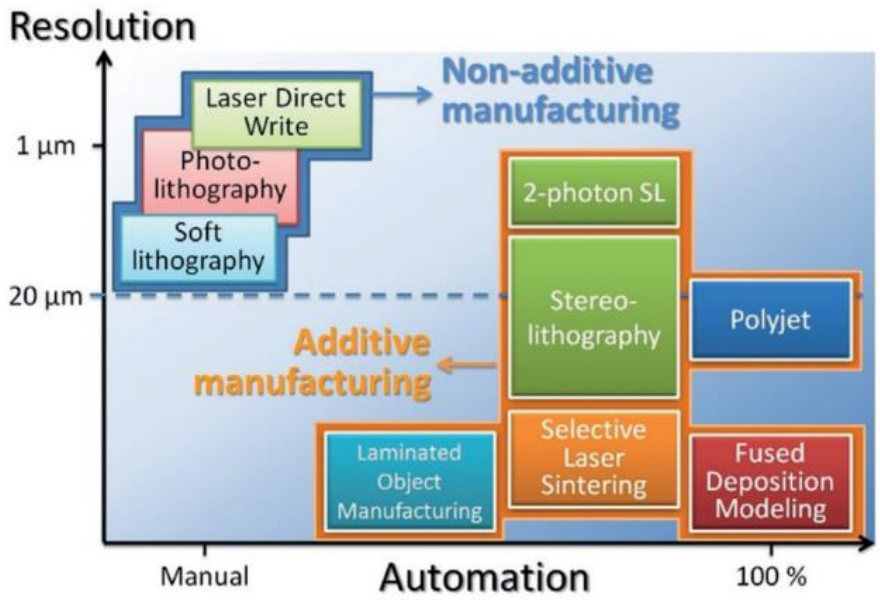

Figure 2.4 Resolution and automation trade-off for conventional microfabrication and AM technologies. Reproduced with permission from reference (Au et al. 2016).

As discussed in Chapter 1, technologies FDM and SLA are two of the most widely used AM methods for microfluidics, yet their resolutions (tens of micrometers, Figure 2.4) are usually insufficient to fabricate complex structures other than microchannels for fluid transport. Moreover, FDM-printed parts usually have rough surfaces owing to intrinsic mechanism of FDM that circular wires are melted and extruded along the designated routes (Walczak and Adamski 2015). On the other hand, SLA is unsuited for creating enclosed microchannels because of the trapped uncured photoresists. To solve these issues, we have done research on the use of microscale AM technology, two-photon polymerization, to create

microstructures that embed in microfluidic devices for different functions. The results of these studies are presented in Chapter 3 to Chapter 6.

2.2.5 Other fabrication techniques

Besides the fabrication methods introduced above, nanofabrication techniques such as electron beam lithography and scanning probe lithography (Mali et al. 2006); self-assembly approaches that use natural attractive forces to build microstructures spontaneously (Folch 2016); electroplating and microextrusion (Beuret et al. 1994; Saotome and Iwazaki 2001), have also been adopted in microfluidic fabrication.

2.3 Two-photon polymerization

Based on the hypothesis that two photons can be absorbed simultaneously as long as their total amount of the energies matches the energy gap between two electronic states, TPP was proposed in 1931 by Göppert-Mayer (Göppert - Mayer 1931). But the realistic experimental achievement was achieved after the invention of laser, which enables the coherent light with higher intensity (Kaiser and Garrett 1961). Along with burgeoning development of stereolithography, the first 3D structure created by TPP was published in 1997 by Maruo and colleagues (Maruo et al. 1997). From then on, TPP has received rapid development, and several excellent reviews and books have already been published (Baldacchini 2015; Han et al. 2016; Lee et al. 2008; Marino et al. 2015; Park et al. 2009; Raimondi et al. 2012; Rumi et al. 2008; Xing et al. 2015; Xu et al. 2013; Yang et al. 2005; Zhang et al. 2010).

As a promising AM technology working at microscale, TPP has superior

merits when it comes to the fabrication of structures that demand complex spatial features with sub-diffraction-limited resolution. Movable components can also be simply created without using sacrificial layers (Schizas et al. 2010). The remaining thin layer of monomers at the exterior surface of the fabricated structure also provides the opportunities for future chemical modifications.

2.3.1 Mechanism and materials of two-photon polymerization

As a type of microstereolithography (micro-SLA), TPP is different from traditional microfabrication techniques operated in a clean room. Owing to its voxel by voxel fashion, extra operations such as chemical or plasma etching, and mask UV exposure are not required, thus facilitating the process of fabrication especially for prototyping designs with irregular features.

Up until now, the configuration in modern machines for TPP does not differ too much from that of the first prototyping machine invented by Maruo and colleagues. Specifically, a mode-locked Ti:sapphire oscillator is used to generate consistent light with wavelength around 780nm, associated with a repetition rate of 80MHz. Afterwards, the light passes through an acousto-optic modulator (AOM), which works as an optical shutter, to generate intermittent laser with a pulse time of around 100 fs. Such short pulse time leads to a focused laser with high intensity and reduces the chance to burn the material. Then laser beam goes through a neutral density filter and a beam expander. Finally, it passes through an objective lens with high numerical aperture and then focuses on preloaded photosensitive materials. In the meanwhile, the position where the polymerization is activated is controlled by piezoelectric tilt mirrors or galvanometric mirrors and a positioning

stage, which are responsible for movements in x, y, and z axes, respectively (Figure 2.5).

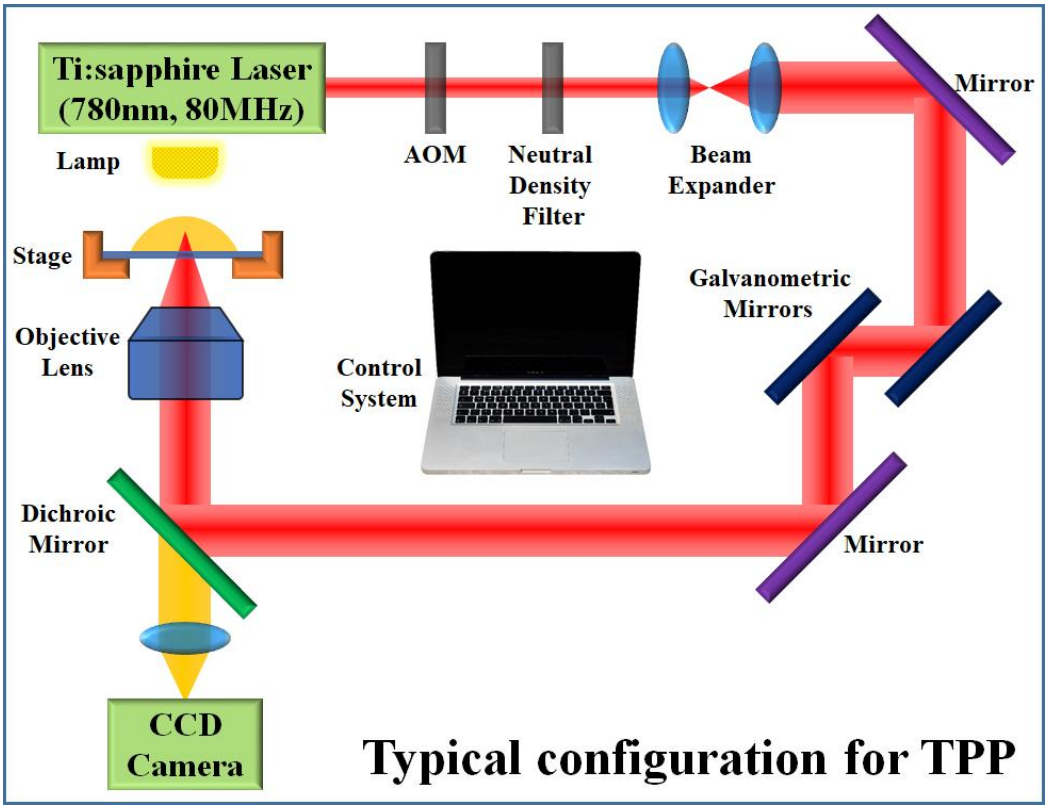

Figure 2.5 Schematic illustration of the configuration for a typical TPP process. First, a Ti:sapphire laser is used to generate consistent light with wavelength around 780nm. Afterwards, the light passes through an optical shutter, followed by a neutral density filter and a beam expander. Finally, it focuses on photosensitive materials through an objective lens. In the meanwhile, two galvanometric mirrors and a positioning stage are used to control the movements in x, y, and z axes, respectively.

Unlike conventional single-photon polymerization, two photons are absorbed simultaneously by photosensitive materials in a typical TPP fabrication process. The total energy from two photons are resonant to the energy difference

between ground state and excited state. Owing to characteristics of nonlinear absorption that occurs in this process, TPP has far higher resolution compared with single-photon polymerization (Sugioka et al. 2014). Considering the fact that only the high intensity near focused volume has the capability to convert the solubility of photosensitive materials, the excitation of polymerization is confined within such region of the beam (a voxel), and its size is normally under the limitation of diffraction.

Most photosensitive materials used in TPP are negative-tone photoresists, whose solubility decreases upon exposure to enough dose of photons. This conversion arises from the cross-linking of soluble monomers or oligomers in the photoresist. There are two common intermediates commonly applied in TPP to excite cross-linking: free radicals or cations (Selimis and Farsari 2017), and they can be initiated by a photoinitiator or a photoacid generator, respectively. For instance, a photoacid generator is used to initiate cationic polymerization in SU-8 (Juodkazis et al. 2005), which is a famous type of negative-tone photoresists. However, it only becomes insoluble upon cross-linking of oligomeric epoxide units after receiving enough heat during postbake. To make fabrication simpler, free radical based photoresists have received more attentions in TPP (Strandwitz et al. 2008).

At present, acrylates and methacrylates have been widely used in TPP as monomers due to their high activity when radicals present. However, the propagation of such reaction between monomers is unstoppable if no action is applied, resulting in a low resolution. Therefore, oxygen or radical inhibitors are normally used to address this issue. During the process of TPP, another inevitable

problem is the shrinkage of the final structure due to the increase of density after cross-linking. Nevertheless, this problem can be solved by offsetting the expected dimensions in advance. Moreover, the increase of refractive index during cross-linking can further cast a shadow over the preciseness of fabrication. Given these concerns, a careful adjustment of different components in the resin including additives such as absorbers and functional materials is inevitable.

2.3.2 Treatments of two-photon polymerization

Although TPP has opened a new door in microfabrication especially for complex 3D structures with high resolution, the polymeric backbones in these structures intrinsically lack mechanical strength and other properties (*e.g.*, conductivity, magnetism, and optical characteristics). Therefore, various treatments have been developed hitherto to enhance the performance of TPP-printed parts, and they can be categorized into two types: material treatments and structural treatments. Obviously, material treatments focus on modifications of photosensitive materials themselves. For instance, ferrofluidic photoresist has been developed by Tian and colleagues through doping synthesized Fe3O4 nanoparticles into original photoresist (Tian et al. 2012). Therefore, magnetism can be incorporated to final structures without further modifications. Conductive photoresists have also been developed recently by Staudinger and colleagues by dispersing single walled carbon nanotubes into matrix polymer (Staudinger et al. 2017). It is worth noting that these functional composites should be carefully optimized to achieve preferably stable, dispersible, and photopolymerizable properties. Imparting extra properties may compromise inherent merits of photosensitive materials. For instance,

microstructures fabricated by magnetic composites usually have rough surfaces, giving rise to unexpected disturbances in a magnetic field.

On the contrary, structural treatments such as coating usually impart functional properties as subsequent processes after TPP fabrication. Conventional techniques such as electron-beam physical vapor deposition, chemical vapor deposition, and sputtering are undoubtedly readily available to coat exterior surfaces. For instance, e-beam evaporation was utilized to coat a nickel and titanium (Ni/Ti) bilayer on structures after fabrication via TPP (Ding et al. 2016). As one of the ferromagnetic metals, Ni imparted magnetic properties to the structures. Moreover, Bauer and collaborators have incorporated a thin layer of alumina onto exterior surfaces of the final structures by atomic layer deposition (ALD) (Bauer et al. 2014). They have proven that such hybrid structures have a better mechanical strength and recoverability compared with pristine one.

Despite the methods described above have the capabilities of imparting special properties to micromachines, these methods normally do not differentiate the surfaces between polymeric structures and substrates. Under most circumstances, only the functionalization on desired part is demanded and other parts should remain intact. Although particular treatments such as shadowed deposition or use of scarified layers are able to treat only desired regions on structures, they can hardly tackle situations involved complicated 3D shapes. Furthermore, even after washing away soluble photoresists by developer thoroughly, the exterior surface of the polymerized structure still has a low concentration of functional groups (*e.g.*, acrylates, methacrylates or epoxides) that

remain unconverted (Chen et al. 2006). This trait has enabled selective treatments for structures fabricated by TPP, and unremitting efforts have been made hitherto. To name a few, Chen et al. have developed a novel treatment on polymeric structures, and it works for various types of photoresists (Chen et al. 2006). Specifically, a lithium aminolysis solution was prepared by mixing n-butyllithium and 1, 3-diaminopropane, and it was used to treat remaining groups on external surfaces of fabricated structures. Hereby, amine groups were created in regions where remaining groups were. Gold was subsequently reduced onto surfaces by these groups. At last, silver was incorporated onto gold via electroless deposition. It is critical to note that only the polymeric structure has been deposited with metal while the substrate remained untreated as indicated by different optical reflective properties (Figure 2.6 a). In addition to selective treatments between structures and substrates, treatments on specific parts of the structures have also been realized (Figure 2.6 b). Farrer and coworkers have creatively fabricated structures using two different types of photoresists (*i.e.*, acrylate and methacrylate based photoresists) (Farrer et al. 2006).

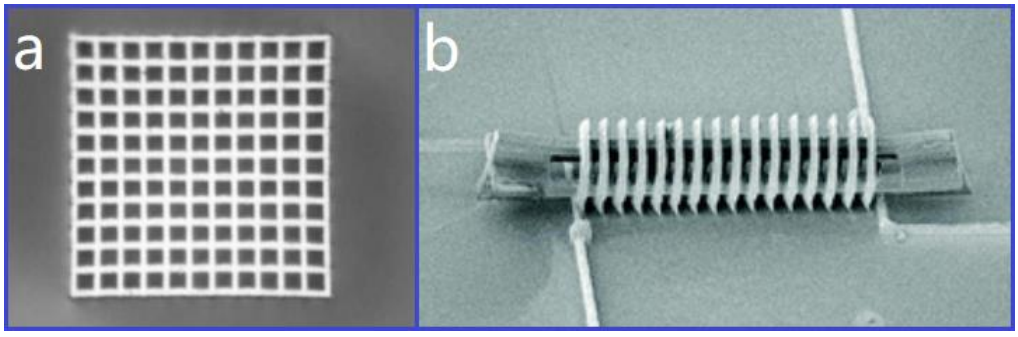

Figure 2.6 a) Optically reflective proof for selectively functionalization on polymeric structure rather than substrate. b) Copper coated acrylic inductor and unmodified

methacrylic support. Reproduced with permission from reference (Lin and Xu 2018).

2.4 Summary

In this Chapter, we first introduce the basics of microfluidics, including governing equations like continuity equation and Navier-Stokes equation, important dimensionless numbers such as Reynolds number and Peclet number, and the Poiseuille-flow in microchannels with its profiles in microstructures with different cross-section shapes. After that, we introduce the hydraulic resistance in microchannels with its expressions for different geometries, and the Stokes drag exerted on suspended substances. In addition, different fabrication methods for creating microstructures and microchannels on polymers, silicon, and glass are introduced, including photolithography, micromolding, micromachining, additive manufacturing techniques, and others. Lastly, we discuss the fundamentals of two-photo polymerization, along with its basic mechanism, materials, and common treatments after fabrication. In the next Chapters, we will present and discuss several applications of two-photon polymerization in microfluidic engineering.

Chapter 3

High resolution master moulds in soft lithography

This chapter has been reprinted with permission from Lin, Y., Gao, C., Gritsenko, D., Zhou, R., & Xu, J. (2018). *Soft lithography based on photolithography and two-photon polymerization*. **Microfluidics and Nanofluidics**, 22 (9), 97. Copyright (2018) by Springer Nature. DOI: https://doi.org/10.1007/s10404-018-2118-5.

3.1 Introduction

Since PDMS only imprints the structures on a master mould, the fabrication of master moulds have become one of the most pivotal steps in soft lithography. To date, numerous mould-creating techniques have been developed, including photolithography (Huh et al. 2010), wet etching (Filipponi et al. 2016), reactive ion etching (Brittman et al. 2017), micromachining (Park et al. 2010), multiphoton lithography (Park et al. 2010), stereolithography (Hwang et al. 2015), electron-beam lithography (Huang et al. 2004), focused ion beam (Li et al. 2003), and so forth. Among these techniques, photolithography is still the mainstream method for soft lithography due to its simplicity and high resolution.

In a typical microfluidic application, negative-tone photoresist SU-8 is the most commonly used photoresist for photolithography due to its good chemical, mechanical properties as well as the capability of creating structures with high

aspect ratio (over 25) (del Campo and Greiner 2007; Mata et al. 2006). Nevertheless, conventional photolithography is not impeccable. Creating 3D structures are still challenging for photolithography. Although stacking multiple layers is able to compensate this drawback, the entire process becomes tedious and allows very little tolerance to operational errors during alignments (Mata et al. 2006). Besides, this approach only works for simple 3D designs, in which the curved structures are not included. To circumvent this issue, other techniques (*e.g.*, 3D printing, electron-beam lithography) have been explored for soft lithography. For instance, 3D printed mould has been applied to fabricate PDMS-based microfluidic device on studies of cell stimulation recently (Kamei et al. 2015). In contrast to photolithography, this method does not require a clean room, and it enables the fabrication of real 3D structures. However, the created master moulds usually possess low resolution and high roughness (Kamei et al. 2015), which inhibit further applications, especially when small features are required. Fortunately, this downside can be solved using other mould-creating techniques such as electron-beam lithography, focused ion beam and so on. They possess the capabilities to fabricate complex 3D structures with high resolution. Furthermore, techniques like deep ultraviolet (DUV) and extreme ultraviolet (EUV) can even achieve resolution as high as several tens of nanometers.

However, most of these advanced fabrication methods require vacuum conditions, herein their procedures and maintenance are usually time-consuming. Recently, TPP technique has also been investigated for soft lithography (Bernardeschi et al. 2016). As introduced in Chapter 2, owing to the nonlinear

absorption, TPP technique confines the volume (*i.e.*, voxel) of photopolymerization at nanoscale, therefore extremely high resolution can be obtained (Lin and Xu 2018). Besides, similar to typical additive manufacturing techniques, TPP directly creates final structures from digital computer-aided design models, resulting in significantly less operation errors compared to other high-resolution techniques mentioned above. Finally, the implementation of laser with long wavelength brings several advantages such as lower absorption scattering, giving rise to a deeper penetration of light into materials, hence microstructures can be directly created inside photoresists.

On the contrary, it is also due to its high resolution, structure is fabricated voxel by voxel in TPP process. Therefore, the fabrication time can be extremely long when it comes to the fabrication of large objects. For instance, writing a solid cubic structure of 50 μm × 50 μm × 10 μm can take up to around 3.5 hours (Weiss and Marom 2015). At present, various methods have been explored and developed to speed up the process. To name a few, instead of writing a complete structure, Weiss and co-workers only wrote the internal skeletal supports as well as the outer shell. Unpolymerized photosensitive materials were encapsulated inside these backbones (Weiss and Marom 2015). Next, an extra UV exposure was used to induce a complete polymerization for the whole structure. Similarly, Kurihara and colleagues first printed the frame structure using TPP and then filled the gaps with Parylene (Kurihara et al. 2012). However, these treatments are still insufficient to make TPP an efficient method for creating master moulds for soft lithography due to their complexity.

It is worth mentioning that in a typical microfluidic device, only small regions require features with high resolution to achieve different purposes such as mixing, filtration or separation, while the remaining parts are mainly used to transport fluids and reagents. Herein, we present an innovative method to fabricate master moulds, which combines the ease of photolithography and high resolution of TPP. Photolithography is used to fabricate the majority of the mould, while TPP is applied only for small regions where high resolution is required. Generally speaking, these two methods can be proceeded separately. First, the main structure is created using SU-8 via photolithography, then the small region is filled by printing structures via TPP using SU-8 or other photosensitive materials. However, when it comes to the connection between the printed parts with existing structures, an overlapping area between two parts is inevitable. That is, the edges of solid SU-8 structures may receive a significantly excessive energy, and result in deformations during the printing process. Additionally, the refractive indices of solid and liquid SU-8 are different, thus deflections may occur during printing. Lastly, the separation of two steps also increases the time cost.

Given these concerns, we perform the TPP process directly in the SU-8 film right after UV exposure of photolithography. Hereby, the same procedures (*e.g.*, softbake and postbake) are applied to both structures exposed using different lights, and problems described above can be avoided.

3.2 Materials and methods

3.2.1 Fabrication of hybrid moulds

A thin glass cover slide (CS-30R15, Warner Instruments, CT) was used as a substrate to create master moulds using hybrid method. Although silicon wafers possess several advantages (*e.g.*, good thermal conductivity) compared to the glass slides for photolithography. It is not favorable for hybrid fabrication. Owing to unwanted opaqueness, the structures fabricated via photolithography can hardly be found under the microscope during TPP process, not to mention the alignment between TPP-fabricated structures with existing ones. Therefore, the glass slides were chosen as substrates to fabricate master moulds. As shown in Figure 3.1, the fabrication process can be divided into several steps:

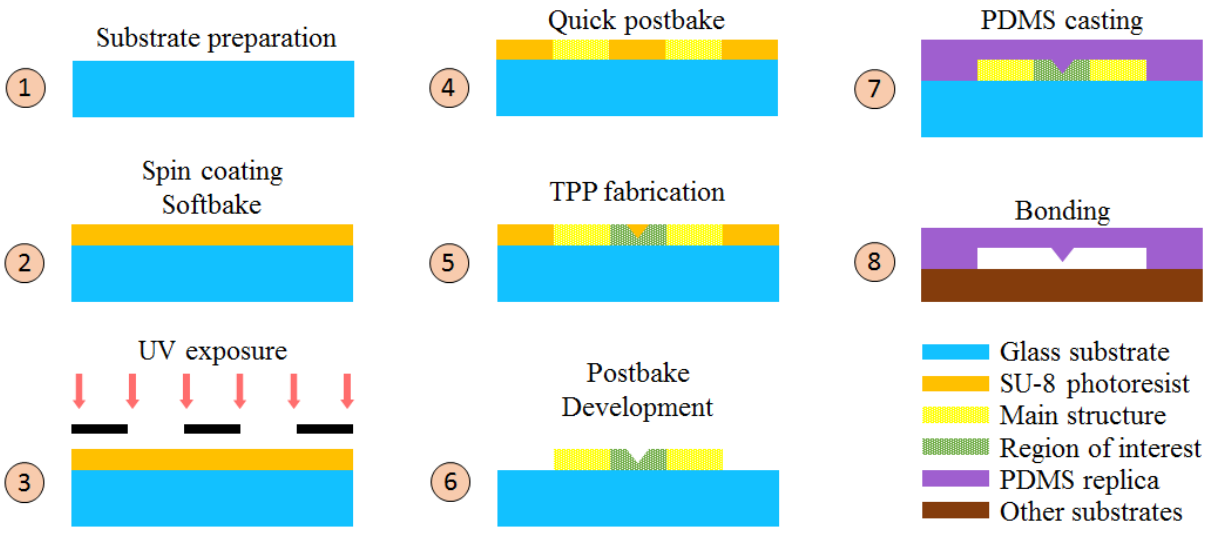

Figure 3.1 Schematic illustration for hybrid fabrication process based on photolithography and two-photon polymerization.

1) Preparation of glass substrate

A glass cover slide was first cleaned thoroughly with acetone, methanol, and isopropyl alcohol (IPA) consecutively. An extra oxygen plasma cleaning (PDC-001, Harrick Scientific Inc.) was also performed to further remove remaining organic residues. Afterwards, the glass slide was transferred to a hotplate (HS61, Torrey Pines Scientific) for 2 hours at 180 °C, assuring better photoresist adhesion after the top surface of the glass slide was completely dehydrated (Kai 2004).

2) Spin coating of SU-8

After dehydration, the glass slide was transferred to a spin coater (Spin Coater, P6700, Specialty Coating Systems Inc.) immediately. SU-8 (SU-8 2025, MicroChem Corporation, MA) was then dispensed using a disposable plastic syringe (10ml BD syringe), covering two thirds of the area of glass slide. The spinning speed was then controlled according to the data sheet of SU-8. In our case, 2000 rpm was used to form a photoresist film with thickness of 40 μm. In addition, the edge beads should be removed for an intimate contact between the glass slide and photomask during UV exposure (Miyajima and Mehregany 1995).

3) Softbake and exposure of SU-8 film

It is worth noting that glass has a smaller thermal conductivity compared to silicon wafer, therefore a longer softbake time is required. Herein, the time used to heat up the glass slide (~ 30 seconds) should be added to the total time. After the sample cooled down to the room temperature, a clear photomask (FineLine Imaging Inc., CO) with segmented pattern was attached to 5 × 5 clear glass (Front Range

PhotoMask, CO) and then loaded in a mask aligner (MA6/BA6, Karl-Süss, Germany). A long bandpass filter (Omega Optical Inc., VT) was also applied to reduce the exposure from UV radiation with wavelength below 350 nm, which may cause non-vertical walls formation. In addition, the exposure time should be elongated when taking glass substrates and optical filter into account.

4) TPP fabrication

As a cationic-type photoresist, SU-8 allows the cross-linking of oligomeric epoxides only after receiving sufficient heat during the postbake (Baldacchini 2015; Sun et al. 2005b). Thereby, a quick postbake is indispensable to visualize the exposed pattern for the alignment. To put it simply, the sample was transferred to the hotplate with the temperature at 95 °C again. In about 20 seconds, the pattern emerged. When the sample was cooled down to the room temperature, it was attached to the holder of TPP system (Nanoscribe GmbH, Germany) using tape, followed by adding immersion oil (518 F Zeiss, Carl Zeiss, NY) on the surfaces (Figure 3.2 a).

The introduction of immersion oil promoted the seeking of interfaces between the substrates and SU-8 films. Additionally, as for the hybrid fabrication method, one should always care about the accuracy of connection between one and the other. Hence, the alignment of printing structures with existing patterns was of the utmost importance (see details in Appendix A). Moreover, the intensity of laser power used in TPP was another crucial factor to be controlled during the fabrication process. A high-intensity laser usually leads to bubbling in the film, thus hindering the fabrication. This phenomenon can be attributed to a remarkable temperature

increase in overexposed regions (Jiang et al. 2014), hence the photoresist may be boiled and generate bubbles. On the other hand, a low-intensity laser gives rise to insufficient cross-linking, thereby the structures maybe deformed during development.

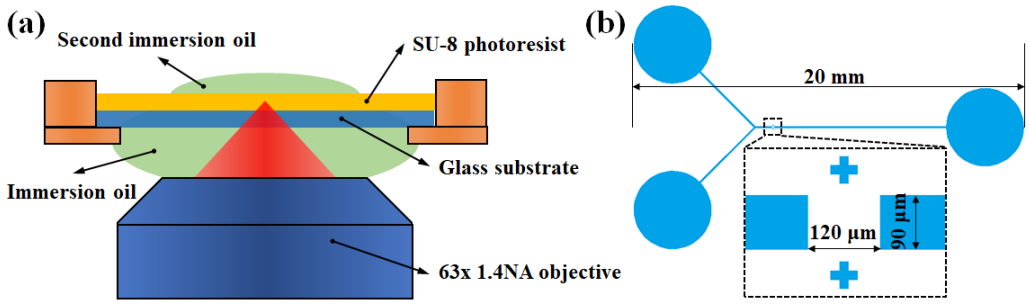

Figure 3.2 a) Schematic illustration of the configuration for TPP process in hybrid method; b) Scheme of a common mixing channel with a rectangular gap in the main channel.

5) Postbake and development

After the printing process finished, the sample was transferred to the hotplate for postbake. Propylene glycol methyl ether acetate (PGMEA, MicroChem Corporation, MA) developer was used to wash unpolymerized SU-8 from the glass after cooling the sample down to the room temperature.

3.2.2 PDMS Casting and Bonding

To prepare PDMS replica using the mould prepared as described above, PDMS mixture (Sylgard 184, Dow Corning, MI) with 10:1 base to curing agent mixing ratio was first stirred vigorously, and then degassed thoroughly using a vacuum desiccator (Bel-Art Scienceware, NJ). Afterwards, the mixture was gently poured

onto the master mould, followed by degassing again. It is worth noting that the glass substrates were very thin, thus they can be easily broken when peeling the PDMS off. Hereby, we fixed them in a bigger container such as a Petri dish with the tape (see details in Appendix A). The container was then transferred to an oven for 2 hours at 65 °C, and PDMS replica was peeled off gently. The replica was then bonded to other substrates such as glass slides.

3.3 Results and discussion

To better understand the performance and limitations of this hybrid fabrication method, we have examined several parameters and key steps that may affect the results using a common mixing channel with a rectangular gap (120 μm in length and 90 μm in width) in the main channel (Figure 3.2 b). In addition, various designs have been adopted to show its capabilities in fabricating master moulds with 3D geometries in the region of interest. Lastly, a simple passive micromixer was fabricated and used to demonstrate its applications in microfluidics.

3.3.1 Influence of adding immersion oil

In order to print 3D structures in the region of interest, one of the key problems to tackle is the seeking of correct interface between the substrates and the photosensitive materials. Otherwise, the laser may start printing inside the glass, resulting in incomplete structures, or the entire structure may float inside photoresist and be washed away after the development. Besides, the interface seeking is usually based on the difference of refractive indices of substrates and photoresists in TPP system. Hereby, adding immersion oil (that has refractive index

identical to glass) between the objective lens and the glass promotes the seeking of interfaces, since it eliminates the interface between substrates and air. But on the other hand, we found that if the immersion oil was only added to the bottom side of the glass, the exposed pattern was difficult to find under the microscope (Figure 3.3 a). Even though the pattern has emerged if the focal point was manually moved away from the substrate, the pattern shown under microscope was shifted to another position as well. Another approach to find a clear exposed pattern was adding one more droplet of immersion oil on the top of the SU-8 film. In this case, the pattern was clear as shown in Figure 3.3 b, and the immersion oil on both sides of the sample can be washed away during development.

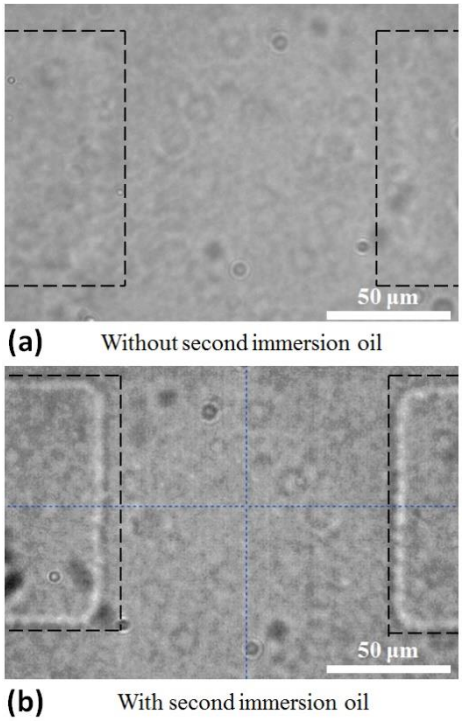

Figure 3.3 Influence of adding second droplet of immersion oil. a) The immersion oil was only added on the bottom side of the substrate. The exposed pattern was hard to find. b) The immersion oil was added on both sides of the substrate. A clear edge

of exposed pattern can be found under microscope.

The enhancement of the microscope viewing maybe ascribed to the backreflection from the second drop of immersion oil, which also affected the laser intensity required for polymerization. We found that laser with lower intensity may induce bubble formation with addition of second drop. Herein, lower laser intensity should be used and it satisfied the requirement of polymerization. This configuration also exerted additional stress on the final structures during development due to the adhesion of immersion oil to the SU-8 photoresist especially when the oil became drier after postbake. Nevertheless, given the fact that a better view of exposed pattern is of the utmost importance for a hybrid method, we have adopted this method for all the further tests.

3.3.2 Influence of quick postbaking time

In contrast to conventional photolithography, our method requires another quick postbake to visualize the exposed pattern. Generally speaking, a longer postbaking time results in better cross-linking of oligomeric epoxides in SU-8. However, it not only increases the time cost, but also makes the SU-8 film more difficult to develop (Narimannezhad et al. 2013). Therefore, we have examined the optimal quick postbaking time to achieve a clear view of exposed pattern. As the exposed pattern became visible after putting the sample on the hotplate at 95 °C for 10 seconds, we have chosen four different samples with different quick postbaking times of 10, 20, 30, 40 seconds, respectively. As shown in Figure 3.4, the exposed pattern in sample A that has undergone 10 seconds of quick postbake was difficult to find, not to mention the alignment. On the contrary, sample B has received more

heat (20 seconds) and its pattern was much clearer under the microscope. However, if the time of quick postbake was further increased, the patterns became a little bit blur again. Herein, we have chosen 20 seconds as an optimal quick postbaking time in the following tests.

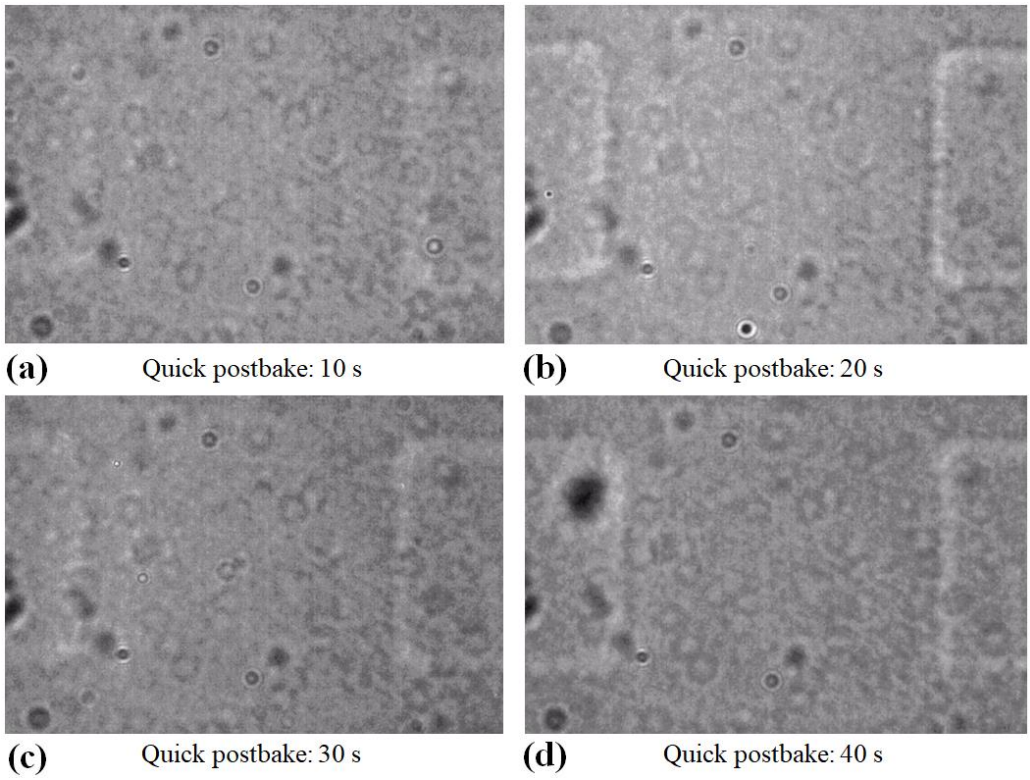

Figure 3.4 Study of the impact of quick postbaking time on finding exposed pattern. A quick postbake of 20 seconds showed the clearest edges of exposed pattern.

3.3.3 Selection of laser intensity

As described above, a high-intensity laser usually induces bubble formation during TPP process while the low-intensity laser results in insufficient cross-linking. Besides, the optimal laser intensity also depends on the properties of the photosensitive materials. Therefore, we have done a series of tests on fabrication of

a truss structure using different power intensities (15 mW, 17.5 mW, 20 mW, 22.5 mW, and 25 mW). We found it was quite challenging to fabricate truss using 15 mW as the structures were too soft and washed away after development. Moreover, weak power intensities (17.5 mW and 20 mW) have given rise to undesired deformation of the final structures (Figure 3.5). This was attributed to insufficient cross-linking, making the structures were vulnerable, and hence some parts of the trusses were washed away. On the contrary, the higher intensity (22.5 mW) resulted in a firm structure that matched the CAD model. However, if the power intensity was too strong (*e.g.*, 25 mW), the bubbling maybe induced and demolished the structures. Nevertheless, it is worth mentioning that the optimal intensity is flexible, as it depends on the structure properties and geometries. When the cross-section of the structures is large enough, the favorable power intensity should be smaller. This can be attributed to the overlapping exposures between the adjacent voxels.

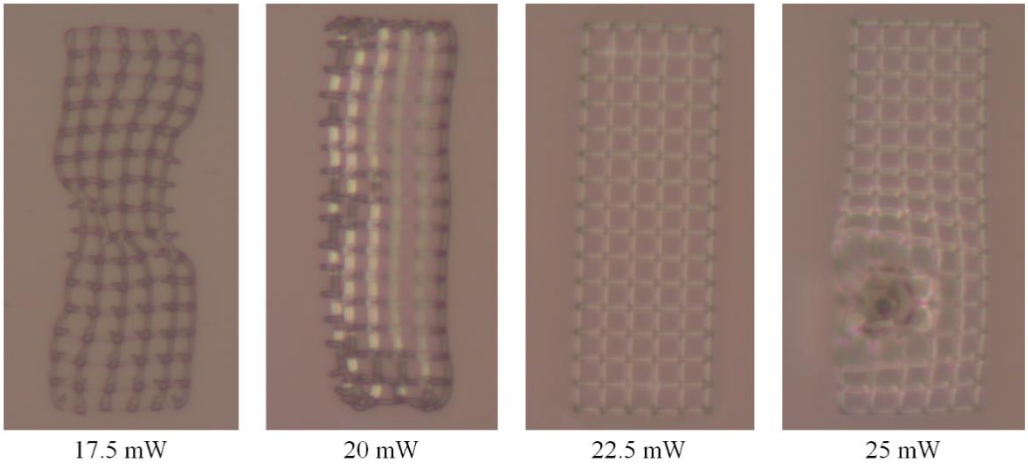

Figure 3.5 Low-intensity laser led to undesired deformation of the final truss structures while a high-intensity laser may induce bubble formation during TPP process. Therefore, a careful calibration of laser intensity is highly recommended

before the fabrication.

3.3.4 Proof-of-the-concept fabrication

The first design used to demonstrate the capability of combining photolithography and TPP is a simple block that connects two segmented microchannels (Figure 3.6 a). Even though the desired thickness of SU-8 film (40 μm as a demonstration) on the glass is predictable according to protocol, it is impossible to know the exact value before the development. Given that there is no SU-8 above the top surface of the photoresist film, TPP process only happens in the immersion oil for the part extruded. Therefore, thick designs that exceed photoresist film should result in identical structures with the same thickness. However, the proper estimation of the final height is still demanding to reduce the fabrication time wasted on the extruded parts. Based on this assumption, we printed a block with the same length and width, but of the larger height (45 μm).

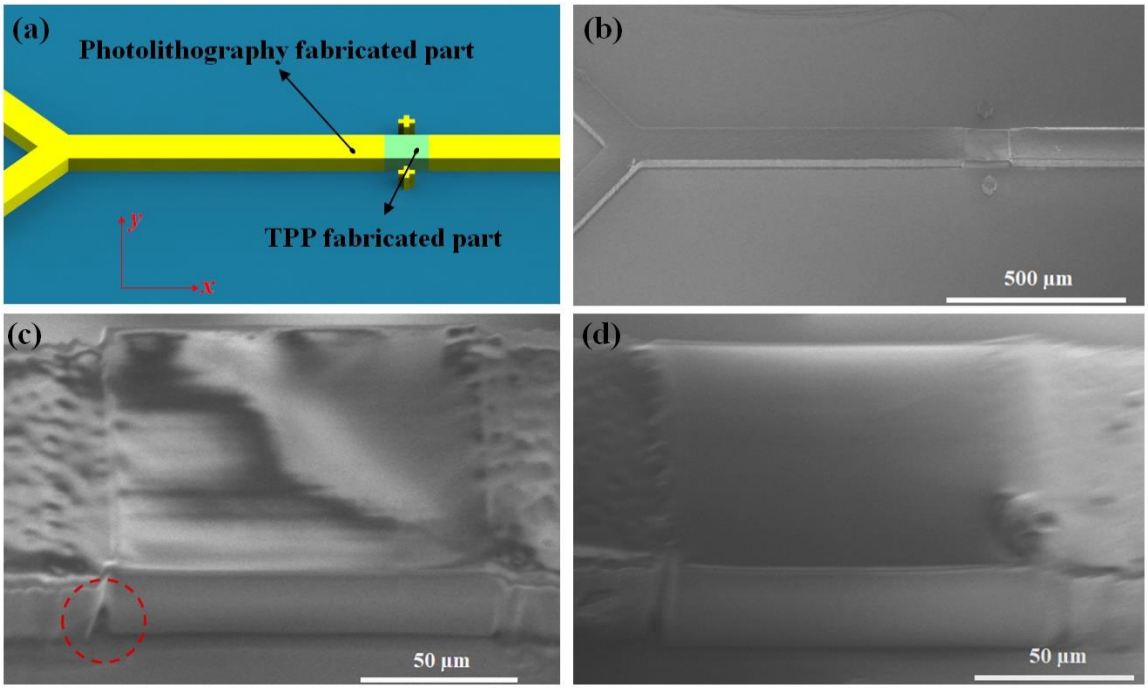

Figure 3.6 A simple block was used to test the feasibility of the proposed method. a) A 3D design that manifests the idea of how the block is used to connect segmented parts. b) SEM image of the hybrid structure fabricated by photolithography and TPP. c) Zoomed SEM images of the regions where the structures connected with the block for the gap of identical dimensions. A small opening between two structures was marked by with red circle. d) Elongated block used to compensate the gap between two structures.

To give a closer look on the final structures, scanning electron microscopy (SEM) system (Hitachi S-3000N-VP-SEM, Japan) was used. As showed in Figure 3.6 b, a simple block fabricated by TPP was successfully connected to the segmented microchannel fabricated using photolithography. Nevertheless, after zooming in, the surface of the final structure was not as smooth as expected (Figure 3.6 c). This thickness variation could arise from the flowing of SU-8 during softbake (Lin et al. 2002). Furthermore, a contact profiler (P7, KLA-Tencor, CA) was used to measure the surface profile in the region where hybrid structures were connected. It was found that the roughness of the surface fabricated by photolithography was around 0.2 μm, which was acceptable for the majority of microfluidic applications.

Additionally, there were two small ridges (less than 1.5 μm in height) in the connecting areas. This problem may be attributed to different shrinkage rates between the photolithography-fabricated parts and TPP-fabricated parts. Nevertheless, compared to the entire thickness of 40 μm, the difference was almost negligible. A small opening was also found in the bottom of the connecting region, which was probably due to low resolution and transmittance from plastic mask, and

can be simply improved if high-resolution masks are used. Alternatively, an elongated structure (*e.g.*, length of 130 μm) with the large overlaps can be adopted to compensate the deficiency (Figure 3.6 d). Last but not least, a small deviation was also found in x direction, and it was an inevitable shortcoming for the proposed hybrid method as the alignment of the printed structure and exposed pattern depended on the clarity of edges in the exposed pattern.

3.3.5 Various microstructures fabricated using hybrid methods

To further investigate the performance of the proposed hybrid method, several microstructures with different designs have been fabricated. As presented in Figure 3.7 a, a series of grooves with same height of 5 μm, but different widths ranging from 0.5 μm to 5.0 μm with an increment of 0.5 μm were fabricated.

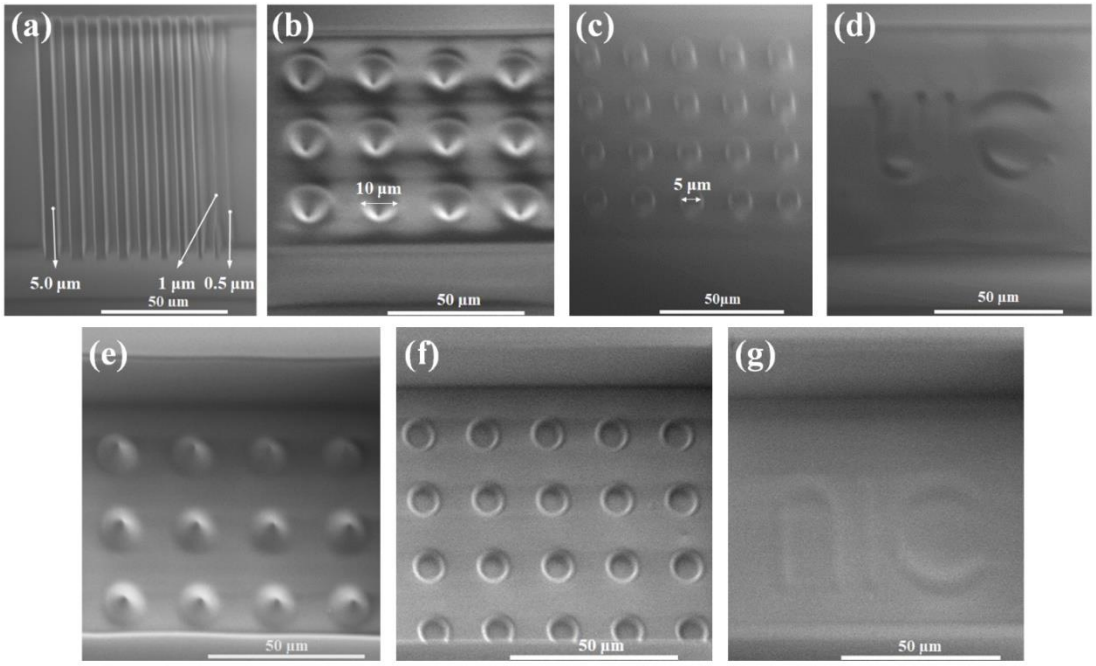

Figure 3.7 a) SEM image of the block with various grooves ranging from 0.5 μm to 5.0μm. b-d) SEM images of various designs fabricated via hybrid method, including

cone-shape cavities, cylindrical pillars, and UIC characters, respectively. e-g) SEM images of corresponding PDMS replicas, respectively.

Specifically, the grooves with the widths more than 1.5 μm were successfully fabricated with the vertical walls as expected. However, two grooves with the widths of 0.5 and 1.0 μm collapsed and the walls between them were connected to each other, which can be attributed to their high aspect ratios. Nonetheless, the results have proven this method to be promising in fabrication of 3D master moulds with high resolution. Additionally, other designs in a connecting block were also fabricated (Figure 3.7 b, c, d), including cone-shape cavities, cylindrical pillars, and UIC characters, respectively. Their PDMS replicas were shown in Figure 3.7 e, f, g, respectively.

In addition, owing to the rapid photolithography process, the time costs for these hybrid structures were much less than that of the structures printed solely by TPP (Table 3.1). For instance, for a micro mixer mould with a connecting block that has structure of cylindrical pillars, the pure TPP for the main channel via solid TPP printing (*i.e.*, solidification at each point with 63x NA 1.4 objective) required 928 hours and 20 minutes, which was almost impossible to achieve. Although adopting scaffold method (*i.e.*, solidification only existed on external surfaces and internal scaffolds) or using other objective (*e.g.*, 25x objective) can mitigate the workload, the final time cost was still huge, not to mention low resolution obtained from 25x objective.

Besides, when printing large structure using TPP, stitching has to be applied because of the limitation of the printing field. Herein, the final structures were made

of numerous small parts, which gave rise to non-smooth surfaces or even steps between them. On the other hand, the connection in the proposed hybrid method is only required between the regions of interest and the main channels, hence the steps only exist in limited areas.

Table 3.1 Time cost for 3 designs (40 μm thick) using hybrid method or pure TPP

Structures	Prebake	Exposure	Quick postbake	TPP	Postbake	Development
Structure-1	10 min	45 sec	20 sec	14 min	8 min	5 min
Structure-2	10 min	45 sec	20 sec	10 min	8 min	5 min
Structure-3	10 min	45 sec	20 sec	15 min	8 min	5 min
Structure-4	10 min	N/A	N/A	928 hr	8 min	5 min
Structure-5	10 min	N/A	N/A	131 hr	8 min	5 min

Note: Structures 1-5 are connecting block with cone-shape cavities, connecting block with cylindrical pillars, connecting block with UIC characters, pure TPP for main channel (solid), and pure TPP for main channel (scaffold), respectively.

3.3.6 Demonstration of microfluidic application: a passive micromixer

As aforementioned, soft lithography has become a commonly used method in microfluidics, and the proposed fabrication method has opened a new door to fabricate reliable master moulds for soft lithography. Micromixer is an important component that has been commonly used in microfluidics due to the fact that viscous force becomes ineligible at microscale and the laminar flow is dominant in the most cases. Hence, mixing in a microchannel is mainly fulfilled by means of passive diffusion, being insufficient for most scenarios.

Nowadays, various micromixers have been developed to facilitate the mixing at microscale, including passive and active micromixers. Here, we have created a

passive micromixer to demonstrate the capability of hybrid fabrication method for microfluidic applications. Specifically, the main channel of micromixer was fabricated using photolithography while three gaps were later filled with three chaotic mixing components using TPP. As presented in Figure 3.8 a and Figure 3.8 b, the chaotic mixing component composed of four triangular blocks that were organized alternatively. Pillars with the diameter of 6 µm and length of 12µm were also added to the surfaces of the blocks to further agitate the flows. After creating the PDMS-based device using as-fabricated mould, we injected the solution of 0.02% w/v fluorescein sodium salt (Sigma Aldrich) and DI water into two inlets at the flow rate of 0.5 ml/min, respectively (Figure 3.8 c). It is worth noting that after two chaotic mixing components, they were mixed completely.

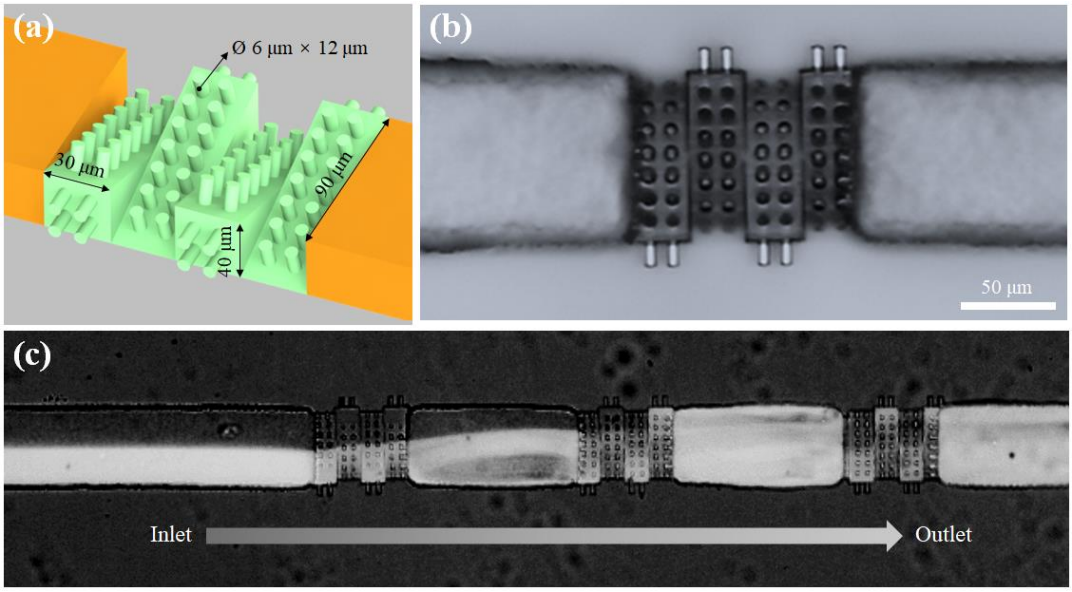

Figure 3.8 A passive mixer fabricated using hybrid fabrication method. a) Schematic illustration of the mixing component composed of four triangular blocks. b) Image of the mixing component in a fabricated soft lithography master mould. c) Image that showed a complete mixing achieved after two mixing components.

3.4 Summary

To summarize, we have successfully developed a new method to create master moulds for soft lithography using the combination of photolithography and TPP. It not only takes the advantages of traditional photolithography, where relatively large structures can be simply and rapidly fabricated, but also incorporates 3D fabrication using TPP. Hereby, the proposed method avoids the huge time expenses that are inevitable when creating the entire structures by TPP. Additionally, various complex 3D structures can be created in the region of interest with high resolution. Moreover, owing to the advantages of soft lithography, even though the master mould should be fabricated in a clean room, it can be used for multiple times to create PDMS replicas, further reducing the costs for single device.

Nevertheless, the hybrid method still has its own deficiencies. For instance, as the exact thickness of SU-8 film remains unknown before the TPP process, a careful prediction is required to minimize the difference in thicknesses between two structures. Additionally, as the alignment of TPP-based structures to existing exposed pattern is based on the clarity of exposed edges, the operational errors are inevitable. Thereby, the small shifts between two structures often exist. Besides, an addition of the second droplet of immersion oil on the top of SU-8 exerts additional stress on final structures, thus requiring a careful development process. An optimal laser intensity is also demanding to obtain reliable master moulds as well as avoiding bubble formation during the TPP process. Nonetheless, this method has proposed a new approach to create complicated microfluidic devices with high resolution in a simpler and faster way.

Chapter 4

Superhydrophobic foil with hierarchical structures

This chapter has been reprinted with permission from Lin, Y., Zhou, R., & Xu, J. (2018). *Superhydrophobic surfaces based on fractal and hierarchical microstructures using two-photon polymerization: toward flexible superhydrophobic films*. **Advanced Materials Interfaces**, 5(21), 1801126. Copyright (2018) by John Wiley & Sons. DOI: https://doi.org/10.1002/admi.201801126.

4.1 Introduction

Nature has long inspired numerous scientific findings and technological innovations, especially after biomimicry was found to be an important approach to tackle human challenges (Benyus 1997). In particular, living systems such as lotus leaves (Cheng and Rodak 2005), insect wings (Byun et al. 2009), and rice leaves (Feng et al. 2002), are usually highly hydrophobic, giving rise to water-repellency, self-cleaning, anti-fouling, and anti-fog and other appealing properties (Liu et al. 2006). Unsurprisingly, these advantages have facilitated the development of artificial hydrophobic materials with a variety of applications coming after, including self-cleaning windows (Yang et al. 2006), non-soiling clothing (Ramaratnam et al. 2007), and wettability treatments on microfluidic devices (Sun et al. 2005a). Specially, surfaces with extremely high water contact angles and low sliding angles, usually greater than 150° and smaller than 10° respectively, are considered as

superhydrophobic surfaces (Synytska et al. 2009). It is worth noting that superhydrophobic properties are governed by both surface chemical composition (*e.g.*, surface free energy) and geometrical microstructures (*e.g.*, surface roughness) on the surfaces (Synytska et al. 2009; Wu et al. 2010b). Therefore, current studies that aim at realizing superhydrophobicity mainly focus on either modifying the chemical properties of the materials or creating efficient microstructures.

Specifically, the impact of geometrical microstructures on surface wetting is attributed to two mechanisms: homogeneous wetting and heterogeneous wetting (Figure 4.1) (Hejazi et al. 2014). The former mechanism is also well-known as the Wenzel State, in which the liquid penetrates into the gaps between microstructures, while the latter mechanism is denoted as the Cassie-Baxter state, in which the liquid is supported by the trapped air inside microstructures. Additionally, transition states exist when the tips of the microstructures and substrates show different degrees of heterogeneity (Berwind et al. 2017). These states result from hierarchical structures, which combine the microscale and nanoscale features. Besides, they have been found in many natural superhydrophobic creations, and proven to be a useful approach to enhance superhydrophobicity (Cha et al. 2010), thus arousing great attentions over the past years.

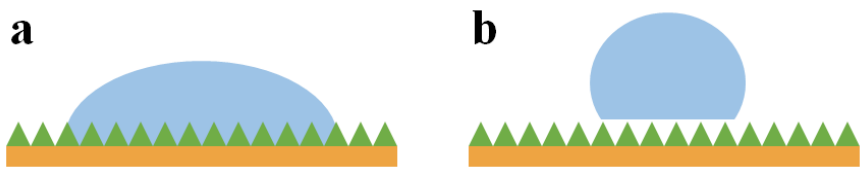

Figure 4.1 Schematic illustration of two different mechanisms for surface wetting. a) Wenzel state. b) Cassie-Baxter state.

At present, a number of fabrication techniques have been investigated and utilized to create hierarchical structures, including chemical etching (Xiu et al. 2010), DRIE (Kwon et al. 2009), replica molding (Choi and Huh 2010), deposition (Wu et al. 2010a), photolithography (Boesel et al. 2010), self-assembly (Pokroy et al. 2009), hydrothermal synthesis (Wu et al. 2010c), electron-beam lithography (Feng et al. 2011), soft lithography (Morariu et al. 2003), laser-assisted etching (Baldacchini et al. 2006), direct laser writing (Tricinci et al. 2015), and so forth.

However, even though these techniques have successfully produced superhydrophobic surfaces, most of them can only fabricate arbitrary features with random secondary structures or simple 3D structures with extruded shapes (Feng et al. 2011). Despite several reports showing that complex 3D shapes can be achieved, their processes are usually quite sophisticated and time-consuming (Liu et al. 2014; Sun et al. 2010). For instance, dual structure with controllable sidewall profile has been successfully created on a silicon wafer using DRIE combined with black silicon effect (Sun et al. 2010). Further, these methods still lack the ability to create real 3D structures with well-defined geometries, thereby the majority of current studies only reflect either statistic results or particular conclusions drawn based on simple 3D structures. Additionally, current studies mainly focus on creating microstructures on rigid substrates, which lack the softness and flexibility that are ubiquitous in nature. Herein, a simple and accurate way to fabricate controllable 3D microstructures on flexible substrates is still highly demanding for in-depth studying of fundamental principles behind surface wetting as well as creating novel engineering and bionic applications.

As discussed in previous chapters, TPP has become a promising method to create real 3D microstructures in microscale or sub-microscale (Lin and Xu 2018). During a typical TPP process, a small region (*i.e.*, voxel) in the photosensitive materials is polymerized when two photons are absorbed simultaneously (Lin et al. 2018), and final structures fabricated are composed of countless voxels that correspond to the digital files after slicing and hatching (Figure 4.2). Owing to the fact that the resolution of TPP can be as high as 100 nm (Ovsianikov and Chichkov 2008), various applications such as creating 3D hierarchical structures on the substrates have been realized over past few years. Besides, fractal structures that possess self-similarity on any length scale have also received much attentions for creating superhydrophobicity (Shibuichi et al. 1996). Recently, such intrinsically hierarchical structures have been successfully fabricated using TPP as well for wetting study (Davis et al. 2017).

Furthermore, conventional methods usually consider the whole surface as an entirety, no particular consideration was taken to convert the wetting performance in different areas on the surface. Nevertheless, owing to the intrinsic convenience from additive manufacturing, spatial control can be incorporated into a digital file, thus creating different microstructures to tune wetting performance at different locations.

In addition, albeit rigid materials such as silicon and silica are the most commonly used substrates for TPP process, flexible materials possess several unique advantages when creating superhydrophobic films (Kwon et al. 2018; Liu et al. 2018; Wang et al. 2016a). Compared to their rigid counterparts, flexible materials

such as plastics are usually cost-effective, soft, flexible, light, thin, and unbreakable. Additionally, natural superhydrophobic materials are usually of good flexibility, whose effect on the wetting performance has long been ignored. That is, it is recently found that substrate flexibility enhances superhydrophobic performance along with surface microstructures synergistically (Vasileiou et al. 2016). For instance, extended water repellency can be attributed to substrate flexibility, and other droplet effects such as impalement resistance and droplet-substrate contact time also benefit from flexible feature. Last but not least, flexible films can also be used for further bionic studies such as raindrop bouncing on hydrophobic insect wings.

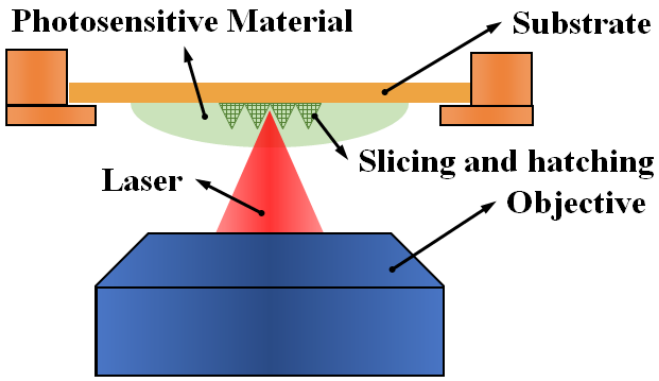

Figure 4.2 Schematic illustration of a typical TPP fabrication configuration. The final structures are composed of voxels in a typical TPP fabrication process.

Here, we first applied the TPP technique to fabricate various 3D hierarchical structures on glass slides, including fractal tetrahedron and pyramids arrays, which investigate the impact of 3D hierarchical structures on superhydrophobic behavior. Afterwards, hexamethyldisiloxane (HMDSO) was coated on all surfaces via plasma enhanced chemical vapor deposition (PECVD) to further enhance hydrophobicity.

Finally, superhydrophobic flexible film was achieved via fabricating hierarchical structures on a plastic polyethylene terephthalate (PET) film using TPP technique, followed by HMDSO coating.

4.2 Materials and methods

Materials and Equipment: ITO-coated square glasses (length: 25 mm, thickness: 0.7 mm) and IP-S photoresist were purchased from Nanoscribe GmbH. ITO-coated PET film (thickness: 0.127 mm) was purchased from Sigma-Aldrich. Propylene glycol monomethyl ether acetate (PGMEA) was purchased from MicroChem. Photonic Professional System from Nanoscribe GmbH was used to create microstructures on either glass or plastic substrates. Polaron E5100 Series II sputter coater was used for gold deposition. JEOL JSM-6320F Field Emission Scanning Electron Microscope (FESEM) was used for SEM imaging. Low-pressure plasma system Tetra 100 PC / PCCE was used for HMDSO deposition with the help of Diener Electronic GmbH. DataPhysics OCA 25 was used to measure the contact angle.

TPP Fabrication on glass substrates: ITO-coated glasses were first thoroughly cleaned with acetone and IPA, followed by blow drying with nitrogen. Afterwards, they were mounted on the holder with tape, and a small drop of IP-S photoresist was carefully added onto the surface of substrates. Then the holder was loaded into Nanoscribe system, and 25 x 0.8 NA objective was selected for fabrication. Although 63x 1.4 NA objective enables a better resolution and surface finishing, associated fabrication time would increase drastically. Slicing distance of 0.4 µm and hatching distance of 0.3 µm were adopted when creating the job files using DeScribe

software. Moreover, as the pattern fabricated was roughly 3 mm by 3 mm, stitching was inevitable due to the limitation from each printing field, as it was only around 270 μm × 270 μm. Therefore, an array of 11 × 11 patterns was adopted during fabrication process, and the fabrication time varied from 1.5 hour to 3.5 hours for different designs (Entirely hierarchical microstructures required much more time: 10 hours). After the fabrication finished, the samples were developed using PGMEA for 10 minutes, followed by IPA rinse and air drying.

TPP Fabrication on PET films: Basically, the fabrication of microstructures on PET films is quite similar to that for glass substrates. However, as the PET film is flexible and much thinner than glass, a square glass (length of 25 mm and thickness of 0.7 mm) has been adopted as a support. Specifically, the glass was first placed on the holder, then cleaned PET film was cut into appropriate size (*e.g.*, 2mm × 2 mm), followed by mounted together with tape. It was also worth noting that Nanoscribe system capitalized on the differences of refractive indices between substrates and photoresist to find interfaces, thereby the interface between PET film and glass support may interfere with correct interface. Given this concern, we added a small droplet of IPA on the glass before mounting the PET film, thus the trapped IPA film has masked the interference from another interface.

SEM Imaging: A 10 nm layer of gold was deposited on the samples before SEM imaging. Afterwards, the samples were transferred to JEOL JSM-6320F FESEM, and an acceleration voltage of 3.0 kV was applied for imaging.

HMDSO treatment: HMDSO treatment was conducted with the help of Diener Electronic GmbH. Basically, the samples were activated with oxygen plasma first,

then PECVD was used to coat a 100 nm layer of HMDSO.

Contact angle measurement: Contact angle was measured using a DataPhysics OCA 25 goniometer. DI water droplets were carefully added onto the surfaces of samples and their sizes varied depending on wetting behaviors. Afterwards, images and contact angles were recorded and measured using SCA20 software. All the measurements were conducted under the temperature of 22° C and humidity of 45%.

4.3 Results and discussion

4.3.1 Design and fabrication of fractal and hierarchical structures

Apart from regular hierarchical structures that add nanoscale features to microscale backbones, Shibuichi and colleagues have reported that hierarchical structures with fractality also have the capability in achieving superhydrophobicity (Shibuichi et al. 1996). However, previous studies mainly focus on forming random fractal structures on substrates (Synytska et al. 2009; Xu et al. 2005), by which the conclusions drawn were statistic. Recently, Davis and co-workers have designed three fractal structures with different fractal dimensions using TPP (Davis et al. 2017), and they found that there was no clear correlation between surface wetting performance and fractal dimensions. This finding deviated from the theory proposed by Shibuichi. Hereby, we have adopted the famous fractal structure (*i.e.*, Sierpinski tetrahedron) to further study the relationship between fractality and surface wetting.

Three stages (0, 1, and 2) of Sierpinski tetrahedron have been adopted. As

shown in Figure 4.3 a, b, c, the stage-0 Sierpinski tetrahedron is basically a single tetrahedron without any modification, while the stage-1 Sierpinski tetrahedron consists of 4 identical stage-0 Sierpinski tetrahedrons with half size. Similarly, stage-2 Sierpinski tetrahedron is composed of 4 stage-1 Sierpinski tetrahedrons with half size. Herein, 4 copies of the former stage Sierpinski tetrahedron are connected to each other with corner touching. It is also worth noting that although the volume decreases (approaching zero) as the iteration goes on, the total surface area remains constant.

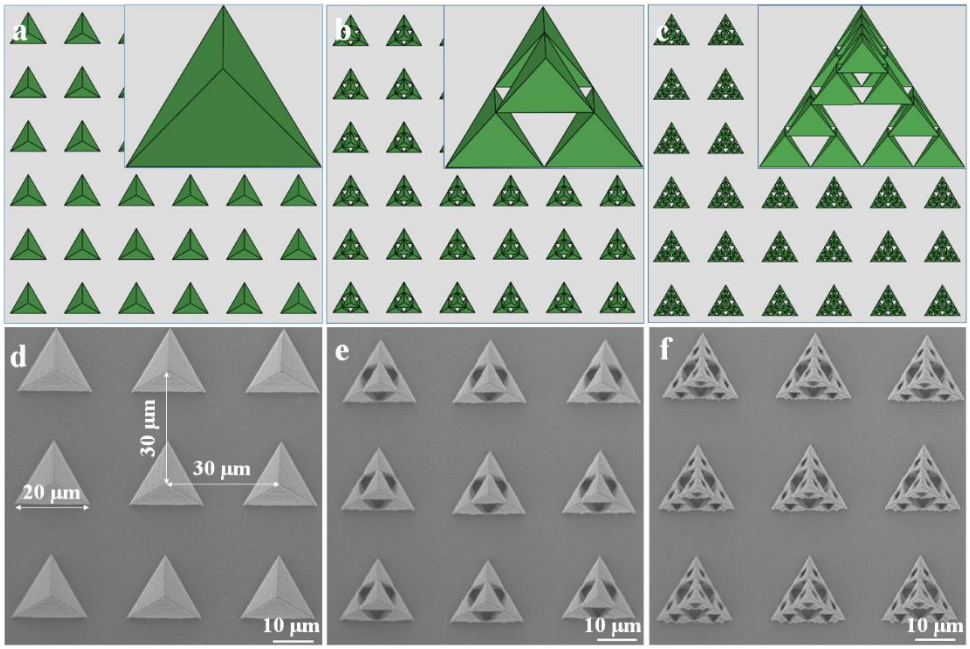

Figure 4.3 CAD models of Sierpinski tetrahedron and corresponding scanning electron microscope (SEM) images of the microstructure array fabricated by TPP. a-c) CAD models of stage-0, stage-1 and stage-2 Sierpinski tetrahedron, respectively. d-f) SEM images of Stage-0, stage-1, and stage-2 Sierpinski tetrahedron array. The length for each Sierpinski tetrahedron unit is 20 μm and the center-to-center distance between units is 30μm. The printed surface area is roughly 3 mm by 3 mm.

In fractal geometry, fractal dimension has been widely used to represent the statistical index of the complexity for objects with self-similarity, and it can be simply calculated using Equation 4.1 (Faloutsos and Gaede 1996),

$$D_f = -\frac{\log N_f}{\log \varepsilon_f} \tag{4.1}$$

where D_f is the fractal dimension, N_f is the number of the parts that form fractal objects, and ε_f stands for the scaling factor. Hereby, we can simply obtain the fractal dimension of Sierpinski tetrahedron: $D_s = -\log(4)/\log(0.5) = 2$.

As the ratio between height and bottom area is constant, it is obviously pointless to create a single big Sierpinski tetrahedron on a glass substrate, not to mention endless time required for fabrication. Given this concern, we have introduced the array of Sierpinski tetrahedron, in which each unit has a length of 20 μm and a center-to-center distance of 30 μm (Figure 4.3 d, e, f). Although when taking the whole array into account, it cannot be considered as a fractal object, but fractality still exist in each unit. Moreover, as the microstructures are polymerized voxel by voxel, the required fabrication time increases drastically if the slicing and hatching distances decrease. Therefore, an appropriate selection of printing parameters is indispensable.

Even though finer slicing and hatching (*e.g.*, 0.2 μm and 0.1 μm, respectively) enable a better result with smoother surface finishing, the time cost can be tens of that for normal slicing and hatching (*e.g.*, 0.4 μm and 0.3 μm used, respectively). However, if they are further increased, the overlaps at corners where tetrahedrons touch become insufficient, thus the top structures may be washed away during

development of photosensitive materials.

In addition to the fractal Sierpinski tetrahedron described above, conventional hierarchical structures with real 3D shapes were also fabricated on glass substrates. Three patterns of microstructure composed of rectangular pyramids have been utilized. The first pattern is an array that consists of single pyramids (Figure 4.4 a), with the length of the square base and height of 20 μm. On the contrary, the second pattern is composed of hierarchical pyramids that contains smaller pyramids (Figure 4.4 b). In spite of the sizes of square base and height being identical to the first pattern, their main bodies are filled with 36 small pyramids with length and height of 2.5 μm.

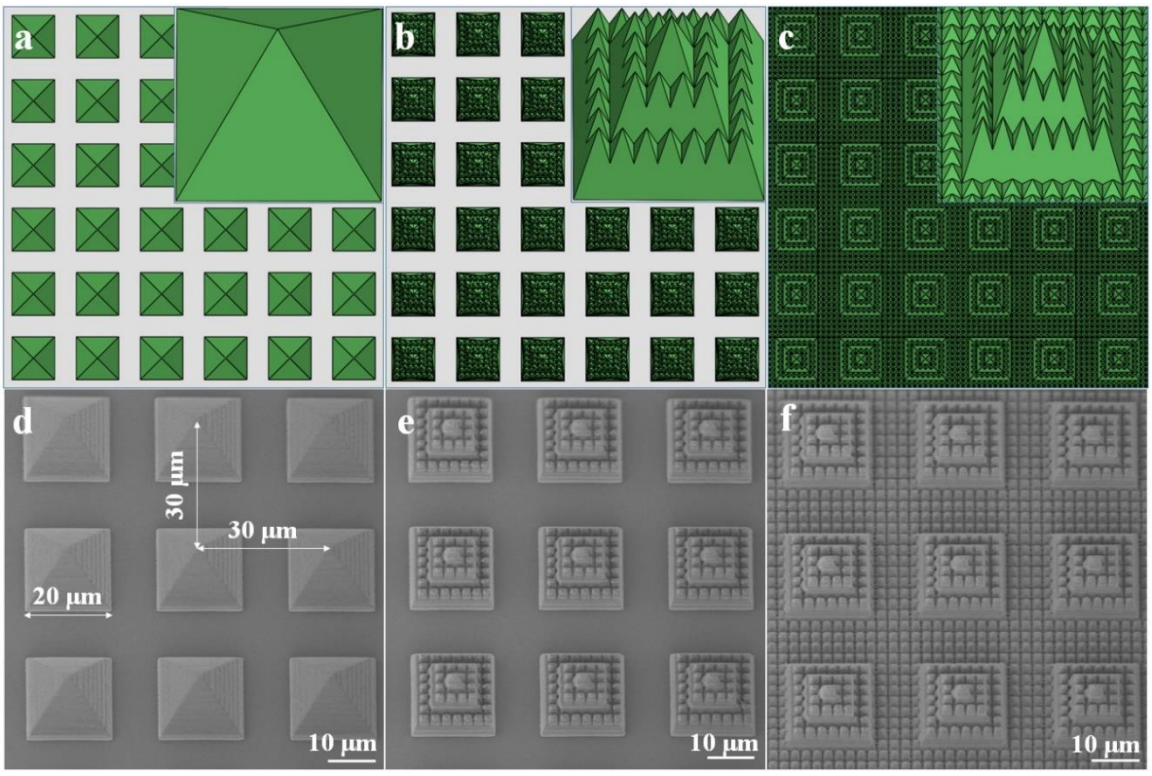

Figure 4.4 CAD models of the hierarchical pyramids and corresponding SEM images of the microstructure array fabricated by TPP. The tilt angle used for SEM is 15°. a)

CAD model of the array of rectangular pyramids, which has a length of 20 μm for square base and height of 20 μm. b) CAD model of the array of hierarchical pyramids, in which the main bodies are filled with 36 smaller rectangular pyramids with length and height of 2.5 μm. c) CAD model of the microstructures by which the entire printing area is covered with hierarchical and small pyramids. d) SEM image of the array with pyramids. e) SEM image of the array with hierarchical pyramids. f) SEM image of the array with entirely hierarchical structures.

Furthermore, we also created the third pattern, in which the entire printing area was covered with hierarchical pyramids as well as the small pyramids in between (Figure 4.4 c). In order to maintain the height of microstructures, the angles of the pyramids in the second and the third patterns were different to that of the first one. It is also worth mentioning that clear ridges were found under SEM (Figure 4.4 d, e, f), and this discrepancy can be alleviated by decreasing the values of slicing and hatching.

4.3.2 Measurement and analysis of surface wettability

After TPP fabrication, we measured the contact angles for all the surfaces with different microstructures described above. Here, we used indium tin oxide (ITO)-coated glass slides as the substrates. The coated ITO allowed the TPP system to find the interface between the glass slides and dropped photosensitive materials. A bare substrate without any printed structure and a substrate with a flat square structure (length of 3 mm and thickness of 10 μm) were used as controls. As shown in Figure 4.5 a, although the array of fractal Sierpinski tetrahedron structures improved the hydrophobicity of the surfaces when the complexity increased, their

wetting performances were still not great. This was attributed to the photosensitive resist (*i.e.*, IP-S) used for TPP, as it displayed a slightly hydrophilic behavior, which has been proved using a flat structure as control. Thereby the wetting was at Wenzel State.

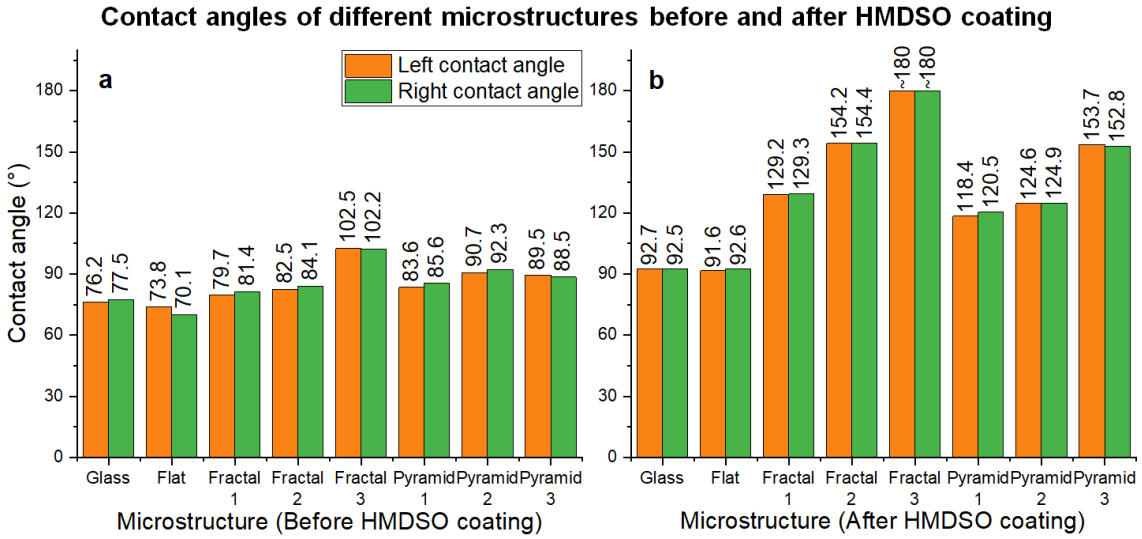

Figure 4.5 Left and right contact angles of the surfaces with different microstructures before and after HMDSO coating. a) All the contact angle measurements were conducted before HMDSO coating. b) All the contact angle measurements were conducted after HMDSO coating. The samples in both bar charts from left to right are bare ITO-coated glass, glasses with flat IP-S structure, stage-0 Sierpinski tetrahedron array, stage-1 Sierpinski tetrahedron array, stage-2 Sierpinski tetrahedron array, rectangular pyramid array, hierarchical pyramid array, and entirely hierarchical pyramid array, respectively.

Moreover, albeit the surface with array of stage-2 Sierpinski tetrahedron structures displayed a hydrophobic behavior, contact angle decreased abruptly within 1 minute, manifesting that the wetting state transferred from Cassie state to

Wenzel state. Additionally, the array of hierarchical pyramids only exhibited a slight hydrophobicity when compared to the original array of rectangular pyramids, while the entirely hierarchical pyramid structure even displayed a hydrophilic behavior.

In order to reduce the surface energy for these surfaces, a thin (C:H:Si:O) film (~ 100 nm) was deposited on all samples using HMDSO via PECVD (Cha et al. 2010). Herein, the negative impact from photoresist was alleviated as shown in Figure 4.5 b. It is worth noting that the flat surface fabricated via TPP possessed a relatively smaller contact angle compared to that of a bare ITO-coated glass slide. However, the other surfaces had exhibited a much more hydrophobic behavior. For example, surface with the array of stage-0 Sierpinski tetrahedrons exhibited a static contact angle of 129°, and surface with the array of stage-1 Sierpinski tetrahedrons displayed superhydrophobicity as its contact angle was larger than 150°. Furthermore, we failed to measure precisely the contact angle from surface of stage-2 Sierpinski tetrahedron as the water droplets merely rolled on the surface rather than forming a sessile drop. This phenomenon manifested that the surface possessed even better superhydrophobicity, indicating a contact angle close to 180°.

Additionally, it is worth noting that the sizes of the sessile water droplets for each design were different since small droplets were difficult to introduce to the surface when the hydrophobicity increased. Herein, larger droplets were adopted for more hydrophobic surfaces. Although the difference of Laplace pressure varied if the size of sessile drop changed, the results shown in Figure 4.6 were sufficient to indicate that fractal structure was more efficient than hierarchical pyramid in terms of imparting hydrophobicity to the surfaces especially when considering that the

fabrication time of fractal structures were significantly less (60%~70% reduction).

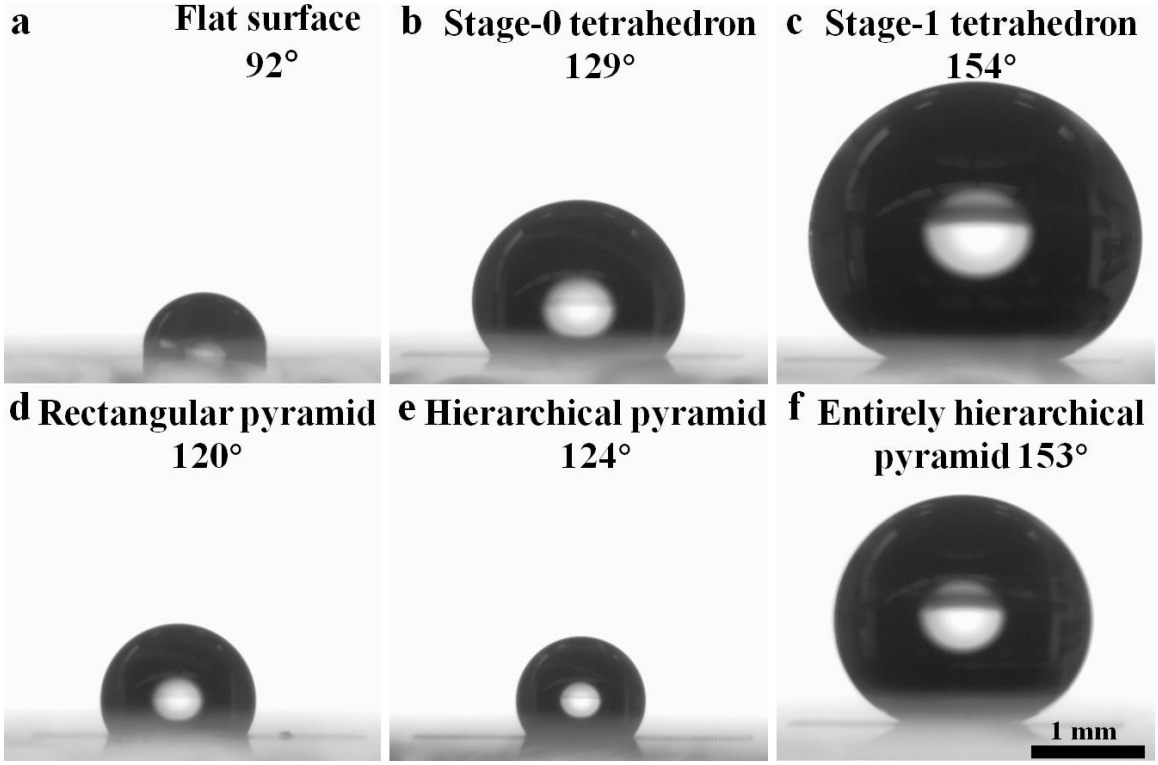

Figure 4.6 Images of the sessile drops sat on surfaces with various structures: a) Flat structure; b) Array of stage-0 Sierpinski tetrahedrons; c) Array of stage-1Sierpinski tetrahedrons; d) Array of rectangular pyramids; e) Array of hierarchical pyramids; f) Structure of entirely hierarchical pyramids.

Despite the fact that all the fractal structures had the same fractal dimension of 2, their hydrophobicity increased when the complexity increased, which was similar to the performance of untreated counterparts. This can be attributed to the fact that small openings between components from these fractal structures inhibited the penetration of the water, thus maintaining the Cassie state. Moreover, this phenomenon also implied that fractal dimension is not the only or main factor that governs the wetting performance for fractal microstructures. Besides, compared to

the untreated surfaces, the contact angle remained almost constant for more than 20 minutes. Even though continuous evaporation of water increased the Laplace pressure of the droplet (due to decreasing radius of curvature), there was no abrupt change of contact angle occurred. This indicated that the microstructures had maintained the Cassie State.

On the other hand, array of hierarchical pyramid was also proven to be efficient for obtaining superhydrophobic surfaces. However, it was worth mentioning that only the entirely hierarchical structure possessed the contact angle more than 150°, associated with a slicing angle of 2°. Herein, it was not as efficient as fractal structures for creating superhydrophobic surfaces in terms of fabrication time. Moreover, as there was no free space in the entirely hierarchical structure, this design is not favorable for bending when it comes to flexible films.

4.3.3 Flexible Hydrophobic Surfaces

As aforementioned, flexibility is ubiquitous in natural superhydrophobic creations, and it has been proven to be beneficial for the performance of surface wetting. Herein, besides creating microstructures on glass slides as described above, we have also investigated the wetting properties of 3D microstructures on a flexible substrate. PET is one of the most commonly used polyesters nowadays due to its attractive properties such as high tensile strength and transparency as well as favorable chemical, mechanical and thermal stability (Ke and Yongping 2005). Recently, PET films have aroused increasing attentions in various applications such as flexible electronics (Zardetto et al. 2011), flexible microfluidics (Yeo et al. 2016), and advanced sensors (Pang et al. 2013). Herein, ITO-coated PET film was chosen as

a demonstration for surface wetting study. During the fabrication process, a glass slide was attached to the PET film as a mechanical support to prevent film deformation.

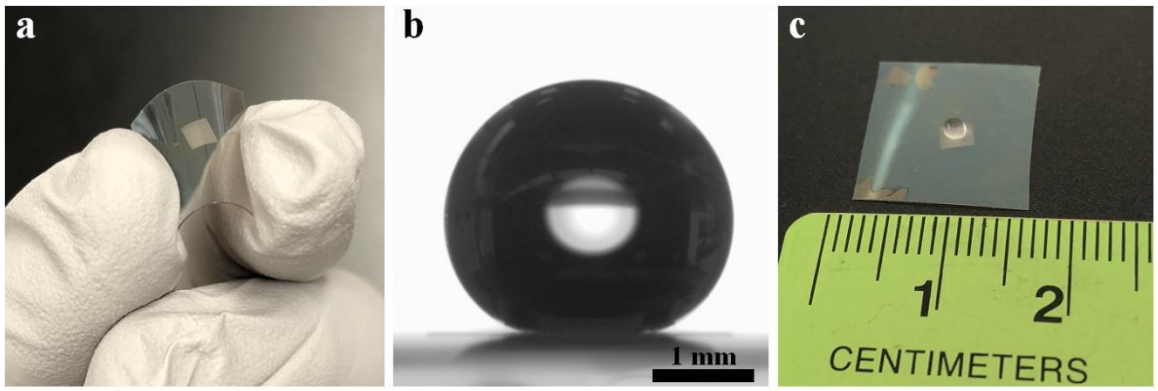

Figure 4.7 Flexible superhydrophobic film achieved by creating microstructures on a PET film using TPP technology. a) Photo of the as-prepared superhydrophobic PET film. b) Image that showed the behavior of superhydrophobicity of PET film with hierarchical microstructures. c) Photo of the sessile drop of water on a PET film. Photos were taken using an iPhone 8.

An array of hierarchical pyramids with HMDSO coating was used as a concept-proofing example (Figure 4.7 a). Since hierarchical microstructures in the array were disconnected from each other, detachment of the microstructures did not happen after 100 cycles of bending and relaxing, giving rise to a robust flexible hydrophobic film.

In addition, the fabricated surface has indicated the performance of superhydrophobicity (Table 4.1), and its left and right contact angles was measured to be 156.5° and 157.8°, respectively (Figure 4.7 b, c), which was larger than that of the same structure on glass slide.

Table 4.1 Contact angles of PET films before and after HMDSO coating

Structure	θ_{left} (before)	θ_{right} (before)	θ_{left} (after)	θ_{right} (after)
Structure-1	77.5°	76.7°	90.1°	90.1°
Structure-2	95.3°	93.2°	156.5°	157.8°

Note: Structure-1 and structure-2 are bare ITO-coated PET film and PET film with hierarchical pyramids, respectively.

4.4 Summary

Various 3D hierarchical structures have been created on glass slides and flexible PET films using TPP technique, including fractal Sierpinski tetrahedron and hierarchical pyramid microstructures. We found that untreated microstructures only slightly increased the hydrophobicity of the surfaces, and this can be attributed to the intrinsic hydrophilicity of the photoresist IP-S. Nevertheless, after depositing a thin layer of HMDSO onto the surfaces, the microstructures have proven to be useful for imparting hydrophobicity. It was worth noting that although all three stages of Sierpinski tetrahedron have the same fractal dimension of 2, better hydrophobicity was obtained when the complexity increased. Stage-1 and stage-2 Sierpinski tetrahedron have proven their ability in creating superhydrophobic surfaces. On the other hand, superhydrophobicity can also be achieved when applying hierarchical pyramids to the surfaces. However, only the microstructures that covered the printing area completely with pyramids had this ability, making the method inefficient when compared to fractal structures as more fabrication time was required.

Moreover, a PET film was also adopted as a demonstration for printing microstructures on flexible substrates using TPP technique. The PET film with

microstructures remained good hydrophobicity after bending and relaxing for more than 100 times. Herein, this method is simple and offers several advantages compared to existing methods. To name a few, it does not require complex operations such as wet etching to obtain 3D structures. Digital files used in TPP are easier to change than other fabrication protocols, hereby promoting prototyping developments. Besides, TPP technique allows the creation of different microstructures at different regions on a surface, making the surface wetting controllable. Lastly, this approach can also be applied in flexible materials that are cheaper, robust and provide a better similarity to natural creations, by which studies on surface wetting and other phenomena in nature can be further investigated.

Nevertheless, there is one downside of using TPP technique, namely, the fabrication speed. Owing to its intrinsic voxel-by-voxel fabrication mechanism, the process of TPP nowadays is still not fast enough to achieve mass production. However, various approaches have been proposed to make TPP process faster. To name a few, novel photoinitiators that possess wide dynamic range have been proven to enable a faster TPP process (Li et al. 2013). Moreover, when considering the fabrication of a pattern using TPP, multiple static or dynamic beams are also good choices (Baldacchini 2015; Xu et al. 2016). For example, multiple focal points (up to hundreds) can be obtained using a microlens array, giving rise to simultaneous polymerization in different areas (Formanek et al. 2006). Thereby, the fabrication time for creating superhydrophobic surfaces using microstructure patterns can be reduced drastically, and large surfaces can also be realized. In addition, an optimal balance of laser intensities, chemical reaction rates as well as

the movements of galvo mirrors and stages also lead to a much faster fabrication speed.

To conclude, we believe the proposed method has opened a new door for further study of surface wetting with respect to the performance of real 3D microstructures on flexible substrates, and it can also be a useful tool for the development of surface engineering and other important fields such as biology, chemistry, flexible electronics and microfluidics.

Chapter 5

Acoustofluidic micromixer on foil

This chapter has been reprinted with permission from Lin, Y., Gao, C., Gao, Y., Wu, M., Yazdi, A. A., & Xu, J. (2019). *Acoustofluidic micromixer on lab-on-a-foil devices*. **Sensors and Actuators B: Chemical**, 287, 312-319. Copyright (2019) by Elsevier. DOI: https://doi.org/10.1016/j.snb.2019.02.050.

5.1 Introduction

Recently, lab-on-a-foil has emerged as a promising research concept with applications in nucleic acid analysis (Lin et al. 2011; Shen et al. 2005), biosensors (Chou et al. 2013), robotics (Wong et al. 2012), electrochemistry (Chen et al. 2015b), and so forth (Focke et al. 2010). In contract to glass and silicon counterparts, lab-on-a-foil devices use thin and flexible films as substrates. These devices often show great cost effectiveness, ease of fabrication, and simplicity of use (Wang et al. 2016b). As lab-on-a-foil devices often consume little materials, they are also considered as environmentally friendly and disposable (Fiorini and Chiu 2005). Moreover, these devices were expected to find huge potential in wearable devices (Liu et al. 2017), thus contributing to future development of Internet of Things and healthcare services.

At present, various fabrication methods have been proposed to create lab-

on-a-foil devices, including micro-thermoforming (Truckenmüller et al. 2008), hot embossing (Li et al. 2007), laser micromachining (Malek et al. 2009), dry resist fabrication (Focke et al. 2010), and xurography (Bartholomeusz et al. 2005). Among them, xurography is often considered as the simplest and cheapest. It relies on a knife plotter to cut thin films, in which microchannels are created. The cut films are then covered with bottom and top layers for enclosed flow paths, and reliable bonding between layers can be achieved using off-the-shelf materials such as adhesive tapes (Yuen and Goral 2010).

Nonetheless, due to size limitation of the knives, the resolution of xurography is relatively low compared to that of soft lithography (Yuen and Goral 2010). Additionally, it is not easy to integrate more functions on these devices other than fluid transportation inside the microchannels created. Therefore, further adoption of the xurography technology for microfluidics is compromised. Here, we propose a novel method to overcome this downside by imparting high-resolution 3D microstructures into xurography-made devices using TPP technology. This fabrication technique is one of the additive manufacturing technologies working at microscale (Kim et al. 2013; Xia et al. 2010), and possessing extremely high resolution (~ 100 nm) (Lin and Xu 2018).

Owing to non-invasive manner and the capabilities in manipulating fluids and particles (Ahmed et al. 2009; Gritsenko et al. 2018), acoustofluidics has become an important branch in microfluidics. For instance, as the flow of fluids in microchannels is usually laminar (Hashmi and Xu 2014), it is challenging to achieve homogenous mixing naturally due to dominance of viscous forces. To address this

problem, acoustofluidics was applied to create efficient micromixers. Generally speaking, acoustic energy induces the pressure fluctuations inside microchannels, giving rise to disturbances for the laminar flows. In addition, bubbles, sharp edges, and solid membranes have also been coupled with acoustic fields to improve the performance (De Vellis et al. 2017; Huang et al. 2013; Liu et al. 2002; Tovar and Lee 2009; Van Phan et al. 2015). As an example, lateral cavity acoustic transducers (LCATs) based on acoustic bubbles were employed in multiple applications, including micropumps (Tovar et al. 2011), particle sorting (Patel et al. 2009), and microfluidic switches (Patel et al. 2012). Similarly, sharp edges were also applied for the developments of micromixers (Huang et al. 2013), chemical signal generators (Huang et al. 2018), and micropumps (Huang et al. 2014).

However, it is difficult to integrate these components in xurography-based microfluidic devices. A serpentine cut in the films for sidewall cavities or sharp edges usually results in ragged edges and undesired debris. On the other hand, TPP is amenable to create high-resolution components, yet direct construction of the entire device would be impractical due to its low fabrication speed (Lin et al. 2018). Given the fact that TPP fabrication time is positively proportional to the volume of printed structures, it is possible to print only the key components in a device. Here, we propose using TPP to fabricate structure inside xurography-made device making it an acoustofluidic lab-on-a-foil device.

In conventional acoustofluidic applications, acoustic bubbles often suffer from instability and dissolution (Bertin et al. 2015; Huang et al. 2012). For instance, the trapped bubbles tend to expand into microchannels at high flow rates (Huang et

al. 2012), and grow or shrink upon the diffusion based on saturation status of the fluids (Epstein and Plesset 1950). To solve this problem, Bertin and coworkers proposed a new type of microbubbles (*i.e.*, armored microbubble) (Bertin et al. 2015). Specifically, hollow-capsule-shaped microstructure was created to trap bubbles and prevent the dissolution. Longer lifetime of bubbles was achieved compared to those unprotected ones. However, because these microbubbles were still standalone, their lifetime remained short (1 minute) when exposed to acoustic actuation.

To prolong the lifetime of acoustic bubbles, or air-liquid interfaces (membranes) *per se*, we propose to connect the oscillating membranes with ambient air instead of bubbles with finite volumes. Specifically, thin shell microstructures with multiple circular pores for trapping membranes are fabricated via TPP and then integrated into devices prepared by xurography. We term these microstructures as defended oscillating membrane equipped structures (DOMES).

As they are created above through holes in the films, the bottom side of membranes is always facing ambient air, and gas diffusion into the liquid is compensated by the atmosphere. Hence, the membrane instability is expected to be alleviated or avoided. Moreover, since the pores on DOMES are generally small, watertight condition for the fluids in the microchannels is achievable if the pressure difference between two sides remains small. We will first investigate the performance of DOMES, and further create a micromixer on the foil. To the best of our knowledge, it is the first time such an active micromixer is created in the lab-on-a-foil devices.

5.2 Material and methods

5.2.1 Overall fabrication process

We used ITO-coated PET films (127 μm in thickness, Sigma-Aldrich, St. Louis) as the substrates to create lab-on-a-foil devices. As introduced in Chapter 4, PET is a common thermoplastic polymer. It possesses several advantages (Hu and Chen 2018; Li et al. 2007; Wang et al. 2016b), including optical transparency, physical, chemical and mechanical stability, as well as good flexibility. ARcare® 90445 double-sided adhesive tape (kindly provided by Adhesives Research, Glen Rock, PA) was used for bonding different layers. It is a transparent medical grade tape with good biocompatibility and aqueous insolubility (Eletxigerra et al. 2015; Patko et al. 2014; Santiago-Felipe et al. 2016). Desktop cutting plotter (QuicKutz Silhouette SD, QuicKutz, Inc., Lindon, UT) was applied for xurography. General fabrication process of a lab-on-a-foil device integrated with DOMES is divided into the following steps:

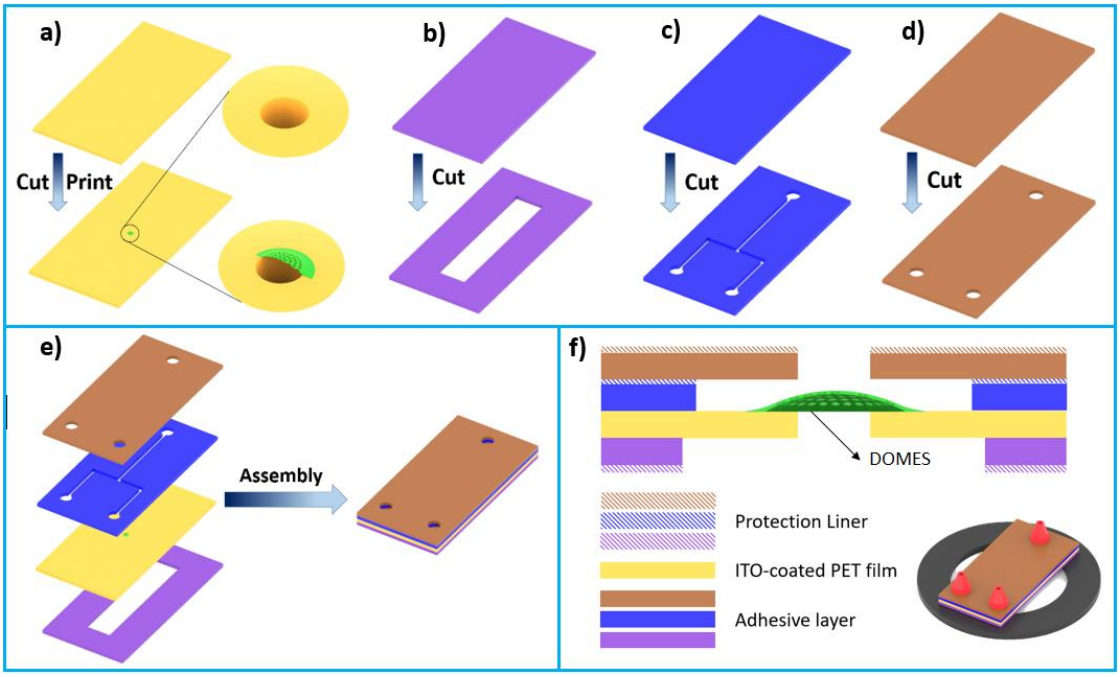

Figure 5.1 Schematic illustration of the fabrication process for a lab-on-a-foil device integrated with DOMES. a) A circular through hole was first cut in PET film, and then DOMES was printed above the hole using TPP; b) Double sided tape with a large rectangular hole in the center was prepared using xurography; c) Microchannels were also cut in the tape using xurography; d) Similarly, inlets and outlets were prepared for the top layer; e) Afterwards, all the layers were aligned and bonded with a homemade tool; f) The as-prepared Lab-on-a-Foil device can be attached to other objects such as piezoelectric instrument and external tubings after revealing the adhesive layers on both sides.

A 200 μm diameter through hole was first cut in the film using a milling machine (CNC Mini-Mill/3, Minitech Machinery Corp., Atlanta, GA). TPP system (Nanoscribe Photonic Professional GT, Nanoscribe GmbH, Germany) was then used to fabricate DOMES above the hole (Figure 5.1 a). Since we will attach the final device to a piezoelectric actuator, a layer of double-sided tape was added to the bottom of the device. A big rectangular opening was cut in the center to maintain DOMES connecting to ambient air (Figure 5.1 b). Microfluidic channels with 600 μm width were similarly created in the tape layer above the film as shown in Figure 5.1 c and Figure B.1 in Appendix B. Inlets and outlets were cut for the top layer (Figure 5.1 d).

Afterwards, all the layers were carefully aligned and pushed together (Figure 5.1 e) with the help of a homemade alignment tool composed of a three-axis linear stage and a USB digital microscope. Finally, the as-prepared device was clamped between two pieces of glass slide and baked overnight to remove the bubbles

trapped during assembly (Figure B.2 in Appendix B). To connect the device to external components, adhesive layers can be revealed after peeling off the protection liners on both sides (Figure 5.1 f). In our cases, the device was bonded to a ring-shaped piezo (APC International, Mackeyville, PA), and tubings were attached through flangeless ferrules (P-200NX, Upchurch Scientific, Oak Harbor, WA) (Figure B.3 in Appendix B).

5.2.2 DOMES fabrication

As aforementioned, DOMES is fabricated above a through hole, and its bottom side is facing ambient air. Therefore, the instability of multiple air-liquid interfaces trapped by the pores on DOMES is expected to be alleviated or avoided. In this study, three types of DOMES are constructed, and all of them have the same contour except for the size and quantity of the pores. As shown in Figure 5.2 a, DOMES is a dome-shaped porous shell with an external diameter of 310 μm, an internal diameter of 230 μm, a curvature radius of 250 μm, and a thickness of 5 μm.

To further study the acoustically induced flow (*i.e.*, microstreaming) with respect to the pore size, the total area of pores for all three types is kept identical. Specifically, the first type of DOMES has 136 pores with diameter of 10.5 μm (Figure 5.2 b). The second type has 71 pores with diameter of 14.55 μm (Figure 5.2 c), and the third one has 25 pores with diameter of 25 μm (Figure 5.2 d). Additionally, a half DOMES is also constructed (Figure 5.2 e), illustrating how the DOMES is created above the hole with bottom side facing ambient air.

For printing microstructures on PET films, we used the same method applied in our previous article (Lin et al. 2018b). Basically, the PET film was thoroughly

cleaned using acetone, IPA, and then blow-dried with nitrogen. Afterwards, the PET film was mounted on a TPP holder with tape. To avoid the bending of films during fabrication, a glass slide (length of 25 mm and thickness of 0.7 mm, Nanoscribe GmbH, Germany) was placed beneath as a support.

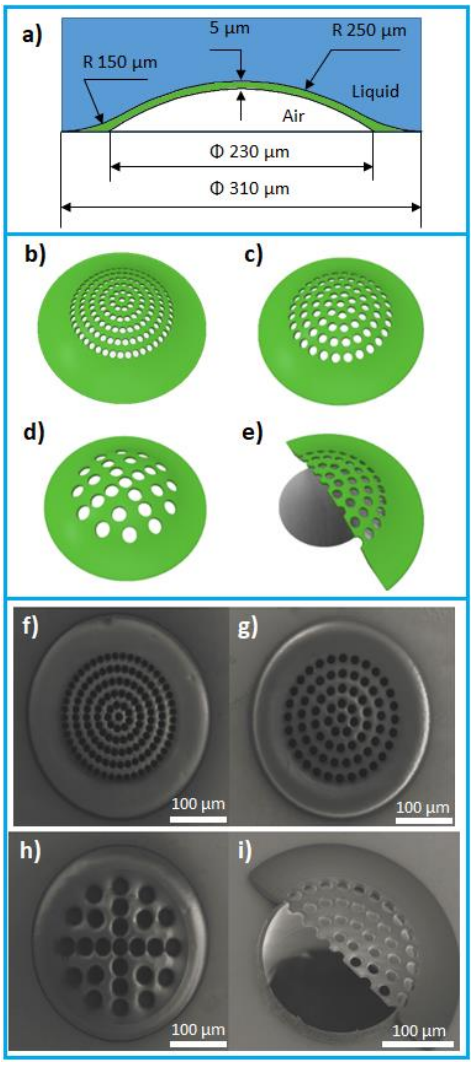

Figure 5.2 Schemes for different types of DOMES and their corresponding SEM images. a) Side view for general DOMES and its dimensions; b-d) Schemes for DOMES with 10.5, 14.55, and 25 µm diameter pores, respectively; e) Scheme for a half DOMES created above a through hole; f-h) Corresponding SEM images for the

DOMES with 10.5, 14.55, and 25 μm diameter pores, respectively. i) SEM image for the half DOMES. The tilt angle used is 30-degree.

A small drop of photoresist (IP-S, Nanoscribe GmbH, Germany) was then dropped onto the top of the through hole at ITO-coated side. The ITO (around 130 nm) coating enabled a quick searching for the interface between PET film and IP-S during printing, due to their difference in refractive indices. After applying adaptive slicing of 1 μm with a minimal distance of 0.2 μm, and a hatching of 0.3 μm, the total fabrication time was found to be 3 minutes.

Additionally, we adjusted the coordinates of the TPP system to match that of the DOMES designs using NanoWrite software (Nanoscribe GmbH, Germany) (Lin et al. 2018). After printing, excessive photoresist was developed using propylene glycol monomethyl ether acetate (MicroChem, Newton, MA), and the device was dried in the air. The SEM images of all three designs were shown in Figure 5.2 f, g, h, respectively. Despite the fact that the gap between each pore in DOMES was only 2 μm, the hatching and slicing distances applied did not lead to any deformation or undesired discrepancies. Additionally, the SEM image of the half DOMES further indicated a good alignment between the printed microstructure and the through hole (Figure 5.2 i).

5.2.3 Driving frequency determination

To determine the driving frequency at which DOMES exert the strongest acoustic microstreaming effect, a free surface PET device without further assembly was attached to a ring-shaped piezo using double-sided tape, and the DOMES on film had 14.55 μm diameter pores. One drop (around 10 μL) of deionized (DI) water

with green aqueous fluorescent particles (2.0 μm Fluoro-Max dyed polystyrene microspheres, Thermo Fisher Scientific, Waltham, MA) was then added to the film. Then, a waveform generator (DG1022U; Rigol Technologies Inc., Beijing, China) was used to generate square wave, followed by the amplification via a voltage amplifier (Tegam 2350, Tegam Inc., Madison, OH).

The driving frequency was swept from 100 Hz to 100 kHz at 5 Vpp, and the performance of acoustic microstreaming was determined based on average velocity of the particles. The particles were excited using a fluorescence illuminator (X-cite 120, Lumen Dynamics, Ontario, Canada), and their trajectories were tracked using a high speed camera (Phantom Miro M310, Vision Research Inc., USA) associated with an inverted microscope system (Nikon Eclipse Ti–S, Nikon Instruments Inc.). Phantom Camera Control software (Vision Research, Wayne, NJ) was applied to analyse the results. At frequency of 32.60 kHz, the DOMES was found to exert strongest microstreaming, thus it was used as the driving frequency for the rest of this study.

5.3 Results and discussion

5.3.1 Theoretical background

In our previous study (Gritsenko et al. 2018), we derived an explicit expression for the displacement of a thin clamped circular membrane,

$$W(r,\theta,t) = w_D(r,\theta)e^{i\omega t} \tag{5.1}$$

where $w_D(r,\theta)$ is the solution of:

$$\nabla^4 w_D(r,\theta) - {\kappa_w}^4 w_D(r,\theta) = 0 \tag{5.2}$$

with the boundary conditions:

$$w_D(a,\theta) = 0,\ \frac{\partial w_D}{\partial r}(a,\theta) = 0 \tag{5.3}$$

That is, the oscillation amplitude of the membrane reads:

$$w_D(r,\theta) = \left(J_n(\kappa_w r) - \frac{J_n(\kappa_w a)}{I_n(\kappa_w a)} I_n(\kappa_w r)\right)(A_1\, cos(n\theta) + B_1\, sin(n\theta)) \tag{5.4}$$

Here W is the time-dependent membrane displacement, and w_D is the classical solution for the displacement equation of a thin clamped circular membrane (Equation 5.2); a, κ_w, r, θ stand for the radius of the membrane, wave number, radial distance, and azimuthal angle, respectively; J_n, I_n stand for the type one and modified Bessel functions, respectively; A_1, B_1 are the arbitrary constants. As the pore size in DOMES increases, the membrane displacement increases, and we expect the microstreaming effect to become stronger with more energy dissipated.

Watertightness is another key factor subjected to the pore size, and the maximum size can be ideally determined using Equation 5.5,

$$d = \frac{4\times\sigma\times cos\varphi}{\Delta p} \tag{5.5}$$

where d is the maximum pore size that is free from liquid leakage; σ, φ denote the surface tension, and the contact angle of the liquid, respectively; Δp is the pressure difference between two sides of the pore. Although this formula does not take into account the interaction between the oscillating membranes with liquid, it provides a straightforward reference when designing the DOMES. For instance, water is one of the most commonly used liquids in microfluidic applications, its surface tension

at 298 K is 0.072 kg/s^2, and the contact angle between water and the material of DOMES (*i.e.*, IP-S) is 73.8° (Lin and Xu 2018). As a result, the pressure barriers (maximum pressure at which the pore still maintains watertightness) for the pores with diameter of 10.5, 14.55, and 25 μm are 3840, 2772, and 1613 Pa, respectively.

To verify these results, DOMES with different pore sizes were integrated in straight microchannels, in which only inlet was left for water injection while outlet was sealed. Hence, the pores on DOMES became the only possible exits for liquids. The pressure difference exerted was varied upon changing the gravitational potential of the water reservoir (Figure B.4 in Appendix B). We found that the actual pressure barriers were 3530, 2620, and 1530 Pa for DOMES with 10.5, 14.55, and 25 μm diameter pores, respectively. The results indicated a good agreement with the theoretical prediction.

5.3.2 Impact of the through hole and pore size

In order to understand the role of through holes in compensating the vulnerability of conventional bubbles due to gas dissolution and acoustic pressure fluctuations, a series of free surface devices with or without through holes was actuated at 5 Vpp.

The results in Figure 5.3 indicated that standalone bubbles trapped in the DOMES built on films without holes were more vulnerable compared to those with holes. The bubble trapped in DOMES with 25 μm pores gradually disappeared as time passed (Figure 5.3 a). This can be attributed to its small pressure barrier. Specifically, after water penetrated the pores, the bubble was first compressed, and then dissolved until completely gone. As a result, corresponding microstreaming

gradually turned weaker and finally disappeared. On the other hand, the membranes in DOMES on through hole were almost identical after the piezoelectric transducer was turned on (Figure 5.3 b), and the microstreaming remained the same for more than 30 minutes. This illustrated that the dissolution of gas was alleviated from ambient air.

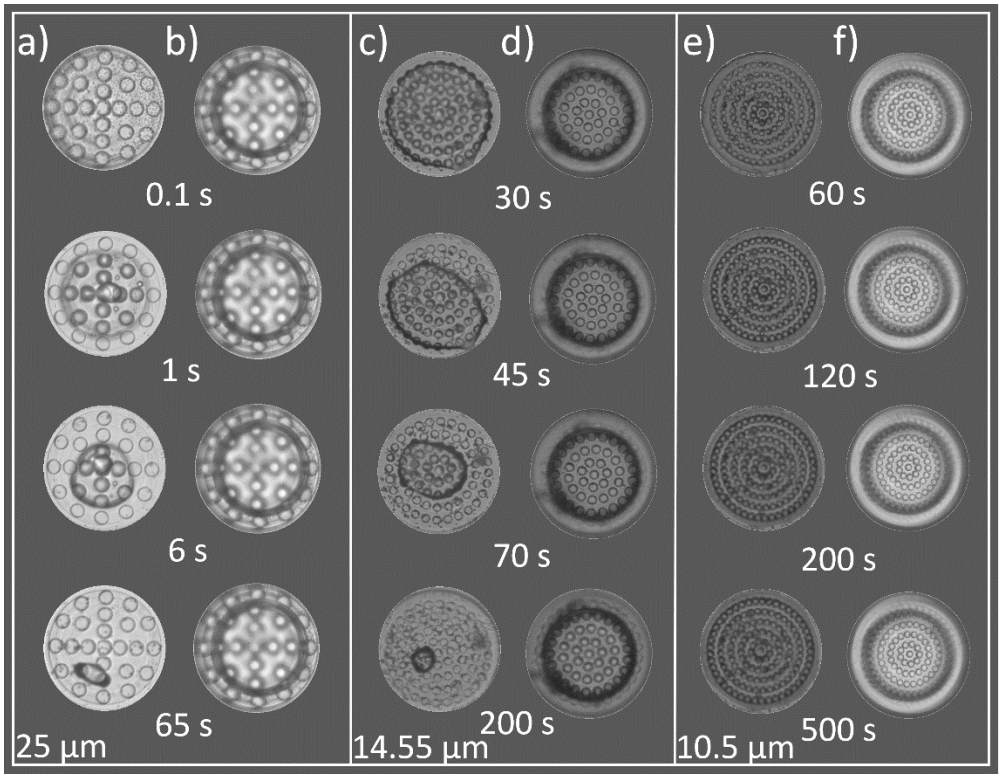

Figure 5.3 Stability study of the standalone bubbles and membranes on DOMES without or with through holes upon the actuation of acoustic microstreaming. a-b) DOMES with 25 µm pores created without or with through holes, respectively. c-d) DOMES with 14.55 µm pores created without or with through holes, respectively. e-f) DOMES with 10.5 µm pores created without or with through holes, respectively.

As the pore size decreases, the pressure barrier and flow resistance increase, making water penetration more difficult, giving rise to a slower shrinkage of the

bubbles. For instance, the bubble trapped in DOMES with 14.55 μm pores became negligible after 200 seconds with acoustic energy being turned on (Figure 5.3 c), while it took only 65 seconds for 25 μm pores. Note that, the standalone bubble in the DOMES with 10.5 μm pores remained almost the same after 500 seconds, indicating a stronger bubble stability due to large pressure barrier (Figure 5.3 e). Similarly, the membranes on DOMES above the through hole almost underwent no change (Figure 5.3 d, f).

We further studied the acoustic performance with respect to the pore size. The first device was created using an intact film, while the second to fourth devices were created using films with through holes. To obtain a straightforward and clear comparison, 24 frames that formed a complete 1-second video clip were superimposed (Figure 5.4).

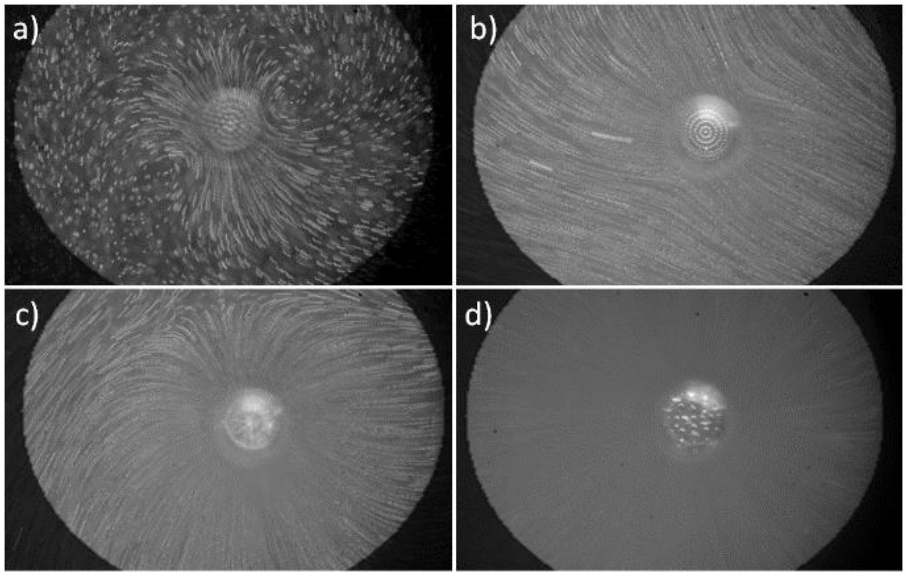

Figure 5.4 Acoustic microstreaming induced by different DOMES: a) DOMES fabricated on an intact film. b-d) DOMES fabricated above through holes with different pore sizes (10.5, 14.55, and 25 μm, respectively).

As described above, standalone bubbles were vulnerable upon acoustic actuation, giving rise to weaker microstreaming as time went by. Hence, the trajectories of particles can be clearly tracked (Figure 5.4 a). However, only blurry trajectories were observable for microstreaming above through holes. Additionally, DOMES with larger pore size exhibited stronger performance. For instance, trajectories were observable in the microstreaming induced by small pores (Figure 5.4 b, c), yet it can barely be noticed for large pores (Figure 5.4 d). This phenomenon indicated a good predication for the theory that larger pores give rise to stronger microstreaming.

Nonetheless, liquid leakage can be a big issue for large pores. After turning the free surface devices into enclosed ones, DOMES with 25 μm diameter pores were no longer able to maintain watertightness, further giving rise to weaker microstreaming. This can be attributed to the pressure drop inside microchannels and the acoustic pressure (around 1100 Pa, measured with a H2a-XLR hydrophone, Aquarian Audio). Moreover, returning flows at the edges may also pose additional hydrodynamic pressure (Hussein et al. 1994).

5.3.3 Lab-on-a-foil acoustofluidic application

To further prove the feasibility of using DOMES for lab-on-a-foil applications, an acoustofluidic micromixer was built and tested as a demonstration. Given that 25 μm pores could not hold membranes well, 14.55 μm pores was adopted. The device included a T-shaped microchannel, two inlets and one outlet (Figure 5.5). The length and the width of the microchannels were 6 mm and 600 μm, respectively. DOMES (green spot in Figure 5.5) was carefully aligned in the center of the main

channel. After assembly, the device was bonded onto a piezo, and connected with tubings (Figure B.3 c in Appendix B). Additionally, DI water and DI water with fluorescent dye (Fluorescein sodium salt, Sigma-Aldrich, St. Louis) were used as two mixing fluids. To quantitatively characterize the performance of mixing, relative mixing index (RMI) was calculated at a measuring line 600 μm away from the center of DOMES after mixing (see the dashed line in Figure 5.5).

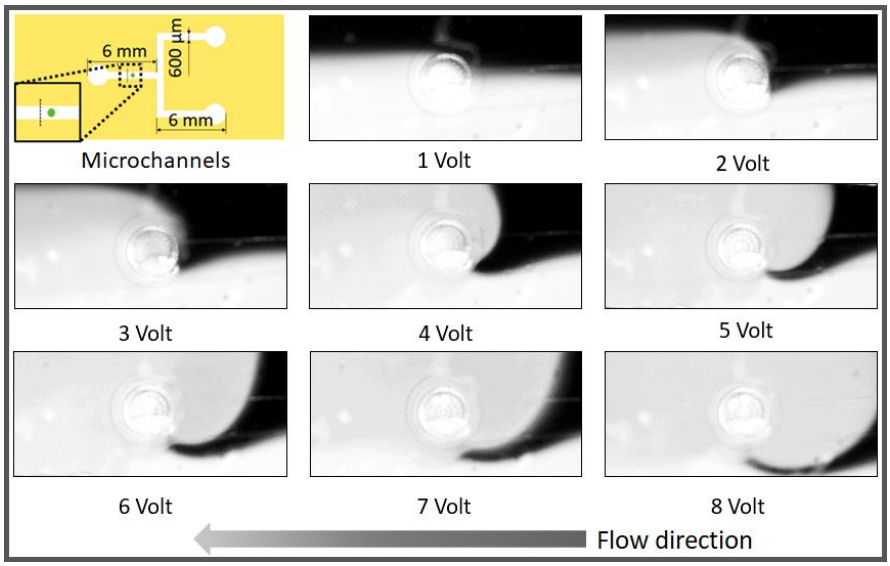

Figure 5.5 Scheme of the microchannels with dimensions, as well as images showing the mixing performance at different driving voltages ranging from 1 to 8 Volt.

In contrast to conventional mixing indices involving rescaling and stretching of grayscale intensities, RMI was used here to preclude the influence of lighting conditions (Hashmi and Xu 2014). It is calculated as follows:

$$RMI = 1 - \frac{\sqrt{\frac{1}{N}\sum_{i=1}^{N}(I_i - \langle I \rangle)^2}}{\sqrt{\frac{1}{N}\sum_{i=1}^{N}(I_{oi} - \langle I \rangle)^2}}, \tag{5.6}$$

where N denotes the number of pixels in the measuring region; I_i and I_{oi} denote the local intensity of the i-th pixel after and before mixing, respectively; $\langle I \rangle$ indicates the average of pixel intensities in the region. Here, a RMI of 0 denotes an unmixed status, while 1 indicates thoroughly mixing. In addition, a threshold of 0.75 was selected as the criteria to determine acceptable mixing performance.

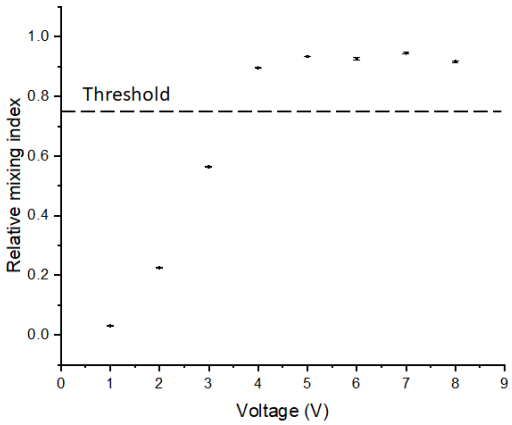

Figure 5.6 Plot of the mixing index versus driving voltage.

Mixing performance was first investigated by applying a series of voltages ranging from 1 to 8 Volt at flow rate of 4 µl/min for each fluid. As illustrated in Figure 5.5 and Figure 5.6, the mixing performance was improved and plateaued with increasing driving voltage. Since the intensity of microstreaming grows quadratically with driving voltage (Xu and Attinger 2007), the mixing index increased rapidly from 1 to 4 Volt, and acceptable mixing was achieved after 4 Volt. Another way of quantifying mixing performance is to look at mixing time τ:

$$\tau = \frac{L_m}{v_f}, \tag{5.7}$$

where L_m is the mixing length, and v_f is the average fluid velocity. Mixing length is usually defined as the distance between the mixer and the downstream location

where complete mixing is achieved. In our experiments, we noticed that as the driving voltage became larger, the microstreaming pattern also became larger and extended into upstream areas. This phenomenon made mixing completed even before fluid reached the location of DOMES at voltages greater than 4 Volt. Therefore, we can consider the mixing length L_m to be 0, proving the potential of DOMES for immediate mixing.

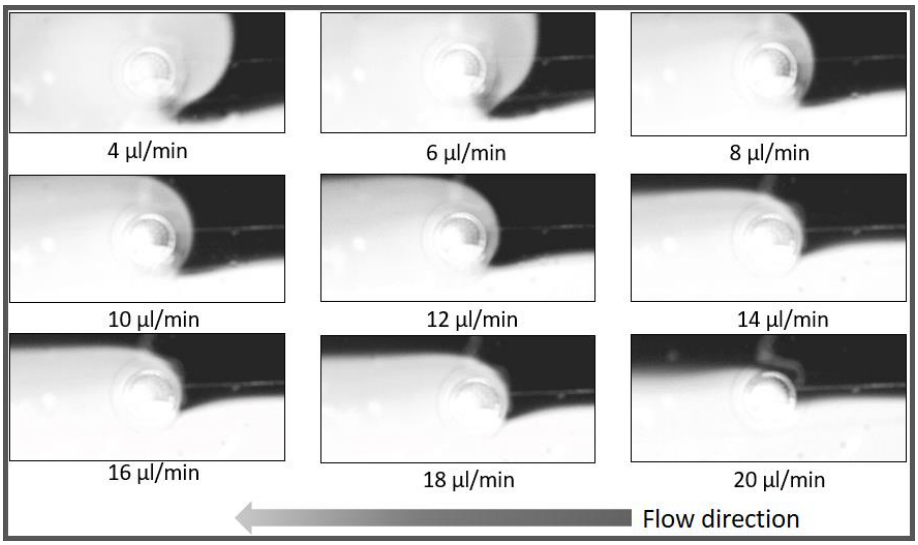

Figure 5.7 Images indicating the mixing performance at different flow rates ranging from 4 to 20 µl/min.

In addition, we investigated the impact of flow rate on mixing performance at 5 Volt. Flow rate ranging from 4 to 20 µl/min were applied to each fluid, and acceptable mixing was obtained when the flow rate was equivalent or smaller than 8 µl/min (Figure 5.7 and Figure 5.8). When the flow rate increased to 8 µl/min, the mixing index reached the threshold value set previously (0.75). In this case, the mixing length can be considered as the distance from measuring line to the centre of DOMES (i.e., 600 µm), from which a mixing time was calculated to be 87.8 ms. As

aforementioned, it was the first time such an active micromixer was achieved in lab-on-a-foil devices, and the mixing time was competitive even compared to most PDMS microfluidic mixers.

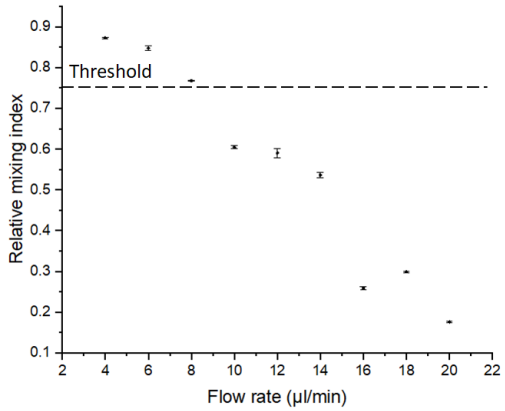

Figure 5.8 Plot of the mixing index versus flow rate.

5.4 Summary

In summary, a novel microstructure termed DOMES was proposed for lab-on-a-foil acoustofluidic applications. The devices were created using off-the-shelf PET films and double-sided tapes via xurography. DOMES was fabricated by two-photon polymerization and integrated in the microchannels. Compared with regular standalone acoustic bubbles, the bottom side of air-liquid interfaces on DOMES was always facing ambient air thanks to the through hole underneath the DOMES. Moreover, common dissolution and compression problems of acoustic bubbles were alleviated, giving rise to a more stable performance. We also investigated the role of pores on DOMES. It is observed that as the pore size increased, the microstreaming induced by DOMES became stronger. However, the pressure tolerance decreased in the meanwhile, which may lead to liquid leakage rather than

maintaining watertightness.

To further prove the capabilities of DOMES in acoustofluidic applications, a micromixer was demonstrated. We found that the mixing efficiency was improved upon the increase of driving voltage, and acceptable mixing can be obtained when the voltage was equivalent or greater than 4 Volt at 4 μl/min (each fluid). Additionally, acceptable mixing can be realized when the flow rate was equivalent or smaller than 8 μl/min at 5 Volt, and the mixing time was 87.8 ms at 8 μl/min. The results suggested that the first acoustofluidic micromixer on the foil possessed a comparable performance compared to those devices fabricated using PDMS.

Admittedly, although xurography itself is cheap and simple, the acoustofluidic performance mainly came from DOMES, which was fabricated using TPP, a technology nowadays is still expensive and not widespread. Nonetheless, methods such as molding or low-cost microscale 3D fabrication techniques may be applied to address this downside in the future. For instance, 3D microfabrication was achieved using a thin multimode optical fiber recently (Delrot et al. 2018), and it did not require bulky and expensive femtosecond laser while maintaining excellent resolution. Alignment and bubble removal process also bring the inconvenience to the fabrication process, yet these problems can be addressed using automation machines when it comes to mass production. Despite the aforementioned limitations, we believe that the proposed lab-on-a-foil devices open a door for a variety of potential microfluidic applications in the future.

Chapter 6

Acoustofluidic micropump on foil for single-cell trapping

This chapter has been reprinted with permission from Lin, Y., Gao, Y., Wu, M., Zhou, R., Chung, D., Caraveo, G., & Xu, J. (2019). *Acoustofluidic stick-and-play micropump built on foil for single-cell trapping*. **Lab on a Chip**. Copyright (2019) by Royal Society of Chemistry. DOI: https://doi.org/10.1039/c9lc00484j.

6.1 Introduction

As discussed in the previous chapters, microfluidics or the so-called lab-on-a-chip has undergone rapid growth and spawned a plethora of applications in different fields such as biology (Wu et al. 2018), chemistry (Weibel and Whitesides 2006), pharmacology (Ainla et al. 2010), environmental monitoring (Lin et al. 2016a), and others (De Vellis et al. 2017; Zhao et al. 2019). Unfortunately, the majority of these applications heavily rely on off-chip equipment (*e.g.*, syringe pumps) to maintain required conditions (*e.g.*, constant flow rates) (Tovar and Lee 2009). Therefore, in most cases, microfluidics nowadays remains an exclusive platform in research laboratories, and the dependence of external devices has become a roadblock for commercialization.

Nevertheless, on-chip functions such as pumping (Huang et al. 2014), mixing (Lin et al. 2018), filtering (Dong et al. 2016), and analysis (Jang et al. 2016), have been

widely explored, towards fully automated microfluidic systems over the past years. Among them, pumping is a fundamental function that bridges the micro and macro environments, and enables precise manipulation of fluids through systems for different purposes, including drug delivery (Patra et al. 2013), cell separation (Patel et al. 2014), biomedical analysis (Amirouche et al. 2009), and so forth (Ma et al. 2019; Patel et al. 2012; Wang et al. 2009; Wang and Fu 2018).

Based on different driving mechanisms, micropumps in microfluidic systems can be primarily categorized into two classes: mechanical and non-mechanical (Wang and Fu 2018). The former one displaces fluids via moving mechanical parts (*e.g.*, pumping diaphragms or check valves) (Chen et al. 2015a; Fong et al. 2015; Wang et al. 2014). Although these micropumps possess attractive pumping performances, sophisticated designs and complex fabrication processes are usually required (Wang and Fu 2018). On the contrary, the alternative type transforms non-mechanical energy into kinetic momentum of fluids by means of magnetohydrodynamics (Lemoff and Lee 2000), electrohydrodynamics (Russel et al. 2016), electroosmosis (Lin et al. 2013), and other effects (Fang and Lee 2015; Oskooei and Günther 2015).

Unsurprisingly, acoustic energy has also been explored for creating micropumps (Ozcelik et al. 2018). For instance, micropumps based on surface acoustic wave (SAW) have been exploited and used for various applications over the past years (Girardo et al. 2008; Schmid et al. 2012). That said, most of these devices were built on rigid piezoelectric substrates (*e.g.*, LiNbO3) and usually required sophisticated vapor deposition for the fabrication of interdigital transducer

(IDT) (Rambach et al. 2017). Therefore, bendable SAW devices built on thin and cheap substrates have become an alternative platform and pioneered several applications (Chen et al. 2014; Jin et al. 2013).

On the other hand, acoustic micropumps based on bulk acoustic waves (usually coupled with acoustic bubbles or sharp edges) have also emerged as promising tools owing to the ease of operation and programmable flow rates (Fang and Lee 2015; Huang et al. 2014; Tovar and Lee 2009; Tovar et al. 2011). Tovar and Lee have developed a micropump termed lateral cavity acoustic transducer (LCAT) (Tovar and Lee 2009), which drives fluids using 20 pairs of air-bubbles trapped in angled lateral cavities. However, similar to free acoustic bubbles, these LCATs suffered from bubble instability and gas dissolution. For example, trapped bubbles can expand into the main microchannels or disappear due to diffusion or dissolution. As a result, pumping performance is challenging to be maintained for a long time.

Apart from acoustic bubbles, solid sharp edges have also been investigated for creating micropumps by Huang and co-workers (Huang et al. 2014). They found the proposed micropumps were capable of tuning the flow rates across a wide range (nL/min to μL/min). Nonetheless, one limitation lay in this device was that the pumping performance was sensitive and subject to undesired bubble-trapping, which may occur at the corners between tilted cantilevers and side walls.

In addition, most of the acoustofluidic devices developed hitherto were placed on glass substrates, and in turn they were inflexible, brittle, and unsuitable for applications involving non-planar and/or flexible surfaces. Moreover, despite

possessing irreversible bonding with high strengths obtained from plasma treatments, such bonding between PDMS and glass substrates in these devices made themselves impossible to be cleaned and reused in a simple way. Therefore, reversible bonding that allows stick-and-play has become an alternative for building microfluidic systems especially when it comes to applications where low bonding strength is sufficient (Nakashoji et al. 2017; Wasay and Sameoto 2015).

In this chapter, we report a robust stick-and-play micropump-on-the-foil with tunable flow rates at a resolution of nanoliter per minute. The device is based on the pore-containing microstructures (*i.e.*, DOMES) introduced in Chapter 5 and a previous article (Lin et al. 2019a). Unlike the previous DOMES, in this chapter, we explore a new type of DOMES with asymmetrical structures and report its ability to produce net flow for pumping biological samples in a lab-on-a-foil device.

In addition, we also applied the micropump-integrated lab-on-a-foil to perform single-cell trapping, which is an important first step that enables downstream single cell analysis. It is well accepted that bulk experiments that account for collecting statistical data from a large number of cells are often not adequate for interpreting the individual differences between cells (Di Carlo et al. 2006; Kuang et al. 2004; Skylaki et al. 2016), and single-cell analysis overcomes this shortcoming and offers invaluable insights at single-cell level (*e.g.*, heterogeneity of stem cells). Thus single cell analysis has gained increasing attentions over the past years (Ahmed et al. 2016; Lawson et al. 2015), along with numerous applications using microfluidics (Wheeler et al. 2003). For example, on-chip flow cytometry has shown excellent capabilities of cellular manipulation and characterization in a high-

throughput way (more than 50,000 cells per second) (Stavrakis et al. 2019). Droplet-based single-cell screening also provides an alternative method to tackle single-cell analysis rapidly (Brouzes et al. 2009; Mazutis et al. 2013).

Nevertheless, these methods lack temporal resolution that reflects the cellular changes over time. In such cases, their results may lead to misinterpreted conclusions. Given this concern, long-term observation or imaging could provide a solution to decipher correlated misunderstandings (Hoppe et al. 2016), and this can be achieved using single-cell trapping methods that retain the cells at preset locations (Tan et al. 2009). In the past, a variety of approaches have been explored to do so, including encaging trapping (Rettig and Folch 2005; Wheeler et al. 2003), hydrodynamic trapping (Di Carlo et al. 2006), dielectrophoretic trapping (Taff and Voldman 2005), optical tweezer trapping (Arai et al. 2005), and others (Hammarström et al. 2010). In this chapter, simple 3D cell cages were adopted, and combined with DOMES-based micropumps for creating self-pumped lab-on-a-foil devices to carry out single-cell trapping on the foil.

6.2 Materials and methods

6.2.1 Overall fabrication process

The stick-and-play microfluidic device consists of two layers: the top PDMS layer and the bottom PET layer (Figure 6.1 a). Through holes (180 μm diameter) were precut in the ITO-coated PET films (127 μm in thickness, Sigma-Aldrich, St. Louis) using a milling machine (CNC Mini-Mill/3, Minitech Machinery Corp., Atlanta, GA). DOMES structures were created using TPP technique. The TPP system used here is

a Nanoscribe system (Nanoscribe Photonic Professional GT, Nanoscribe GmbH, Germany). As shown in Figure 6.1 d, thanks to the through hole in the PET substrate, the air-liquid interfaces formed in the pores of the DOMES structure is now open to the ambient air subject to atmospheric pressure. These air-liquid interfaces (or membranes) acted in a similar way to a bubble surface in an acoustic field, *i.e.*, oscillating upon acoustic actuation and creating microstreaming flow.

The fabrication process is similar to that in Chapter 5, and briefly described as follows. The PET film with a through hole in it was first cleaned with acetone and IPA rinse, followed by nitrogen blow-drying. Afterwards, a small amount of the photoresist (IP-S, Nanoscribe GmbH, Germany) was added onto the ITO-coated side of the film. During fabrication, an adaptive slicing (0.2-1.0 μm) and a hatching of 0.3 μm were applied, upon which the total fabrication time for a DOMES was found to be approximately 5 minutes. To remove excessive photoresist, the final device with DOMES was immersed in propylene glycol monomethyl ether acetate (PGMEA, MicroChem, Newton, MA) for a few minutes, followed by IPA rinse. Since such microstructure was printed right above the through hole, the trapped resin was readily dissolved using PGMEA, giving rise to a shorter development time compared to those microstructures created on intact films.

Soft lithography was utilized to fabricate top PDMS layer. Basically, any fabrication method that satisfies the resolution requirements can be used for creating master moulds, including photolithography (Lin et al. 2018), 3D printing (Kamei et al. 2015), micromachining (Park et al. 2010), and others (Bartholomeusz et al. 2005; Brittman et al. 2017). Afterwards, PDMS cover was attached directly onto

PET substrate manually without additional treatments.

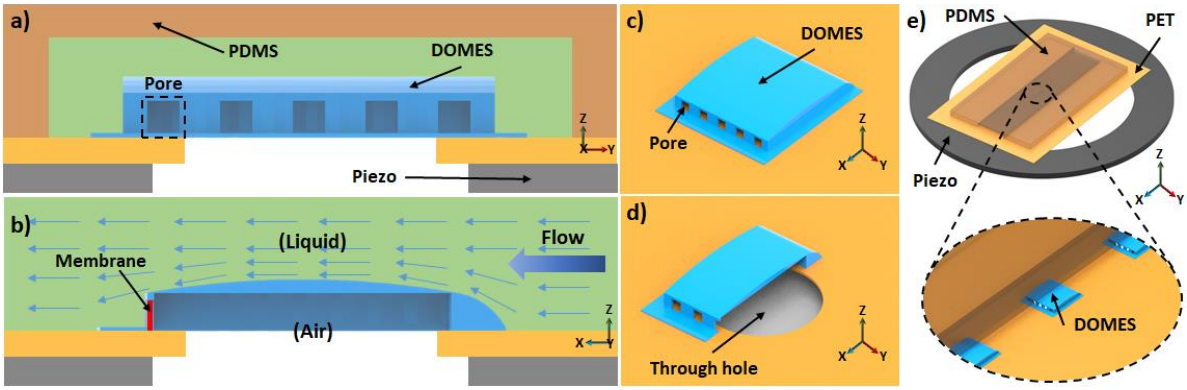

Figure 6.1 Schematic illustration of the micropump based on DOMES. a) Cross section of the stick-and-play micropump on the foil. A PET film with printed DOMES was attached on a ring-shaped piezo using double-sided tape. Thereafter, the PDMS cover with microchannels was attached manually and carefully onto the PET substrate without further treatment; b) Side view of micropump based on the DOMES created above a through hole in the PET film. The interfaces were kept facing ambient air across the holes in the PET film and the piezo; c) 3D model of the DOMES; d) 3D model of the half DOMES created above a through hole; e) Schematic illustration of the final device attached to the piezo. Schemes only represent relative position of objects rather than actual size.

As the bonding was performed manually, cares should be taken during the whole process. Moreover, both surfaces should be cleaned thoroughly before contacting each other so as to give a stronger molecular contact between them via van der Waals forces (Wasay and Sameoto 2015). Despite the fact that such reversible bonding did not provide comparable sealing strength compared to other methods such as plasma bonding, it allowed for the realization of the concept of

stick-and-play. Moreover, microchannels became available for a direct cleaning upon the separation of the cover and the substrate, thus making the reuse possible. Lastly, we attached the device to a ring-shaped piezo (APC International, Mackeyville, PA) with the help of the transparent double-sized tape. The piezo had a resonant frequency of 99.0 kHz with a 40 mm external diameter and a 20 mm diameter hole in the center, through which we were able to observe the pumping effects under microscope.

In contrast to the micromixer reported in Chapter 5 and our previous work (Lin et al. 2019a), the DOMES adopted in this chapter had a rectangular profile with a curved contour in its top and tail (Figure 6.1 b), which allowed incoming flows to pass by smoothly without exerting extra pressure to the microstructures. Moreover, the pores for creating air-liquid interfaces only existed on one side of the microstructures (Figure 6.1 c). Since the microstreaming was only expected to occur in the vicinity of these interfaces, the hypothesis is that rectified flows can be generated upon the activation of acoustic waves. Moreover, to obtain a stable adhesion between the DOMES and the PET film, an expanded base with larger contact area was applied in the design. Figure 6.1 d illustrated schematically the 3D model for a half DOMES, which was created above a through hole. This clearly indicates how the DOMES was deployed. Finally, a scheme illustrated the whole setup for the final device was shown in Figure 6.1 e.

6.2.2 DOMES and associated acoustic performance

Since through holes were precut in the PET substrates, and DOMES were printed right above these holes, the trapped air-liquid interfaces were found to be

very stable, thus maintaining stable acoustic microstreaming upon acoustic actuation. This benefit can be attributed to the fact that the bottom sides of these interfaces were always facing ambient air.

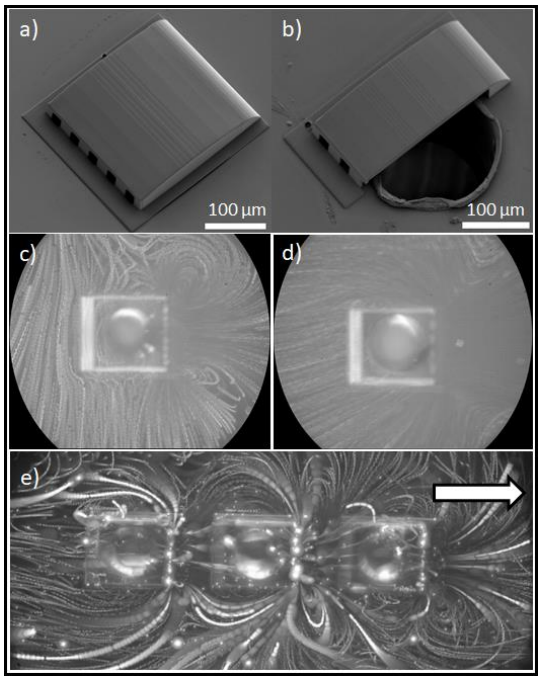

Figure 6.2 SEM images of the DOMES as well as associated acoustic performances. a) SEM image of the DOMES with 20 µm pore; b) SEM image illustrating how a half DOMES was created above a through hole; c) Rectified flows generated by the DOMES with 15 µm pores; d) Stronger rectified flows generated by the DOMES with 20 µm pores; e) A net flow (indicated by the arrow) was created using three DOMES. All the images for microstreaming were obtained by superimposing 24 frames in a 1-second video clip.

In this study, two different designs of DOMES were adopted, and both had the same profile except for the pore size. Basically, the DOMES had a cuboid base (300 µm in length, 270 µm in width, and 2 µm in thickness) and a curved shell (265

μm in length, 230 μm in width, and 25 μm in height) with pores in its front wall. Note that the total area of the pores in two designs was kept the same. The first design had 9 square pores with length of 15 μm, and the second design had 5 square pores with length of 20 μm.

DOMES with 20 μm square pore was printed above a through hole, and the corresponding SEM image taken by a SEM system (Hitachi S-3000N-VP-SEM, Japan) was shown in Figure 6.2 a. It illustrated that the adaptive slicing and hatching parameters used successfully led to a smooth surface with a curved tail. In addition, we also created a half DOMES, and its SEM image was shown in Figure 6.2 b. Despite the fact that protruding edges formed during hole preparation may apply undesired obstructions in TPP fabrication, the half microstructure remained intact without any deformation or undesired partition.

To further validate the value of the through hole for maintaining acoustic performance, we created one DOMES with 20 μm pores above the hole, and another identical one on intact PET film. Afterwards, small droplets of DI water with 2.0 μm diameter fluorescent microparticles (Fluoro-Max dyed polystyrene microspheres, Thermo Fisher Scientific, Waltham, MA) were added to both films to visualize the corresponding pumping performance. It should be noted that both tests were carried out on free surface films without any top layer. Thereafter, they were attached to a ring-shaped piezo (APC International, Mackeyville, PA), which was actuated by a function generator (DG1022U; Rigol Technologies Inc., Beijing, China), associated with a voltage amplifier (Tegam 2350, Tegam Inc., Madison, OH). It is worth noting that by simplifying the air-liquid interfaces into a flat rectangular

shaped membrane and neglecting the influence of other membranes in the array, we can find the theoretical resonant frequency of the interfaces to be around 140 kHz (Chindam et al. 2013). This frequency was used as a guideline for us to determine the frequency sweeping range in the experiment.

Indeed, upon sweeping the frequency from 100 Hz to 150 kHz at 5 Vpp, we found that the DOMES exhibited strongest microstreaming at 32.6 kHz with the aid of a fluorescence illuminator (X-cite 120, Lumen Dynamics, Ontario, Canada), an inverted microscope system (Nikon Eclipse Ti–S, Nikon Instruments Inc.), and a high-speed camera (Phantom Miro M310, Vision Research Inc., USA). As a result, we used 32.6 kHz as the driving frequency hereafter. In addition, the air trapped in the microstructures on intact PET film disappeared in less than 1 minute, while the other one remained effective for more than 30 minutes (total experimental time).

Furthermore, by comparing the acoustic performance of the DOMES printed above through holes (Figure 6.2 c, d), we also observed that larger pore led to stronger acoustic effect. This can be attributed to more energy dissipated along with increasing interface displacement (Gritsenko et al. 2018). It is worth mentioning that the phenomena were characterized at the height where DOMES were (the height of DOMES was much smaller compared to that of the entire liquid domain, *i.e.* the liquid droplet on the surface), as the microstreaming became weaker upon increasing the height of focal plane (away from the substrate). Notwithstanding, both DOMES indicated the pumping ability to generate rectified flows pointing from their tails to front walls. Moreover, two vortices were observed near the corners of DOMES on the pumping side. In addition, micropump based on multiple DOMES

was also demonstrated. Three identical DOMES were deployed in a line, and each of them had a through hole cut beneath in advance. After the piezoelectric transducer was activated, a strong microstreaming occurred near the vicinity of the microstructures. Hereby, a net flow (towards right in Figure 6.2 e) was generated, and the microparticles suspended in the liquid were pushed consecutively.

6.3 Theory and simulations

6.3.1 Theoretical background

Besides the experimental results obtained above using free surface PET devices, computational studies pertinent to the proposed acoustofluidic micropump were also conducted to gain in-depth understanding of the physical mechanisms behind these phenomena. Generally speaking, acoustofluidic manipulation stems from two hydrodynamic properties that are commonly ignored in conventional cases, the non-linearity of the well-known Navier-Stokes equation and the compressibility of fluids (Bruus 2008). Moreover, to achieve such ability, two phenomena are of the utmost importance. The first one is the microstreaming, where an extra steady component of the velocity field in the bulk of liquids is induced by acoustic energy (Hashmi et al. 2013). The second phenomenon is the secondary radiation force (*i.e.*, Bjerknes force), which accounts for the movement of suspended objects such as microparticles and cells together with Stokes drag force (Chen et al. 2016).

To simulate and characterize the microstreaming induced by acoustic energy, two methods can be applied: simulation based on directly solving the nonlinear

Navier-Stokes equation, or based on the separation of time scales (Bruus 2008; Muller et al. 2012). The latter one solves the thermoacoustic equations first to first order, associated with the impact of thermoviscous boundary layer near walls. Afterwards, the results of first-order fields could be applied to solve the time-averaged second-order equations, determining the final forces acting on the objects suspended (Muller et al. 2012). Specifically, thermoacoustic fields can be described using four scalar parameters (density ρ, pressure p, temperature T, and entropy s) and the velocity vector field $\boldsymbol{v}$. Moreover, the changes of ρ and s can be determined by the following two equations,

$$d\rho = \gamma\kappa\rho dp - \alpha\rho dT, \tag{6.1}$$

$$ds = \frac{C_p}{T}dT - \frac{\alpha}{\rho}dp, \tag{6.2}$$

where C_p, γ, κ, and α denote the specific heat capacity, the specific heat capacity ratio, the isentropic compressibility, and the isobaric thermal expansion coefficient, respectively.

In addition, given the fact that solving the governing differential equations analytically is only achievable in several ideal scenarios, approximation methods such as perturbation theory are of the great value in conducting simulations. Hereby, we applied this theory. Accordingly, parameters $T, p, \rho,$ and velocity $\boldsymbol{v}$ can be represented as follows:

$$T = T_0 + T_1 + T_2, \tag{6.3}$$

$$p = p_0 + p_1 + p_{2,} \tag{6.4}$$

$$\rho = \rho_0 + \rho_1 + \rho_{2,} \tag{6.5}$$

$$\boldsymbol{v} = \boldsymbol{0} + \boldsymbol{v}_1 + \boldsymbol{v}_{2.} \tag{6.6}$$

No-slip boundary conditions were applied to all the walls with constant temperature ($T = T_0$), and velocity ($\boldsymbol{v} = \boldsymbol{0}$). Furthermore, a harmonic time-dependent velocity component should be added to the oscillating interfaces. In our case,

$$\boldsymbol{n} \cdot \boldsymbol{v}_1 = v_0 e^{-i\omega t} \tag{6.7}$$

was applied to the air-liquid interfaces formed in DOMES. Note that $\boldsymbol{n}$ is the normal vector pointing out of the interfaces, and $v_0, \omega,$ and t represent the velocity amplitude, the angular frequency, and the time, respectively.

To solve the first order acoustic field, here we used the *Thermoviscous Acoustics, Frequency Domain* interface in the Acoustic Module of COMSOL Multiphysics. It was also worth mentioning that the thermodynamic heat transfer equation, the kinematic continuity equation, and the Navier-Stokes equation now become (Muller et al. 2012):

$$\partial_t T_1 = D_{th} \nabla^2 T_1 + \frac{\alpha T_0}{\rho_0 C_p} \partial_t p_1, \tag{6.8}$$

$$\partial_t p_1 = \frac{1}{\gamma \kappa} [\alpha \partial_t T_1 - \nabla \cdot \boldsymbol{v}_1], \tag{6.9}$$

$$\rho_0 \partial_t \boldsymbol{v}_1 = -\nabla p_1 + \mu \nabla^2 \boldsymbol{v}_1 + \beta \mu \nabla (\nabla \cdot \boldsymbol{v}_1), \tag{6.10}$$

where $D_{th}, \mu,$ and β represent the thermal diffusivity, the dynamic viscosity, and the viscosity ratio of fluids, respectively. Afterwards, the second order time averaged microstreaming can be solved using the *Laminar Flow* interface based on the first order results. Thereby, the continuity equation and Navier-Stokes equation have

been transformed to:

$$\rho_0 \nabla \cdot \langle \boldsymbol{v}_2 \rangle = -\nabla \cdot \langle \rho_1 \boldsymbol{v}_1 \rangle, \tag{6.11}$$

$$\mu \nabla^2 \langle \boldsymbol{v}_2 \rangle + \beta \mu \nabla (\nabla \cdot \boldsymbol{v}_2) - \langle \nabla p_2 \rangle = \langle \rho_1 \partial_t \boldsymbol{v}_1 \rangle + \rho_0 \langle (\boldsymbol{v}_1 \cdot \nabla) \boldsymbol{v}_1 \rangle. \tag{6.12}$$

As a result, the first, second order acoustic fields can be calculated, which were further applied for determining the forces acting on the objects suspended. The secondary radiation force F_{rad}, and Stokes drag force F_{drag} can be calculated using the following equations (Karlsen and Bruus 2015; Muller et al. 2012; Settnes and Bruus 2012),

$$F_{rad} = -\pi {R_0}^3 \left[\frac{2\kappa_0}{3} Re[f_1^* p_1^* \nabla p_1] - \rho_0 Re[f_2^* \boldsymbol{v}_1^* \cdot \nabla \boldsymbol{v}_1] \right], \tag{6.13}$$

$$F_{drag} = 6\pi \mu R_0 (\langle \boldsymbol{v}_2 \rangle - \boldsymbol{u}), \tag{6.14}$$

where $R_0, \kappa_0, f_1, f_2, \boldsymbol{u}$, and the asterisk symbol represent the radius of the spherical particle suspended, the compressibility of the fluid, the two pre-factors, the velocity of the particle, and the complex conjugation, respectively. Here, we applied the *Particle Tracing for Fluid Flow* interface to simulate the trajectories of the microparticles.

6.3.2 Simulation results

To simplify the geometry and avoid the heavy workload of calculation using 3D model, two-dimensional (2D) model (Figure 6.3 a) was adopted for the simulation of DOMES-based micropump. Basically, the microchannel and the DOMES were represented by a block with the length and width of 600 μm, and a square polygon (width of 220 μm) with several segments, respectively. It is worth noting that the

interfaces were marked in red with a length of 20 μm. The horizontal lines in the external block denoted the walls of the microchannel, and their mechanical conditions were set to be no-slip. Similarly, the walls on the DOMES except the interfaces were set to be no-slip. Thereafter, a harmonic time-dependent velocity component was added to the interfaces, associated with an amplitude of 50 nm, and a frequency of 32.6 kHz. It should also be noted that since the microchannel was far longer than 600 μm, periodic conditions should be applied to the vertical lines (orange) of the external block. Moreover, the liquid used in the fluid domain (area between the block and the DOMES) was set to be regular water, and the initial flow velocity was set to be 0.

As shown in Figure 6.3 b, the microstreaming plot indicated that the result had a great agreement with the experimental results. That was, a net flow was generated by the DOMES. The water in the fluid domain first bypassed the DOMES, and then converged in the center, giving rise to a continuous flow. Similar to the experimental results, two vortices were generated near the corners of DOMES in the pumping side, where the flows and objects suspended can be trapped.

Additionally, we also simulated the case, in which multiple DOMES were utilized to generate pumping effects (Figure 6.3 c). Specifically, three DOMES were adopted and deployed in a line, the gap between them was 350 μm, identical to that in the experiments. Here, the harmonic time-dependent velocity component was added to 15 interfaces and all the other walls were set to be no-slip. After the calculation, we found that multiple DOMES also had the capability to generate rectified flow along the microchannel, and vortices still existed near the corners.

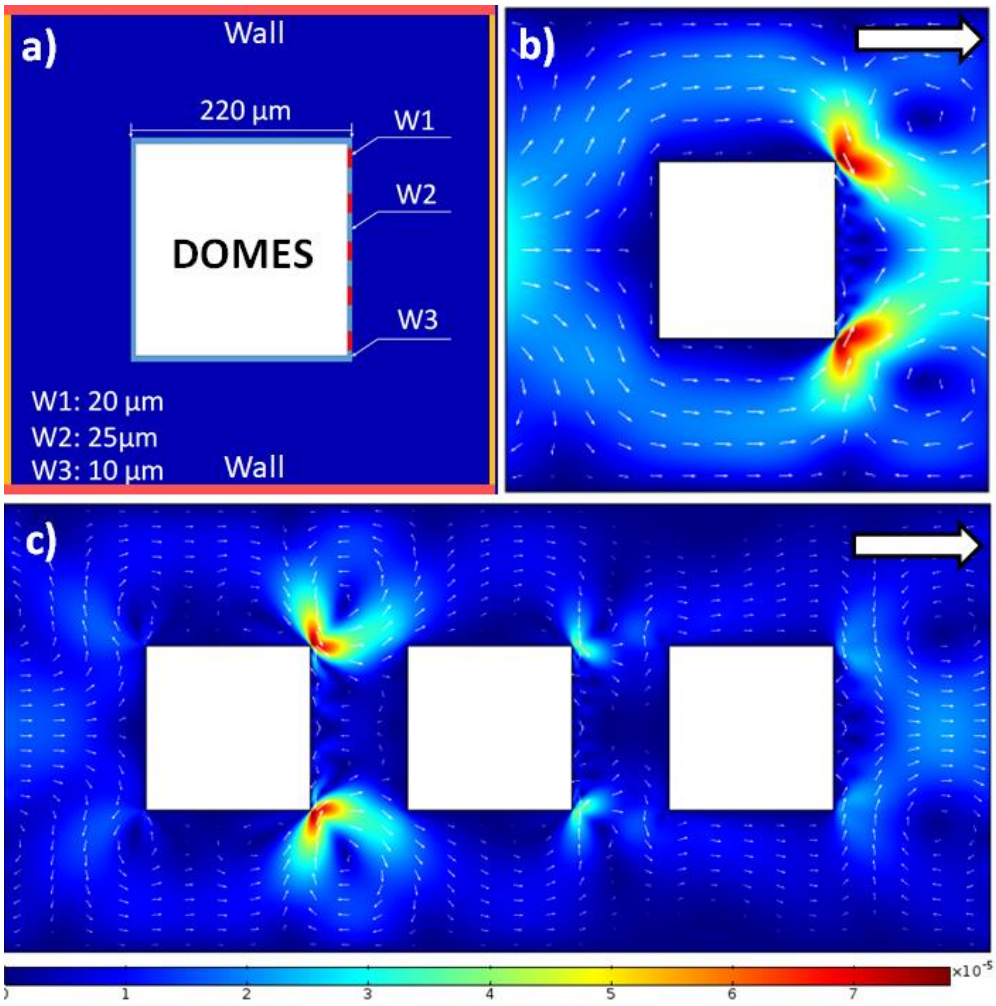

Figure 6.3 The geometry and simulation results for DOMES-based micropump. a) The scheme illustrating the geometry and dimensions used in the simulation. W1, W2, and W3 denoted the widths of interfaces (red lines), walls between interfaces, and side walls, respectively. The horizontal lines (pink) represented the walls of the microchannel, while the vertical lines (orange) were set to periodic conditions; b) Velocity field illustrating the acoustofluidic pumping effect due to single DOMES (color legend was not shown); c) Velocity field illustrating acoustofluidic pumping effect due to multiple DOMES. The arrows in the microstreaming velocity plots indicated the flow directions, and the unit of the color legend was m/s.

However, it was worth mentioning that the flows in the regions between the DOMES had an opposite flow direction, which was contradictory to the experimental findings. This can be attributed to the fact that the fluids were capable of flowing above the DOMES in a 3D case, while in a 2D case, the flows were blocked by the front microstructure and had to turn back. Notwithstanding this limitation, the simulated results manifested that the DOMES was able to achieve pumping effects, and had shown the capabilities in assisting future designs. Furthermore, the *Particle Tracing for Fluid Flow* interface of COMSOL Multiphysics was applied for tracking the trajectories of the particles suspended in the fluid domain. The involving particles were set to be 2.0 μm diameter polystyrene beads, which had the same properties of the fluorescent particles used in the aforementioned experiments.

6.4 Experimental results and discussion

6.4.1 Pumping performance

As aforementioned, stick-and-play method provides several advantages in those cases, where strong bonding is not required. Given that acoustic micropumps usually do not generate high pressure, PDMS cover with microchannel created by standard soft lithography was reversibly bonded to PET film manually. The PDMS cover contained a straight microchannel (length of 12mm and width of 600 μm) as well as two holes punched in advance using a biopsy punch (Ted Pella, Redding, CA), working as the inlet and outlet. Three DOMES with 20 μm pores and a center-to-center distance of 350 μm were incorporated in the microchannel. The final as-prepared lab-on-a-foil device was then attached to the ring-shaped piezo and activated at 32.6 kHz.

Note that these microstructures were deployed preferably close to the inlet in the center of the microchannel, by which DI water suspended with 2.0 μm diameter fluorescent microparticles could initially pass the microstructures via capillary action, forming the interfaces on the pores. Hereafter, micropump was activated to generate continuous flow inside the microchannel. However, after the flow reached the outlet, the micropump was deactivated to set the equilibrium state for the fluid. This step was inevitable since the pressure heads between the inlet and outlet could negatively affect the actual flow rate generated by DOMES.

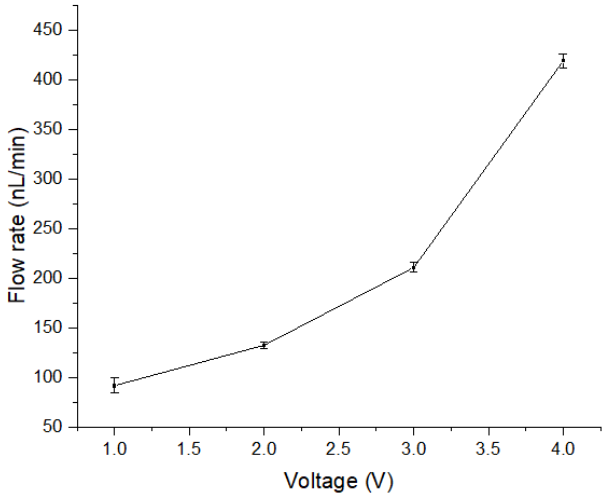

Figure 6.4 Plot of pumping flow rate versus voltage illustrating the fact that flow rate increased along with the increase of input voltage.

After the equilibrium state was obtained, the micropump was activated again, and its initial performance was adopted for the quantification of the flow rates due to possible influence from different pressure heads between inlet and outlet after pumping for a while. Specifically, the average flow rate was calculated from the average velocities of the microparticles observed. Since our channel has a

rectangular cross-sectional shape with an aspect ratio of 1:6, the velocity profile will deviate from parabolic shape in the width direction mimicking a Hele-Shaw flow condition (Bruus 2008; Tabeling 2005). The average flow rate was estimated from the microparticle velocities observed in videos with the assumption of parabolic velocity profile along the height and plug-like flow along the width of the channel, which agreed with the profile introduced in Chapter 2.

We also investigated the impact of input voltage on pumping performance (Figure 6.4). It was found that as the voltage increased, the flow rate generated by the micropump increased accordingly. When the input voltage was 1 Vpp, the flow rate was only 90 nL/min, yet it increased dramatically to 420 nL/min when the voltage was 4 Vpp. Despite having a relatively low flow rate when compared to other acoustic micropumps such as sharp edge based devices (Huang et al. 2013; Nama et al. 2014), the proposed micropump did not suffer from bubble instability and undesired bubble-trapping in the corners. Moreover, DOMES-based micropump possessed a high resolution in terms of flow rate control. That said, it was capable of tuning the flow rates in a fine range upon adjusting the input voltage carefully.

6.4.2 Microparticle and single-cell trapping

Similar to conventional microfluidic devices, to a large extent, single-cell traps based on encaging designs developed hitherto were generally fabricated using 2D designs (Di Carlo et al. 2006; Wheeler et al. 2003). Although these traps were capable of trapping an individual cell, the involving cages were usually large. Therefore, only large cells (more than 10 μm in diameter) can be entrapped. Additionally, these devices were only able to trap cells in a fixed height due to the

limitations from 2D designs. Hence, spatial impacts from vertical axis were commonly ignored.

Advantages of TPP such as high resolution and capabilities in 3D printing were exploited to create single-cell trapping microstructures, which were finally incorporated for creating self-pumped lab-on-a-foil single-cell trapping devices. Specifically, the single-cell trap used was a cylindrical open cage with tapering inlet and straight outlet (Figure 6.5 a), which were designed to trap cells and discharge fluids, respectively. The tapering inlet had a maximal diameter of 8 μm, a minimal diameter of 4 μm and a depth of 5 μm. Moreover, the straight outlet microchannel had a diameter of 4 μm. Herein, it was expected that single microparticle or cell with size around 5 μm could be trapped in the cage. To support the cage, another cylindrical microstructure was created underneath, by which the height of the region where the trapping carried out can be adjusted.

Prior to the use of actual cells to validate the functionality of such trapping approach, 4.8 μm diameter fluorescent microparticles (Fluoro-Max dyed polystyrene microspheres, Thermo Fisher Scientific, Waltham, MA) were utilized for initial investigation. That was, stick-and-play microfluidic device identical to the one described above was used in this case, yet a 3 by 3 array of traps were also built and incorporated in the center of the microchannel after the DOMES region. After the fluid with microparticles was pumped through upon the activation of the micropump, we found that despite microparticle trapping happening in the microstructure, a number of microparticles were also attached to the base (Figure 6.5 b). This can be attributed to the fact that a thin layer of unpolymerized photoresist

still remained on the exterior surfaces of the polymerized microstructure even after a thorough development (Lin and Xu 2018). As a result, the surface could be sticky and readily for microparticle attachment.

Given this concern, a post polymerization using an UV lamp would be preferable. Herein, BlueWave® 200 Light-Curing Spot Lamp (Dymax Corporation, Torrington, CT) was used to conduct 5-minute polymerization on the final trapping microstructures. As shown in the Figure 6.5 c, the microstructure became less sticky, only a few microparticles were attached to the surface. Nevertheless, the result also demonstrated that the proposed microstructure was capable of trapping a single microparticle in the cage.

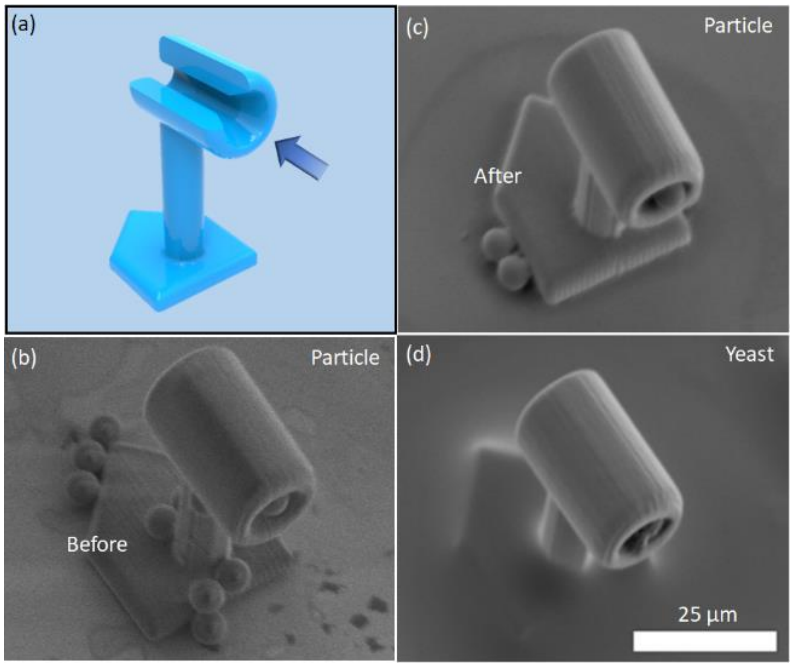

Figure 6.5 Single-cell trap used in the self-pumped lab-on-a-foil device. a) A 3D model of the cell trap illustrating its working mechanism. The blue arrow indicates the flow direction; b) Microparticle trapping using the cell trap without post

polymerization. A number of microparticles were found to be attached to the microstructure; c) Microparticle trapping using the cell trap with post polymerization. Only a few microparticles were found to be attached to the microstructure; d) Single-cell trapping on the foil using yeasts as a test type.

To test the feasibility of our single-cell trap using live cells, we used the budding yeast *Saccharomyces cerevisiae*. Yeast offers several advantages: size is amenable for the trap (~5 μm), and compared to the microparticles, it is less sticky which enable us to trap them inside the cage (Figure 6.5 d). Importantly, we did not find yeast attached to the base or other areas. Note that the budding event was also observed in this SEM image.

Yeast are a powerful model system for basic eukaryotic biology due to its genetic tractability, ability to perform high-throughput experiments and the conservation of many signaling pathways to humans. Yeast has been used as a pioneer model system in aging research (Jo et al. 2015), cellular signaling pathways (Caraveo et al. 2014), and even to understand basic biology of highly complex neurological diseases (Auluck et al. 2010; Khurana and Lindquist 2010). Therefore, our microfluidics design can provide an important tool to facilitate high-throughput studies needed to circumvent major roadblocks in the field of aging, which can speed and enrich for large quantities of the replicative aged cells for RNA sequencing and other type of studies.

6.5 Summary

To sum up, we developed a novel stick-and-play acoustofluidic micropump on the foil based on the microstructures termed DOMES. Compared to regular

acoustic bubbles or sharp edge based micropumps, our devices did not suffer from problems such as bubble instability, gas dissolution and undesired bubble-trapping in the corners, which could affect or even cease the pumping performance.

More specifically, the DOMES were created above the through holes precut in flexible PET films using TPP, and the pores designed on these microstructures were able to form air-liquid interfaces upon the arrival of fluids. As the pores were deployed asymmetrically, rectified flows can be generated after acoustic energy was activated. It was worth mentioning that larger pores were found to be able to generate stronger microstreaming, further leading to rapider flows. We also capitalized on multiple DOMES to create better pumping performance, and the results indicated a good agreement with simulation results.

PDMS cover was utilized to form enclosed microchannels in a stick-and-play mode for characterizing the pumping performance. Herein, the final device could be disassembled and cleaned for reuse. A maximal flow rate of 420 nL/min was obtained using three DOMES at 4 Vpp. Although such performance was not competitive to those obtained using other methods such as sharp edges, it did not suffer from problems such as bubble instability. Moreover, conventional microfluidic devices were built on rigid substrates such as glass slides, hence they lacked the capabilities of bending in the future work. The objective of this work was to demonstrate the possibility of building a reliable micropump on the foils and avoid the drawbacks such as gas dissolution for long-term use. Finally, we incorporated the proposed micropump with 3D cell traps for creating a self-pumped single-cell trapping device. That was, a simple 3D encaging trap was created using

TPP, and the cumulative results indicated that it was capable of trapping single microparticle or yeast, as a test type. Compared to conventional single-cell cages with 2D designs, spatial control in the vertical axis could be considered in such 3D design, thus offering new possibilities in the future studies.

Admittedly, a few shortcomings to this proof-of-concept device still existed. For instance, compared to LCAT-based micropumps, multiple pumping components cannot be created simply through soft lithography, yet they should be created one by one via TPP, leading to a relatively long fabrication time. Moreover, TPP technology is currently still not a widely accessible method, thereby the applicability of this method is temporarily limited. In the future work, non-planar piezoelectric transducers such as film or 3D printed piezoelectric transducers could be used to further exploit the flexibility of such proposed micropump. We believe with such feature, acoustofluidic micropumps could become a promising tool with tremendous advantages and make invaluable contributions to various applications.

Chapter 7

Conclusions and Prospects

7.1 Conclusions

Additive manufacturing technologies have emerged as a powerful tool in the field of microfluidic engineering, owing to their powerful capabilities in fabrication of 3D microstructures for diverse functions. However, a majority of the applications in microfluidics only adopt these technologies to create simple microchannels for the transport of fluids rather than functional components, due to the limitation of resolution. On the other hand, components such as micromixers, micropumps, cellular traps and filters, often require sophisticated designs. To create these miniaturized components, microfabrication technologies such as photolithography and soft lithography have been widely used over the past decades. However, unlike 2D extruded parts, arbitrary 3D microstructures are very difficult to build using these microfabrication technologies. Herein, two-photon polymerization, an additive manufacturing technique with extremely high resolution, has emerged and started to play a critical role for fabrication of microfluidic components.

Given the fact that two-photon polymerization builds objects through a voxel-by-voxel manner, the time of fabrication could be significantly long, therefore it is more suitable to create only the essential parts at regions of interest in a microfluidic device, instead of creating the whole device. In this dissertation, we contribute to

the use of two-photon polymerization in several applications of microfluidics: novel fabrication method for soft lithography, superhydrophobic foil with hierarchical structures, acoustofluidic micromixer and micropump, as well as the cell traps. Specifically, we have achieved several milestones as follows:

1) High resolution master moulds for soft lithography

A novel hybrid fabrication method based on photolithography and two-photon polymerization was developed to create master moulds in soft lithography. More specifically, photolithography was applied to build the main structures, while two-photon polymerization was successively used to create high resolution microstructures in the regions of interest after careful alignment. As a result, this proposed method prevented the huge time expenses from printing the entire parts using two-photon polymerization, along with taking advantages of conventional photolithography.

2) Superhydrophobic surfaces on glass slides and flexible foils

Fractal Sierpinski tetrahedron and hierarchical pyramid microstructures were created on glass slides and flexible PET films using two-photon polymerization, aiming to create superhydrophobic surfaces. Despite only slight hydrophobicity being obtained due to intrinsic hydrophilicity of the photoresists, these printed microstructures imparted superhydrophobicity on the surfaces after the coating of HMDSO. In addition, when it comes to the superhydrophobicity on flexible PET films, the property retained even after tens of bending and relaxing cycles. Since different microstructures can be built at different regions, the proposed method could be applied for a controllable management of surface wetting.

3) Acoustofluidic micromixer on flexible foils

Based on the experience of creating microstructures on flexible foils, we presented a novel acoustofluidic micromixer by means of embedding 3D printed microstructures in flexible devices made of off-the-shelf materials such as PET films and double-sided tapes. The mixing effect was generated from 3D printed microstructures termed DOMES, through which the acoustically oscillated air-liquid interfaces were connected to the ambient air, thus preventing the oscillation of these interfaces from dissolution and compression. It is found that the mixing effect became stronger if the pores on these microstructures were enlarged, yet larger pores may result in liquid leakage from the pores. Nevertheless, the mixing time was found to be 87.8 ms when the flow rate was set to 8 μl/min, indicating that such lab-on-a-foil acoustofluidic micromixer possessed a competitive performance even compared with other PDMS-based counterparts.

4) Self-pumped lab-on-a-foil devices for single-cell trapping

Extending the capabilities of the DOMES proposed above, we developed an acoustofluidic micropump on the foils. Since the pores on DOMES were deployed asymmetrically, net flows can be generated by acoustic microstreaming upon acoustic actuation. A maximal flow rate of 420 nL/min was obtained when the driving voltage was set to 4 Vpp. To further investigate the pumping abilities of the proposed micropump, it was utilized to drive flows in a single-cell trapping device. Here, the cell traps were also printed using two-photon polymerization, and it exhibited good performances in the capture of suspended objects such as the microparticles and yeasts.

7.2 Prospects

This dissertation has focused on the development of various microfluidic devices using two-photon polymerization, an additive manufacturing technique working at micro and nanoscale. Despite the successful development and implementation of devices in several applications, the work has been not comprehensive enough. This is because the field is still at its beginning stage, and encompasses numerous uncovered matters and possibilities. Therefore, fundamental studies on topics such as photopolymerization, hydrophobicity, post treatments, acoustofluidics, and others, have to be done in the next stage to further improve the performance of two-photon polymerization in these applications and expand its capabilities in other fields.

On the other hand, two-photon polymerization is still not a widely accessible technique, since it requires expensive fabrication systems and sophisticated operations. Meanwhile, the fabrication speed of this technique is still not fast enough to achieve mass production, thus significantly constraining its developments and progress of commercialization. Given these concerns, future works should empathize on further improvements in critical aspects such as the speed, cost of fabrication, and corresponding processes involving alignment and connections between microscale and macroscale components.

Admittedly, the implementation of nanoscale additive manufacturing technique in microfluidics is still quite limited, but we truly believe the proposed devices and applications in this dissertation have manifested its capabilities in various fields, along with more applications expected in the near future. We are

confident that such approach will become a powerful tool not only in the field of microfluidics, but also inspire a variety of possibilities for our society and the world.

Appendices

Appendix A

Alignment of the printed structures to exposed patterns

Since the sample was attached to the holder manually, the direction by which the structure should be printed was usually different to that from the coordinates of TPP system. Thereby, before printing the actual structures, the coordinates of the TPP system should be calibrated based on real samples. To put it simply, a small test spot was printed first, followed by dragging and dropping the cross hair (NanoWrite, Nanoscribe GmbH, Germany) to the identical printing position on the screen (Figure A.1 a).

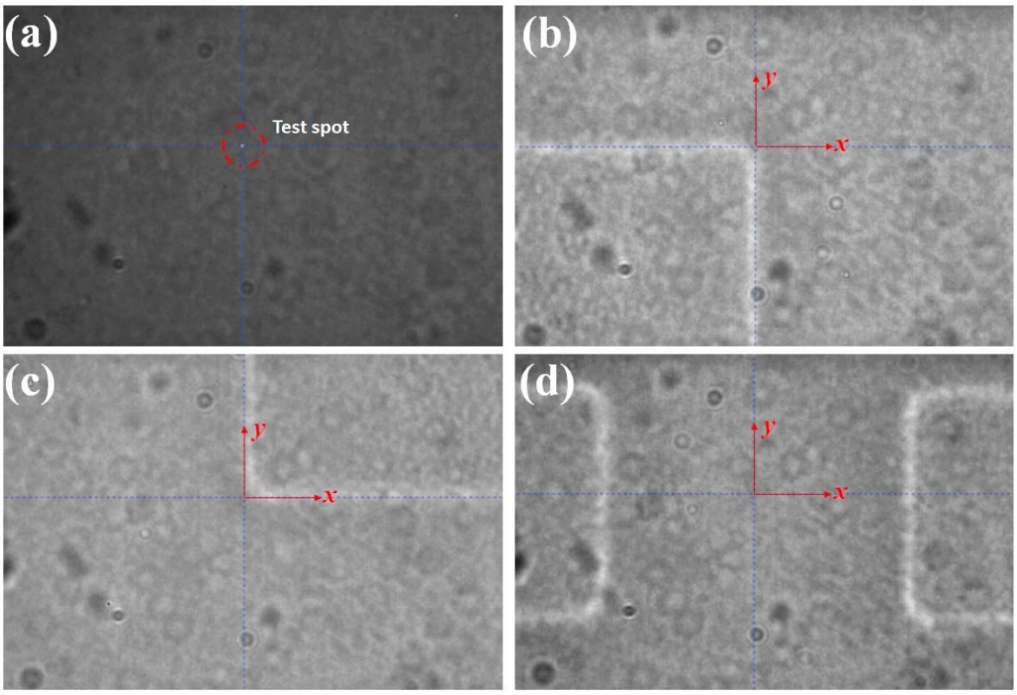

Figure A.1 a) A test spot printed to calibrate the coordinates of the TPP system. b) Image showed the top left corner of the gap. c) Image showed the bottom right corner of the gap. d) Move the origin of the TPP system to the center of gap.

Herein, the position where cross hair appeared on NanoWrite was set as the origin. Additionally, x and y axes of systematic coordinates were also adjusted based on the directions from the edges of rectangular edges. Next, the top left corner and bottom right corner of the gap were tracked as reference points (Figure A.1 b, c), followed by moving the cross hair to the center of gap using GWL script control. Thus, this position was set as the origin of printed structures (Figure A.1 d).

PDMS casting in a Petri dish

To avoid the breakage of glass slides during PDMS peeling, we have fixed them in a Petri dish with tape (Figure A.2).

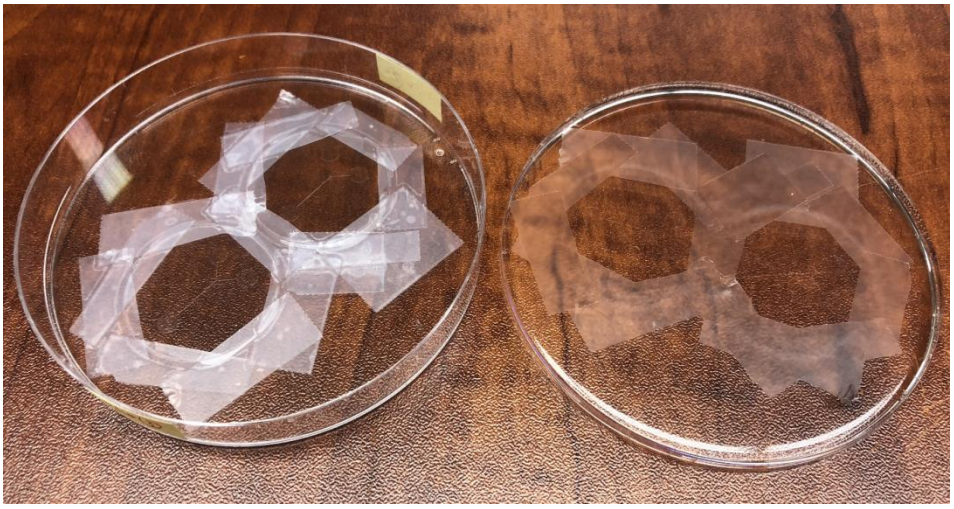

Figure A.2 Photo of fixing the as-fabricated master mould onto a bigger container using tape, avoiding the possibility of breaking the thin glass when peeling the PDMS off.

Appendix B

Xurography performance

Since the resolution of xurography is limited by the size of the cutting edge of the knife used in a cutting plotter, we investigated the smallest achievable microchannel using xurography. As shown in Figure B.1, a series of microchannels with designed widths of 200, 300, 400, 500, and 600 μm was created by the cutting plotter, while 100 μm width microchannel was failed due to drastic deformation.

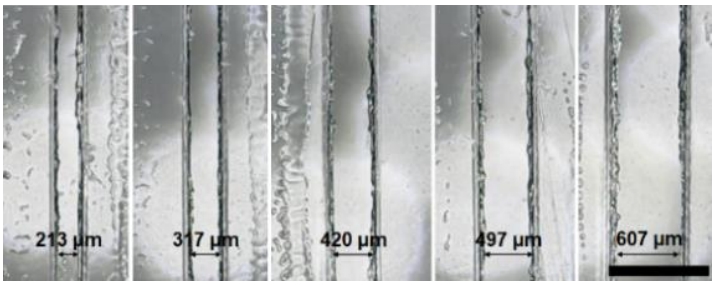

Figure B.1 Images of the microchannels with different widths ranging from 200-600 μm created via xurography. The scale bar is 1 mm.

Another issue for the xurography-based acoustofluidic devices is the bubbles trapped between layers during cutting and assembly. Conventionally, these bubbles are not harmful to the applications because they are confined in tween layers. However, we observed that after the acoustic energy was applied, the oscillation resulted in the escape of bubbles towards microchannels. As a result, these bubbles exerted additional microstreaming on the experiments, giving rise to random results. Therefore, we clamped the as-prepared devices between two pieces of glass slide, followed by baking overnight. After 2 hours, the majority of bubbles near

edges disappeared (Figure B.2), and two clear bubble-free bands can be obtained after baking overnight.

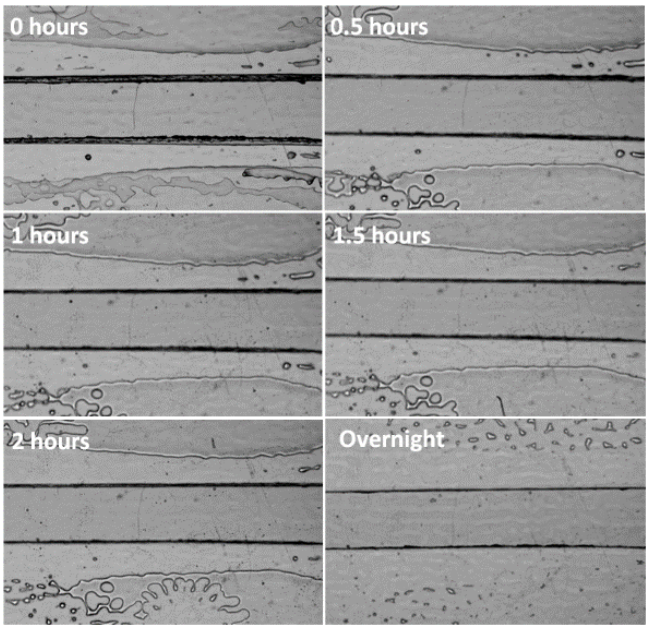

Figure B.2 Bubble removal process for xurography-based acoustofluidic devices.

Assembly and world-to-chip connection

A homemade alignment tool that consists of a three-axis linear stage and a USB digital microscope was used for assembly (Figure B.3 a). Hereby, PET film was first attached to the platform. Afterwards, the as-prepared double sided tape was placed on the three-axis linear stage. After moving the stage up, they can be aligned and bonded under microscope. Finally, all the layers were bonded together (Figure B.3 b), and the final device was attached to a ring-shaped piezo. External tubings were also bonded directly onto the top sticky side (Figure B.3 c).

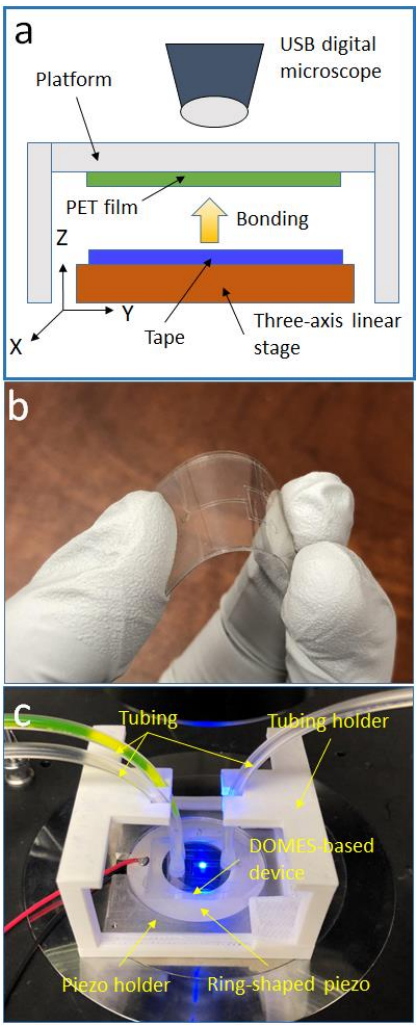

Figure B.3 Assembly and world-to-chip connection of the xurography-based devices. a) Schematic illustration of the homemade alignment tool used for assembly. b) Photo of the DOMES-based device. c) Experimental setup for the device. All the photos were taken using an iPhone 8.

Figure B.4 Experimental setup used to determine the watertightness of DOMES.

Appendix C

Permissions

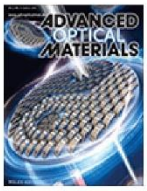

Title: Microstructures Fabricated by Two-Photon Polymerization and Their Remote Manipulation Techniques: Toward 3D Printing of Micromachines
Author: Yang Lin, Jie Xu
Publication: Advanced Optical Materials
Publisher: John Wiley and Sons
Date: Mar 24, 2018

Logged in as:
Yang Lin
Account #:
3000995684
LOGOUT

Order Completed

Thank you for your order.

This Agreement between Yang Lin ("You") and John Wiley and Sons ("John Wiley and Sons") consists of your license details and the terms and conditions provided by John Wiley and Sons and Copyright Clearance Center.

Your confirmation email will contain your order number for future reference.

printable details

License Number	4685570854549
License date	Oct 10, 2019
Licensed Content Publisher	John Wiley and Sons
Licensed Content Publication	Advanced Optical Materials
Licensed Content Title	Microstructures Fabricated by Two-Photon Polymerization and Their Remote Manipulation Techniques: Toward 3D Printing of Micromachines
Licensed Content Author	Yang Lin, Jie Xu
Licensed Content Date	Mar 24, 2018
Licensed Content Volume	6
Licensed Content Issue	8
Licensed Content Pages	11
Type of use	Dissertation/Thesis
Requestor type	Author of this Wiley article
Format	Print and electronic
Portion	Full article
Will you be translating?	No
Title of your thesis / dissertation	Microfluidics with Nanoscale Additive Manufacturing: Devices and Applications
Expected completion date	Nov 2019
Expected size (number of pages)	200
Requestor Location	Yang Lin 842 W Taylor St. 2039 ERF MC 251 CHICAGO, IL 60607

	United States Attn: Yang Lin
Publisher Tax ID	EU826007151
Total	0.00 USD

Would you like to purchase the full text of this article? If so, please continue on to the content ordering system located here: Purchase PDF

If you click on the buttons below or close this window, you will not be able to return to the content ordering system.

ORDER MORE CLOSE WINDOW

Order Completed

Thank you for your order.

This Agreement between Yang Lin ("You") and Springer Nature ("Springer Nature") consists of your license details and the terms and conditions provided by Springer Nature and Copyright Clearance Center.

Your confirmation email will contain your order number for future reference.

printable details

License Number	4685571110012
License date	Oct 10, 2019
Licensed Content Publisher	Springer Nature
Licensed Content Publication	Microfluids and Nanofluids
Licensed Content Title	Soft lithography based on photolithography and two-photon polymerization
Licensed Content Author	Yang Lin, Can Gao, Dmitry Gritsenko et al
Licensed Content Date	Jan 1, 2018
Licensed Content Volume	22
Licensed Content Issue	9
Type of Use	Thesis/Dissertation
Requestor type	academic/university or research institute
Format	print and electronic
Portion	full article/chapter
Will you be translating?	no
Circulation/distribution	1 - 29
Author of this Springer Nature content	yes
Title	Microfluidics with Nanoscale Additive Manufacturing: Devices and Applications
Institution name	University of Illinois at Chicago
Expected presentation date	Nov 2019
Requestor Location	Yang Lin 842 W Taylor St. 2039 ERF MC 251 CHICAGO, IL 60607 United States Attn: Yang Lin
Total	0.00 USD

ORDER MORE CLOSE WINDOW

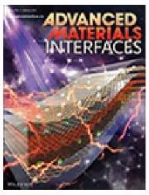

Title: Superhydrophobic Surfaces Based on Fractal and Hierarchical Microstructures Using Two-Photon Polymerization: Toward Flexible Superhydrophobic Films

Author: Yang Lin, Ran Zhou, Jie Xu

Publication: Advanced Materials Interfaces

Publisher: John Wiley and Sons

Date: Sep 19, 2018

Order Completed

Thank you for your order.

This Agreement between Yang Lin ("You") and John Wiley and Sons ("John Wiley and Sons") consists of your license details and the terms and conditions provided by John Wiley and Sons and Copyright Clearance Center.

Your confirmation email will contain your order number for future reference.

printable details

License Number	4685571298663
License date	Oct 10, 2019
Licensed Content Publisher	John Wiley and Sons
Licensed Content Publication	Advanced Materials Interfaces
Licensed Content Title	Superhydrophobic Surfaces Based on Fractal and Hierarchical Microstructures Using Two-Photon Polymerization: Toward Flexible Superhydrophobic Films
Licensed Content Author	Yang Lin, Ran Zhou, Jie Xu
Licensed Content Date	Sep 19, 2018
Licensed Content Volume	5
Licensed Content Issue	21
Licensed Content Pages	8
Type of use	Dissertation/Thesis
Requestor type	Author of this Wiley article
Format	Print and electronic
Portion	Full article
Will you be translating?	No
Title of your thesis / dissertation	Microfluidics with Nanoscale Additive Manufacturing: Devices and Applications
Expected completion date	Nov 2019
Expected size (number of pages)	200
Requestor Location	Yang Lin 842 W Taylor St. 2039 ERF MC 251 CHICAGO, IL 60607

	United States Attn: Yang Lin
Publisher Tax ID	EU826007151
Total	0.00 USD

Would you like to purchase the full text of this article? If so, please continue on to the content ordering system located here: Purchase PDF

If you click on the buttons below or close this window, you will not be able to return to the content ordering system.

ORDER MORE CLOSE WINDOW

Account Info Help

Title:	Lab on a chip
Article ID:	1473-0189
Publication:	Publication1
Publisher:	CCC Republication
Date:	Jan 1, 2001

Logged in as:
Yang Lin
Account #:
3000995684

LOGOUT

Order Completed

Thank you for your order.

This Agreement between Yang Lin ("You") and Royal Society of Chemistry ("Royal Society of Chemistry") consists of your order details and the terms and conditions provided by Royal Society of Chemistry and Copyright Clearance Center.

License number	Reference confirmation email for license number
License date	Oct, 11 2019
Licensed content publisher	Royal Society of Chemistry
Licensed content title	Lab on a chip
Licensed content date	Jan 1, 2001
Type of use	Thesis/Dissertation
Requestor type	Academic institution
Format	Print, Electronic
Portion	chapter/article
The requesting person/organization	Yang Lin/University of Illinois at Chicago
Title or numeric reference of the portion(s)	Full article
Title of the article or chapter the portion is from	Acoustofluidic stick-and-play micropump built on foil for single-cell trapping
Editor of portion(s)	Sarah Holmes
Author of portion(s)	Yang Lin, Yuan Gao, Mengren Wu, Ran Zhou, Daayun Chung, Gabriela Caraveo, Jie Xu
Volume of serial or monograph	19
Issue, if republishing an article from a serial	N/A
Page range of portion	
Publication date of portion	5th August 2019
Rights for	Main product and any product related to main product
Duration of use	Life of current edition
Creation of copies for the disabled	no
With minor editing privileges	yes
For distribution to	Worldwide
In the following language(s)	Original language of publication
With incidental promotional use	no
Lifetime unit quantity of new product	Up to 499
Title	Microfluidics with Nanoscale Additive Manufacturing: Devices and Applications
Institution name	University of Illinois at Chicago

Expected presentation date	Nov 2019
Requestor Location	Yang Lin 842 W Taylor St. 2039 ERF MC 251 CHICAGO, IL 60607 United States Attn: Yang Lin
Billing Type	Invoice
Billing address	Yang Lin 842 W Taylor St. 2039 ERF MC 251 CHICAGO, IL 60607 United States Attn: Yang Lin
Total (may include CCC user fee)	0.00 USD
Total	0.00 USD

CLOSE WINDOW

Science AAAS

Title: Long-Term Monitoring of Bacteria Undergoing Programmed Population Control in a Microchemostat

Author: Frederick K. Balagaddé,Lingchong You,Carl L. Hansen,Frances H. Arnold,Stephen R. Quake

Publication: Science

Publisher: The American Association for the Advancement of Science

Date: Jul 1, 2005

Order Completed

Thank you for your order.

This Agreement between Yang Lin ("You") and The American Association for the Advancement of Science ("The American Association for the Advancement of Science") consists of your license details and the terms and conditions provided by The American Association for the Advancement of Science and Copyright Clearance Center.

Your confirmation email will contain your order number for future reference.

printable details

License Number	4685580982179
License date	Oct 10, 2019
Licensed Content Publisher	The American Association for the Advancement of Science
Licensed Content Publication	Science
Licensed Content Title	Long-Term Monitoring of Bacteria Undergoing Programmed Population Control in a Microchemostat
Licensed Content Author	Frederick K. Balagaddé,Lingchong You,Carl L. Hansen,Frances H. Arnold,Stephen R. Quake
Licensed Content Date	Jul 1, 2005
Licensed Content Volume	309
Licensed Content Issue	5731
Volume number	309
Issue number	5731
Type of Use	Thesis / Dissertation
Requestor type	Scientist/individual at a research institution
Format	Print and electronic
Portion	Figure
Number of figures/tables	1
Order reference number	
Title of your thesis / dissertation	Microfluidics with Nanoscale Additive Manufacturing: Devices and Applications
Expected completion date	Nov 2019
Estimated size(pages)	200

Requestor Location	Yang Lin 842 W Taylor St. 2039 ERF MC 251 CHICAGO, IL 60607 United States Attn: Yang Lin
Total	0.00 USD

ORDER MORE CLOSE WINDOW

Copyright Clearance Center

Note: Copyright.com supplies permissions but not the copyrighted content itself.

1 PAYMENT 2 REVIEW 3 CONFIRMATION

Step 3: Order Confirmation

Thank you for your order! A confirmation for your order will be sent to your account email address. If you have questions about your order, you can call us 24 hrs/day, M-F at +1.855.239.3415 Toll Free, or write to us at info@copyright.com. This is not an invoice.

Confirmation Number: 11858703
Order Date: 10/10/2019

If you paid by credit card, your order will be finalized and your card will be charged within 24 hours. If you choose to be invoiced, you can change or cancel your order until the invoice is generated.

Payment Information

Yang Lin
ylin212@uic.edu
+1 (312) 937-4209
Payment Method: n/a

Order Details

Analytical methods

Order detail ID:	72041547
Order License Id:	4685581259722
ISSN:	1759-9679
Publication Type:	e-Journal
Volume:	
Issue:	
Start page:	
Publisher:	RSC Publishing
Author/Editor:	Royal Society of Chemistry (Great Britain)

Permission Status: Granted
Permission type: Republish or display content
Type of use: Thesis/Dissertation

Requestor type	Academic institution
Format	Print, Electronic
Portion	chart/graph/table/figure
Number of charts/graphs/tables/figures	1
The requesting person/organization	Yang Lin/University of Illinois at Chicago
Title or numeric reference of the portion(s)	Figure 4 a
Title of the article or chapter the portion is from	A simple procedure to produce FDM-based 3D-printed microfluidic devices with an integrated PMMA optical window

Editor of portion(s)	N/A
Author of portion(s)	Lucas P. Bressan , Cristina B. Adamo , Reverson F. Quero , Dosil P. de Jesus and José A. F. da Silva
Volume of serial or monograph	11
Issue, if republishing an article from a serial	N/A
Page range of portion	1014-1020
Publication date of portion	9th January 2019
Rights for	Main product
Duration of use	Life of current edition
Creation of copies for the disabled	no
With minor editing privileges	yes
For distribution to	Worldwide
In the following language(s)	Original language of publication
With incidental promotional use	no
Lifetime unit quantity of new product	Up to 499
Title	Microfluidics with Nanoscale Additive Manufacturing: Devices and Applications
Institution name	University of Illinois at Chicago
Expected presentation date	Nov 2019

Note: This item will be invoiced or charged separately through CCC's **RightsLink** service. More info **$ 0.00**

This is not an invoice.

Total order items: 1

Order Total: 0.00 USD

Confirmation Number: 11858703

Special Rightsholder Terms & Conditions

The following terms & conditions apply to the specific publication under which they are listed

Analytical methods
Permission type: Republish or display content
Type of use: Thesis/Dissertation

TERMS AND CONDITIONS

The following terms are individual to this publisher:

None

Other Terms and Conditions:

STANDARD TERMS AND CONDITIONS

1. Description of Service; Defined Terms. This Republication License enables the User to obtain licenses for republication of one or more copyrighted works as described in detail on the relevant Order Confirmation (the "Work(s)"). Copyright Clearance Center, Inc. ("CCC") grants licenses through the Service on behalf of the rightsholder identified on the Order Confirmation (the "Rightsholder"). "Republication", as used herein, generally means the inclusion of a Work, in whole or in part, in a new work or works, also as described on the Order Confirmation. "User", as used herein, means the person or entity making such republication.

2. The terms set forth in the relevant Order Confirmation, and any terms set by the Rightsholder with respect to a particular Work, govern the terms of use of Works in connection with the Service. By using the Service, the person transacting for a republication license on behalf of the User represents and warrants that he/she/it (a) has been duly authorized by the User to accept, and hereby does accept, all such terms and conditions on behalf of User, and (b) shall inform User of all such terms and conditions. In the event such person is a "freelancer" or other third party independent of User and CCC, such party shall be deemed jointly a "User" for purposes of these terms and conditions. In any event, User shall be deemed to have accepted and agreed to all such terms and conditions if User republishes the Work in any fashion.

3. Scope of License; Limitations and Obligations.

3.1 All Works and all rights therein, including copyright rights, remain the sole and exclusive property of the Rightsholder. The license created by the exchange of an Order Confirmation (and/or any invoice) and payment by User of the full amount set forth on that document includes only those rights expressly set forth in the Order Confirmation and in these terms and conditions, and conveys no other rights in the Work(s) to User. All rights not expressly granted are hereby reserved.

3.2 General Payment Terms: You may pay by credit card or through an account with us payable at the end of the month. If you and we agree that you may establish a standing account with CCC, then the following terms apply: Remit Payment to: Copyright Clearance Center, 29118 Network Place, Chicago, IL 60673-1291. Payments Due: Invoices are payable upon their delivery to you (or upon our notice to you that they are available to you for downloading). After 30 days, outstanding amounts will be subject to a service charge of 1-1/2% per month or, if less, the maximum rate allowed by applicable law. Unless otherwise specifically set forth in the Order Confirmation or in a separate written agreement signed by CCC, invoices are due and payable on "net 30" terms. While User may exercise the rights licensed immediately upon issuance of the Order Confirmation, the license is automatically revoked and is null and void, as if it had never been issued, if complete payment for the license is not received on a timely basis either from User directly or through a payment agent, such as a credit card company.

3.3 Unless otherwise provided in the Order Confirmation, any grant of rights to User (i) is "one-time" (including the editions and product family specified in the license), (ii) is non-exclusive and non-transferable and (iii) is subject to any and all limitations and restrictions (such as, but not limited to, limitations on duration of use or circulation) included in the Order Confirmation or invoice and/or in these terms and conditions. Upon completion of the licensed use, User shall either secure a new permission for further use of the Work(s) or immediately cease any new use of the Work(s) and shall render inaccessible (such as by deleting or by removing or severing links or other locators) any further copies of the Work (except for copies printed on paper in accordance with this license and still in User's stock at the end of such period).

3.4 In the event that the material for which a republication license is sought includes third party materials (such as photographs, illustrations, graphs, inserts and similar materials) which are identified in such material as having been used by permission, User is responsible for identifying, and seeking separate licenses (under this Service or otherwise) for, any of such third party materials; without a separate license, such third party materials may not be used.

3.5 Use of proper copyright notice for a Work is required as a condition of any license granted under the Service. Unless otherwise provided in the Order Confirmation, a proper copyright notice will read substantially as follows: "Republished with permission of [Rightsholder's name], from [Work's title, author, volume, edition number and year of copyright]; permission conveyed through Copyright Clearance Center, Inc. " Such notice must be provided in a reasonably legible font size and must be placed either immediately adjacent to the Work as used (for example, as part of a by-line or footnote

but not as a separate electronic link) or in the place where substantially all other credits or notices for the new work containing the republished Work are located. Failure to include the required notice results in loss to the Rightsholder and CCC, and the User shall be liable to pay liquidated damages for each such failure equal to twice the use fee specified in the Order Confirmation, in addition to the use fee itself and any other fees and charges specified.

3.6 User may only make alterations to the Work if and as expressly set forth in the Order Confirmation. No Work may be used in any way that is defamatory, violates the rights of third parties (including such third parties' rights of copyright, privacy, publicity, or other tangible or intangible property), or is otherwise illegal, sexually explicit or obscene. In addition, User may not conjoin a Work with any other material that may result in damage to the reputation of the Rightsholder. User agrees to inform CCC if it becomes aware of any infringement of any rights in a Work and to cooperate with any reasonable request of CCC or the Rightsholder in connection therewith.

4. Indemnity. User hereby indemnifies and agrees to defend the Rightsholder and CCC, and their respective employees and directors, against all claims, liability, damages, costs and expenses, including legal fees and expenses, arising out of any use of a Work beyond the scope of the rights granted herein, or any use of a Work which has been altered in any unauthorized way by User, including claims of defamation or infringement of rights of copyright, publicity, privacy or other tangible or intangible property.

5. Limitation of Liability. UNDER NO CIRCUMSTANCES WILL CCC OR THE RIGHTSHOLDER BE LIABLE FOR ANY DIRECT, INDIRECT, CONSEQUENTIAL OR INCIDENTAL DAMAGES (INCLUDING WITHOUT LIMITATION DAMAGES FOR LOSS OF BUSINESS PROFITS OR INFORMATION, OR FOR BUSINESS INTERRUPTION) ARISING OUT OF THE USE OR INABILITY TO USE A WORK, EVEN IF ONE OF THEM HAS BEEN ADVISED OF THE POSSIBILITY OF SUCH DAMAGES. In any event, the total liability of the Rightsholder and CCC (including their respective employees and directors) shall not exceed the total amount actually paid by User for this license. User assumes full liability for the actions and omissions of its principals, employees, agents, affiliates, successors and assigns.

6. Limited Warranties. THE WORK(S) AND RIGHT(S) ARE PROVIDED "AS IS". CCC HAS THE RIGHT TO GRANT TO USER THE RIGHTS GRANTED IN THE ORDER CONFIRMATION DOCUMENT. CCC AND THE RIGHTSHOLDER DISCLAIM ALL OTHER WARRANTIES RELATING TO THE WORK(S) AND RIGHT(S), EITHER EXPRESS OR IMPLIED, INCLUDING WITHOUT LIMITATION IMPLIED WARRANTIES OF MERCHANTABILITY OR FITNESS FOR A PARTICULAR PURPOSE. ADDITIONAL RIGHTS MAY BE REQUIRED TO USE ILLUSTRATIONS, GRAPHS, PHOTOGRAPHS, ABSTRACTS, INSERTS OR OTHER PORTIONS OF THE WORK (AS OPPOSED TO THE ENTIRE WORK) IN A MANNER CONTEMPLATED BY USER; USER UNDERSTANDS AND AGREES THAT NEITHER CCC NOR THE RIGHTSHOLDER MAY HAVE SUCH ADDITIONAL RIGHTS TO GRANT.

7. Effect of Breach. Any failure by User to pay any amount when due, or any use by User of a Work beyond the scope of the license set forth in the Order Confirmation and/or these terms and conditions, shall be a material breach of the license created by the Order Confirmation and these terms and conditions. Any breach not cured within 30 days of written notice thereof shall result in immediate termination of such license without further notice. Any unauthorized (but licensable) use of a Work that is terminated immediately upon notice thereof may be liquidated by payment of the Rightsholder's ordinary license price therefor; any unauthorized (and unlicensable) use that is not terminated immediately for any reason (including, for example, because materials containing the Work cannot reasonably be recalled) will be subject to all remedies available at law or in equity, but in no event to a payment of less than three times the Rightsholder's ordinary license price for the most closely analogous licensable use plus Rightsholder's and/or CCC's costs and expenses incurred in collecting such payment.

8. **Miscellaneous.**

8.1 User acknowledges that CCC may, from time to time, make changes or additions to the Service or to these terms and conditions, and CCC reserves the right to send notice to the User by electronic mail or otherwise for the purposes of notifying User of such changes or additions; provided that any such changes or additions shall not apply to permissions already secured and paid for.

8.2 Use of User-related information collected through the Service is governed by CCC's privacy policy, available online here: http://www.copyright.com/content/cc3/en/tools/footer/privacypolicy.html.

8.3 The licensing transaction described in the Order Confirmation is personal to User. Therefore, User may not assign or transfer to any other person (whether a natural person or an organization of any kind) the license created by the Order Confirmation and these terms and conditions or any rights granted hereunder; provided, however, that User may assign such license in its entirety on written notice to CCC in the event of a transfer of all or substantially all of User's rights in the new material which includes the Work(s) licensed under this Service.

8.4 No amendment or waiver of any terms is binding unless set forth in writing and signed by the parties. The Rightsholder and CCC hereby object to any terms contained in any writing prepared by the User or its principals, employees, agents or affiliates and purporting to govern or otherwise relate to the licensing transaction described in the Order Confirmation, which terms are in any way inconsistent with any terms set forth in the Order Confirmation and/or in these terms and conditions or CCC's standard operating procedures, whether such writing is prepared prior to, simultaneously with or subsequent to the Order Confirmation, and whether such writing appears on a copy of the Order Confirmation or in a separate instrument.

8.5 The licensing transaction described in the Order Confirmation document shall be governed by and construed under the law of the State of New York, USA, without regard to the principles thereof of conflicts of law. Any case, controversy, suit, action, or proceeding arising out of, in connection with, or related to such licensing transaction shall be brought, at CCC's sole discretion, in any federal or state court located in the County of New York, State of New York, USA, or in any federal or state court whose geographical jurisdiction covers the location of the Rightsholder set forth in the Order Confirmation. The parties expressly submit to the personal jurisdiction and venue of each such federal or state court.If you have any comments or questions about the Service or Copyright Clearance Center, please contact us at 978-750-8400 or send an e-mail to info@copyright.com.

v 1.1

Close

Confirmation Number: 11858703

Citation Information

Order Detail ID: 72041547

Analytical methods by Royal Society of Chemistry (Great Britain) Reproduced with permission of RSC Publishing in the format Thesis/Dissertation via Copyright Clearance Center.

Close

Title: Microfluidic devices fabricated using stereolithography for preparation of monodisperse double emulsions

Author: Toshimitsu Kanai,Masaki Tsuchiya

Publication: Chemical Engineering Journal

Publisher: Elsevier

Date: 15 April 2016

Order Completed

Thank you for your order.

This Agreement between Yang Lin ("You") and Elsevier ("Elsevier") consists of your license details and the terms and conditions provided by Elsevier and Copyright Clearance Center.

Your confirmation email will contain your order number for future reference.

printable details

License Number	4685590083609
License date	Oct 10, 2019
Licensed Content Publisher	Elsevier
Licensed Content Publication	Chemical Engineering Journal
Licensed Content Title	Microfluidic devices fabricated using stereolithography for preparation of monodisperse double emulsions
Licensed Content Author	Toshimitsu Kanai,Masaki Tsuchiya
Licensed Content Date	Apr 15, 2016
Licensed Content Volume	290
Licensed Content Issue	n/a
Licensed Content Pages	5
Type of Use	reuse in a thesis/dissertation
Portion	figures/tables/illustrations
Number of figures/tables/illustrations	1
Format	both print and electronic
Are you the author of this Elsevier article?	No
Will you be translating?	No
Original figure numbers	Figure 1
Title of your thesis/dissertation	Microfluidics with Nanoscale Additive Manufacturing: Devices and Applications
Publisher of new work	University of Illinois at Chicago
Expected completion date	Nov 2019
Estimated size (number of pages)	200
Requestor Location	Yang Lin 842 W Taylor St. 2039 ERF MC 251 CHICAGO, IL 60607

	United States Attn: Yang Lin
Publisher Tax ID	98-0397604
Total	0.00 USD

ORDER MORE CLOSE WINDOW

Copyright Clearance Center

Note: Copyright.com supplies permissions but not the copyrighted content itself.

1 PAYMENT 2 REVIEW 3 CONFIRMATION

Step 3: Order Confirmation

Thank you for your order! A confirmation for your order will be sent to your account email address. If you have questions about your order, you can call us 24 hrs/day, M-F at +1.855.239.3415 Toll Free, or write to us at info@copyright.com. This is not an invoice.

Confirmation Number: 11858707
Order Date: 10/10/2019

If you paid by credit card, your order will be finalized and your card will be charged within 24 hours. If you choose to be invoiced, you can change or cancel your order until the invoice is generated.

Payment Information

Yang Lin
ylin212@uic.edu
+1 (312) 937-4209
Payment Method: n/a

Order Details

Annual review of materials research

Order detail ID:	72041552
Order License Id:	4685590361265
ISSN:	1545-4118
Publication Type:	e-Journal
Volume:	
Issue:	
Start page:	
Publisher:	ANNUAL REVIEWS

Permission Status: Granted
Permission type: Republish or display content
Type of use: Thesis/Dissertation

Requestor type	Academic institution
Format	Print, Electronic
Portion	chart/graph/table/figure
Number of charts/graphs/tables/figures	1
The requesting person/organization	Yang Lin/University of Illinois at Chicago
Title or numeric reference of the portion(s)	Figure 5
Title of the article or chapter the portion is from	Soft lithography
Editor of portion(s)	N/A

Author of portion(s)	Younan Xia and George M. Whitesides
Volume of serial or monograph	28
Issue, if republishing an article from a serial	1
Page range of portion	153-184
Publication date of portion	1998
Rights for	Main product
Duration of use	Life of current edition
Creation of copies for the disabled	no
With minor editing privileges	yes
For distribution to	Worldwide
In the following language(s)	Original language of publication
With incidental promotional use	no
Lifetime unit quantity of new product	Up to 499
Title	Microfluidics with Nanoscale Additive Manufacturing: Devices and Applications
Institution name	University of Illinois at Chicago
Expected presentation date	Nov 2019

Note: This item will be invoiced or charged separately through CCC's **RightsLink** service. More info **$ 0.00**

This is not an invoice.

Total order items: 1 **Order Total: 0.00 USD**

Confirmation Number: 11858707

Special Rightsholder Terms & Conditions

The following terms & conditions apply to the specific publication under which they are listed

Annual review of materials research
Permission type: Republish or display content
Type of use: Thesis/Dissertation

TERMS AND CONDITIONS

The following terms are individual to this publisher:

None

Other Terms and Conditions:

STANDARD TERMS AND CONDITIONS

1. Description of Service; Defined Terms. This Republication License enables the User to obtain licenses for republication of one or more copyrighted works as described in detail on the relevant Order Confirmation (the "Work(s)"). Copyright Clearance Center, Inc. ("CCC") grants licenses through the Service on behalf of the rightsholder identified on the Order Confirmation (the "Rightsholder"). "Republication", as used herein, generally means the inclusion of a Work, in whole or in part, in a new work or works, also as described on the Order Confirmation. "User", as used herein, means the person or entity making such republication.

2. The terms set forth in the relevant Order Confirmation, and any terms set by the Rightsholder with respect to a particular Work, govern the terms of use of Works in connection with the Service. By using the Service, the person transacting for a republication license on behalf of the User represents and warrants that he/she/it (a) has been duly authorized by the User to accept, and hereby does accept, all such terms and conditions on behalf of User, and (b) shall inform User of all such terms and conditions. In the event such person is a "freelancer" or other third party independent of User and CCC, such party shall be deemed jointly a "User" for purposes of these terms and conditions. In any event, User shall be deemed to have accepted and agreed to all such terms and conditions if User republishes the Work in any fashion.

3. Scope of License; Limitations and Obligations.

3.1 All Works and all rights therein, including copyright rights, remain the sole and exclusive property of the Rightsholder. The license created by the exchange of an Order Confirmation (and/or any invoice) and payment by User of the full amount set forth on that document includes only those rights expressly set forth in the Order Confirmation and in these terms and conditions, and conveys no other rights in the Work(s) to User. All rights not expressly granted are hereby reserved.

3.2 General Payment Terms: You may pay by credit card or through an account with us payable at the end of the month. If you and we agree that you may establish a standing account with CCC, then the following terms apply: Remit Payment to: Copyright Clearance Center, 29118 Network Place, Chicago, IL 60673-1291. Payments Due: Invoices are payable upon their delivery to you (or upon our notice to you that they are available to you for downloading). After 30 days, outstanding amounts will be subject to a service charge of 1-1/2% per month or, if less, the maximum rate allowed by applicable law. Unless otherwise specifically set forth in the Order Confirmation or in a separate written agreement signed by CCC, invoices are due and payable on "net 30" terms. While User may exercise the rights licensed immediately upon issuance of the Order Confirmation, the license is automatically revoked and is null and void, as if it had never been issued, if complete payment for the license is not received on a timely basis either from User directly or through a payment agent, such as a credit card company.

3.3 Unless otherwise provided in the Order Confirmation, any grant of rights to User (i) is "one-time" (including the editions and product family specified in the license), (ii) is non-exclusive and non-transferable and (iii) is subject to any and all limitations and restrictions (such as, but not limited to, limitations on duration of use or circulation) included in the Order Confirmation or invoice and/or in these terms and conditions. Upon completion of the licensed use, User shall either secure a new permission for further use of the Work(s) or immediately cease any new use of the Work(s) and shall render inaccessible (such as by deleting or by removing or severing links or other locators) any further copies of the Work (except for copies printed on paper in accordance with this license and still in User's stock at the end of such period).

3.4 In the event that the material for which a republication license is sought includes third party materials (such as photographs, illustrations, graphs, inserts and similar materials) which are identified in such material as having been used by permission, User is responsible for identifying, and seeking separate licenses (under this Service or otherwise) for, any of such third party materials; without a separate license, such third party materials may not be used.

3.5 Use of proper copyright notice for a Work is required as a condition of any license granted under the Service. Unless otherwise provided in the Order Confirmation, a proper copyright notice will read substantially as follows: "Republished with permission of [Rightsholder's name], from [Work's title, author, volume, edition number and year of copyright]; permission conveyed through Copyright Clearance Center, Inc. " Such notice must be provided in a reasonably legible font size and must be placed either immediately adjacent to the Work as used (for example, as part of a by-line or footnote

but not as a separate electronic link) or in the place where substantially all other credits or notices for the new work containing the republished Work are located. Failure to include the required notice results in loss to the Rightsholder and CCC, and the User shall be liable to pay liquidated damages for each such failure equal to twice the use fee specified in the Order Confirmation, in addition to the use fee itself and any other fees and charges specified.

3.6 User may only make alterations to the Work if and as expressly set forth in the Order Confirmation. No Work may be used in any way that is defamatory, violates the rights of third parties (including such third parties' rights of copyright, privacy, publicity, or other tangible or intangible property), or is otherwise illegal, sexually explicit or obscene. In addition, User may not conjoin a Work with any other material that may result in damage to the reputation of the Rightsholder. User agrees to inform CCC if it becomes aware of any infringement of any rights in a Work and to cooperate with any reasonable request of CCC or the Rightsholder in connection therewith.

4. Indemnity. User hereby indemnifies and agrees to defend the Rightsholder and CCC, and their respective employees and directors, against all claims, liability, damages, costs and expenses, including legal fees and expenses, arising out of any use of a Work beyond the scope of the rights granted herein, or any use of a Work which has been altered in any unauthorized way by User, including claims of defamation or infringement of rights of copyright, publicity, privacy or other tangible or intangible property.

5. Limitation of Liability. UNDER NO CIRCUMSTANCES WILL CCC OR THE RIGHTSHOLDER BE LIABLE FOR ANY DIRECT, INDIRECT, CONSEQUENTIAL OR INCIDENTAL DAMAGES (INCLUDING WITHOUT LIMITATION DAMAGES FOR LOSS OF BUSINESS PROFITS OR INFORMATION, OR FOR BUSINESS INTERRUPTION) ARISING OUT OF THE USE OR INABILITY TO USE A WORK, EVEN IF ONE OF THEM HAS BEEN ADVISED OF THE POSSIBILITY OF SUCH DAMAGES. In any event, the total liability of the Rightsholder and CCC (including their respective employees and directors) shall not exceed the total amount actually paid by User for this license. User assumes full liability for the actions and omissions of its principals, employees, agents, affiliates, successors and assigns.

6. Limited Warranties. THE WORK(S) AND RIGHT(S) ARE PROVIDED "AS IS". CCC HAS THE RIGHT TO GRANT TO USER THE RIGHTS GRANTED IN THE ORDER CONFIRMATION DOCUMENT. CCC AND THE RIGHTSHOLDER DISCLAIM ALL OTHER WARRANTIES RELATING TO THE WORK(S) AND RIGHT(S), EITHER EXPRESS OR IMPLIED, INCLUDING WITHOUT LIMITATION IMPLIED WARRANTIES OF MERCHANTABILITY OR FITNESS FOR A PARTICULAR PURPOSE. ADDITIONAL RIGHTS MAY BE REQUIRED TO USE ILLUSTRATIONS, GRAPHS, PHOTOGRAPHS, ABSTRACTS, INSERTS OR OTHER PORTIONS OF THE WORK (AS OPPOSED TO THE ENTIRE WORK) IN A MANNER CONTEMPLATED BY USER; USER UNDERSTANDS AND AGREES THAT NEITHER CCC NOR THE RIGHTSHOLDER MAY HAVE SUCH ADDITIONAL RIGHTS TO GRANT.

7. Effect of Breach. Any failure by User to pay any amount when due, or any use by User of a Work beyond the scope of the license set forth in the Order Confirmation and/or these terms and conditions, shall be a material breach of the license created by the Order Confirmation and these terms and conditions. Any breach not cured within 30 days of written notice thereof shall result in immediate termination of such license without further notice. Any unauthorized (but licensable) use of a Work that is terminated immediately upon notice thereof may be liquidated by payment of the Rightsholder's ordinary license price therefor; any unauthorized (and unlicensable) use that is not terminated immediately for any reason (including, for example, because materials containing the Work cannot reasonably be recalled) will be subject to all remedies available at law or in equity, but in no event to a payment of less than three times the Rightsholder's ordinary license price for the most closely analogous licensable use plus Rightsholder's and/or CCC's costs and expenses incurred in collecting such payment.

8. **Miscellaneous.**

8.1 User acknowledges that CCC may, from time to time, make changes or additions to the Service or to these terms and conditions, and CCC reserves the right to send notice to the User by electronic mail or otherwise for the purposes of notifying User of such changes or additions; provided that any such changes or additions shall not apply to permissions already secured and paid for.

8.2 Use of User-related information collected through the Service is governed by CCC's privacy policy, available online here: http://www.copyright.com/content/cc3/en/tools/footer/privacypolicy.html.

8.3 The licensing transaction described in the Order Confirmation is personal to User. Therefore, User may not assign or transfer to any other person (whether a natural person or an organization of any kind) the license created by the Order Confirmation and these terms and conditions or any rights granted hereunder; provided, however, that User may assign such license in its entirety on written notice to CCC in the event of a transfer of all or substantially all of User's rights in the new material which includes the Work(s) licensed under this Service.

8.4 No amendment or waiver of any terms is binding unless set forth in writing and signed by the parties. The Rightsholder and CCC hereby object to any terms contained in any writing prepared by the User or its principals, employees, agents or affiliates and purporting to govern or otherwise relate to the licensing transaction described in the Order Confirmation, which terms are in any way inconsistent with any terms set forth in the Order Confirmation and/or in these terms and conditions or CCC's standard operating procedures, whether such writing is prepared prior to, simultaneously with or subsequent to the Order Confirmation, and whether such writing appears on a copy of the Order Confirmation or in a separate instrument.

8.5 The licensing transaction described in the Order Confirmation document shall be governed by and construed under the law of the State of New York, USA, without regard to the principles thereof of conflicts of law. Any case, controversy, suit, action, or proceeding arising out of, in connection with, or related to such licensing transaction shall be brought, at CCC's sole discretion, in any federal or state court located in the County of New York, State of New York, USA, or in any federal or state court whose geographical jurisdiction covers the location of the Rightsholder set forth in the Order Confirmation. The parties expressly submit to the personal jurisdiction and venue of each such federal or state court.If you have any comments or questions about the Service or Copyright Clearance Center, please contact us at 978-750-8400 or send an e-mail to info@copyright.com.

v 1.1

Close

Confirmation Number: 11858707

Citation Information

Order Detail ID: 72041552

Annual review of materials research by ANNUAL REVIEWS. Reproduced with permission of ANNUAL REVIEWS in the format Thesis/Dissertation via Copyright Clearance Center.

Close

Title: 3D-Printed Microfluidics
Author: Albert Folch, Lisa F. Horowitz, Wilson Huynh, et al
Publication: Angewandte Chemie International Edition
Publisher: John Wiley and Sons
Date: Feb 8, 2016

Order Completed

Thank you for your order.

This Agreement between Yang Lin ("You") and John Wiley and Sons ("John Wiley and Sons") consists of your license details and the terms and conditions provided by John Wiley and Sons and Copyright Clearance Center.

Your confirmation email will contain your order number for future reference.

printable details

License Number	4687961426542
License date	Oct 14, 2019
Licensed Content Publisher	John Wiley and Sons
Licensed Content Publication	Angewandte Chemie International Edition
Licensed Content Title	3D-Printed Microfluidics
Licensed Content Author	Albert Folch, Lisa F. Horowitz, Wilson Huynh, et al
Licensed Content Date	Feb 8, 2016
Licensed Content Volume	55
Licensed Content Issue	12
Licensed Content Pages	20
Type of use	Dissertation/Thesis
Requestor type	University/Academic
Format	Print and electronic
Portion	Figure/table
Number of figures/tables	1
Original Wiley figure/table number(s)	Figure 10
Will you be translating?	No
Title of your thesis / dissertation	Microfluidics with Nanoscale Additive Manufacturing: Devices and Applications
Expected completion date	Nov 2019
Expected size (number of pages)	200
Requestor Location	Yang Lin 842 W Taylor St. 2039 ERF MC 251 CHICAGO, IL 60607 United States Attn: Yang Lin
Publisher Tax ID	EU826007151
Total	0.00 USD

Cited Literature

Abgrall, P., Gue, A., 2007. Lab-on-chip technologies: making a microfluidic network and coupling it into a complete microsystem—a review. Journal of micromechanics and microengineering 17(5), R15.

Ahmed, D., Mao, X., Juluri, B.K., Huang, T.J., 2009. A fast microfluidic mixer based on acoustically driven sidewall-trapped microbubbles. Microfluidics and nanofluidics 7(5), 727.

Ahmed, D., Ozcelik, A., Bojanala, N., Nama, N., Upadhyay, A., Chen, Y., Hanna-Rose, W., Huang, T.J., 2016. Rotational manipulation of single cells and organisms using acoustic waves. Nature communications 7, 11085.

Ainla, A., Jansson, E.T., Stepanyants, N., Orwar, O., Jesorka, A., 2010. A microfluidic pipette for single-cell pharmacology. Analytical chemistry 82(11), 4529-4536.

Ambrosi, A., Moo, J.G.S., Pumera, M., 2016. Helical 3D‐printed metal electrodes as custom‐shaped 3D platform for electrochemical devices. Advanced Functional Materials 26(5), 698-703.

Amirouche, F., Zhou, Y., Johnson, T., 2009. Current micropump technologies and their biomedical applications. Microsystem technologies 15(5), 647-666.

Arai, F., Ng, C., Maruyama, H., Ichikawa, A., El-Shimy, H., Fukuda, T., 2005. On chip single-cell separation and immobilization using optical tweezers and thermosensitive hydrogel. Lab on a Chip 5(12), 1399-1403.

Au, A.K., Huynh, W., Horowitz, L.F., Folch, A., 2016. 3D‐printed microfluidics. Angewandte Chemie International Edition 55(12), 3862-3881.

Auluck, P.K., Caraveo, G., Lindquist, S., 2010. α-Synuclein: membrane interactions and toxicity in Parkinson's disease. Annual review of cell and developmental biology 26, 211-233.

Balagaddé, F.K., You, L., Hansen, C.L., Arnold, F.H., Quake, S.R., 2005. Long-term monitoring of bacteria undergoing programmed population control in a microchemostat. Science 309(5731), 137-140.

Baldacchini, T., 2015. Three-dimensional microfabrication using two-photon polymerization: fundamentals, technology, and applications. William Andrew.

Baldacchini, T., Carey, J.E., Zhou, M., Mazur, E., 2006. Superhydrophobic surfaces prepared by microstructuring of silicon using a femtosecond laser. Langmuir 22(11), 4917-4919.

Bartholomeusz, D.A., Boutté, R.W., Andrade, J.D., 2005. Xurography: rapid prototyping of microstructures using a cutting plotter. Journal of

Microelectromechanical systems 14(6), 1364-1374.

Bauer, J., Hengsbach, S., Tesari, I., Schwaiger, R., Kraft, O., 2014. High-strength cellular ceramic composites with 3D microarchitecture. Proceedings of the National Academy of Sciences 111(7), 2453-2458.

Benyus, J.M., 1997. Biomimicry: Innovation inspired by nature. Morrow New York.

Bernardeschi, I., Tricinci, O., Mattoli, V., Filippeschi, C., Mazzolai, B., Beccai, L., 2016. Three-dimensional soft material micropatterning via direct laser lithography of flexible molds. ACS applied materials & interfaces 8(38), 25019-25023.

Bertin, N., Spelman, T.A., Stephan, O., Gredy, L., Bouriau, M., Lauga, E., Marmottant, P., 2015. Propulsion of bubble-based acoustic microswimmers. Physical Review Applied 4(6), 064012.

Berwind, M., Hashibon, A., Fromm, A., Gurr, M., Burmeister, F., Eberl, C., 2017. Rapidly prototyping biocompatible surfaces with designed wetting properties via photolithography and plasma polymerization. Microfluidics and Nanofluidics 21(9), 144.

Beuret, C., Racine, G.-A., Gobet, J., Luthier, R., De Rooij, N., 1994. Microfabrication of 3D multidirectional inclined structures by UV lithography and electroplating. Proceedings IEEE Micro Electro Mechanical Systems An Investigation of Micro Structures, Sensors, Actuators, Machines and Robotic Systems, pp. 81-85. IEEE.

Boesel, L.F., Greiner, C., Arzt, E., Del Campo, A., 2010. Gecko - inspired surfaces: a path to strong and reversible dry adhesives. Advanced Materials 22(19), 2125-2137.

Bohl, B., Steger, R., Zengerle, R., Koltay, P., 2005. Multi-layer SU-8 lift-off technology for microfluidic devices. Journal of micromechanics and microengineering 15(6), 1125.

Borenstein, J.T., Tupper, M.M., Mack, P.J., Weinberg, E.J., Khalil, A.S., Hsiao, J., García-Cardeña, G., 2010. Functional endothelialized microvascular networks with circular cross-sections in a tissue culture substrate. Biomedical microdevices 12(1), 71-79.

Bressan, L.P., Adamo, C.B., Quero, R.F., de Jesus, D.P., da Silva, J.A., 2019. A simple procedure to produce FDM-based 3D-printed microfluidic devices with an integrated PMMA optical window. Analytical methods 11(8), 1014-1020.

Brittman, S., Oener, S.Z., Guo, K., Āboliņš, H., Koenderink, A.F., Garnett, E.C., 2017. Controlling crystallization to imprint nanophotonic structures into halide perovskites using soft lithography. Journal of Materials Chemistry C 5(32), 8301-8307.

Brouzes, E., Medkova, M., Savenelli, N., Marran, D., Twardowski, M., Hutchison, J.B., Rothberg, J.M., Link, D.R., Perrimon, N., Samuels, M.L., 2009. Droplet microfluidic technology for single-cell high-throughput screening.

Proceedings of the National Academy of Sciences 106(34), 14195-14200.

Bruus, H., 2008. Theoretical microfluidics. Oxford university press Oxford.

Byun, D., Hong, J., Ko, J.H., Lee, Y.J., Park, H.C., Byun, B.-K., Lukes, J.R., 2009. Wetting characteristics of insect wing surfaces. Journal of Bionic Engineering 6(1), 63-70.

Caraveo, G., Auluck, P.K., Whitesell, L., Chung, C.Y., Baru, V., Mosharov, E.V., Yan, X., Ben-Johny, M., Soste, M., Picotti, P., 2014. Calcineurin determines toxic versus beneficial responses to α-synuclein. Proceedings of the National Academy of Sciences 111(34), E3544-E3552.

Carugo, D., Lee, J.Y., Pora, A., Browning, R.J., Capretto, L., Nastruzzi, C., Stride, E., 2016. Facile and cost-effective production of microscale PDMS architectures using a combined micromilling-replica moulding (μMi-REM) technique. Biomedical microdevices 18(1), 4.

Cha, T.-G., Yi, J.W., Moon, M.-W., Lee, K.-R., Kim, H.-Y., 2010. Nanoscale patterning of microtextured surfaces to control superhydrophobic robustness. Langmuir 26(11), 8319-8326.

Chen, J., He, X., Wang, W., Xuan, W., Zhou, J., Wang, X., Dong, S., Garner, S., Cimo, P., Luo, J., 2014. Bendable transparent ZnO thin film surface acoustic wave strain sensors on ultra-thin flexible glass substrates. Journal of Materials Chemistry C 2(43), 9109-9114.

Chen, J., Huang, D., Feng, Z.H., 2015a. A U-shaped piezoelectric resonator for a compact and high-performance pump system. Smart Materials and Structures 24(10), 105009.

Chen, J., Zhou, Y., Wang, D., He, F., Rotello, V.M., Carter, K.R., Watkins, J.J., Nugen, S.R., 2015b. UV-nanoimprint lithography as a tool to develop flexible microfluidic devices for electrochemical detection. Lab on a Chip 15(14), 3086-3094.

Chen, Y., Fang, Z., Merritt, B., Strack, D., Xu, J., Lee, S., 2016. Onset of particle trapping and release via acoustic bubbles. Lab on a Chip 16(16), 3024-3032.

Chen, Y.S., Tal, A., Torrance, D.B., Kuebler, S.M., 2006. Fabrication and characterization of three - dimensional silver - coated polymeric microstructures. Advanced Functional Materials 16(13), 1739-1744.

Cheng, Y.-T., Rodak, D.E., 2005. Is the lotus leaf superhydrophobic? Applied physics letters 86(14), 144101.

Childs, W.R., Nuzzo, R.G., 2002. Decal transfer microlithography: a new soft-lithographic patterning method. Journal of the American Chemical Society 124(45), 13583-13596.

Chindam, C., Nama, N., Ian Lapsley, M., Costanzo, F., Jun Huang, T., 2013. Theory and experiment on resonant frequencies of liquid-air interfaces trapped in

microfluidic devices. Journal of applied physics 114(19), 194503.

Choi, J.-H., Lee, S.-K., Lim, J.-M., Yang, S.-M., Yi, G.-R., 2010. Designed pneumatic valve actuators for controlled droplet breakup and generation. Lab on a Chip 10(4), 456-461.

Choi, S.J., Huh, S.Y., 2010. Direct structuring of a biomimetic anti - reflective, self - cleaning surface for light harvesting in organic solar cells. Macromolecular rapid communications 31(6), 539-544.

Chou, J.-C., Tsai, Y.-L., Cheng, T.-Y., Liao, Y.-H., Ye, G.-C., Yang, S.-Y., 2013. Fabrication of arrayed flexible screen-printed glucose biosensor based on microfluidic framework. IEEE Sensors Journal 14(1), 178-183.

Davis, E., Liu, Y., Jiang, L., Lu, Y., Ndao, S., 2017. Wetting characteristics of 3-dimensional nanostructured fractal surfaces. Applied Surface Science 392, 929-935.

De Vellis, A., Gritsenko, D., Lin, Y., Wu, Z., Zhang, X., Pan, Y., Xue, W., Xu, J., 2017. Drastic sensing enhancement using acoustic bubbles for surface-based microfluidic sensors. Sensors and Actuators B: Chemical 243, 298-302.

del Campo, A., Greiner, C., 2007. SU-8: a photoresist for high-aspect-ratio and 3D submicron lithography. Journal of micromechanics and microengineering 17(6), R81.

Delrot, P., Loterie, D., Psaltis, D., Moser, C., 2018. Single-photon three-dimensional microfabrication through a multimode optical fiber. Optics express 26(2), 1766-1778.

Di Carlo, D., Aghdam, N., Lee, L.P., 2006. Single-cell enzyme concentrations, kinetics, and inhibition analysis using high-density hydrodynamic cell isolation arrays. Analytical chemistry 78(14), 4925-4930.

Ding, Y., Qiu, F., Casadevall i Solvas, X., Chiu, F., Nelson, B., deMello, A., 2016. Microfluidic-based droplet and cell manipulations using artificial bacterial flagella. Micromachines 7(2), 25.

Dong, L., Cornaglia, M., Lehnert, T., Gijs, M.A., 2016. Versatile size-dependent sorting of C. elegans nematodes and embryos using a tunable microfluidic filter structure. Lab on a Chip 16(3), 574-585.

Ehrfeld, W., Schmidt, A., 1998. Recent developments in deep X-ray lithography. Journal of Vacuum Science & Technology B: Microelectronics and Nanometer Structures Processing, Measurement, and Phenomena 16(6), 3526-3534.

Eletxigerra, U., Martinez-Perdiguero, J., Merino, S., 2015. Disposable microfluidic immuno-biochip for rapid electrochemical detection of tumor necrosis factor alpha biomarker. Sensors and Actuators B: Chemical 221, 1406-1411.

Epstein, P.S., Plesset, M.S., 1950. On the stability of gas bubbles in liquid - gas

solutions. The Journal of Chemical Physics 18(11), 1505-1509.

Faloutsos, C., Gaede, V., 1996. Analysis of n-dimensional quadtrees using the Hausdorff fractal dimension. Computer Science Department, 548.

Fang, J., Wang, W., Zhao, S., 2015. Fabrication of 3D microfluidic structures. Encyclopedia of Microfluidics and Nanofluidics, 1069-1082.

Fang, W.-F., Lee, A.P., 2015. LCAT pump optimization for an integrated microfluidic droplet generator. Microfluidics and nanofluidics 18(5-6), 1265-1275.

Farrer, R.A., LaFratta, C.N., Li, L., Praino, J., Naughton, M.J., Saleh, B.E., Teich, M.C., Fourkas, J.T., 2006. Selective functionalization of 3-D polymer microstructures. Journal of the American Chemical Society 128(6), 1796-1797.

Feng, J., Tuominen, M.T., Rothstein, J.P., 2011. Hierarchical superhydrophobic surfaces fabricated by dual - scale electron - beam - lithography with well - ordered secondary nanostructures. Advanced Functional Materials 21(19), 3715-3722.

Feng, L., Li, S., Li, Y., Li, H., Zhang, L., Zhai, J., Song, Y., Liu, B., Jiang, L., Zhu, D., 2002. Super - hydrophobic surfaces: from natural to artificial. Advanced materials 14(24), 1857-1860.

Filipponi, L., Livingston, P., Kašpar, O., Tokárová, V., Nicolau, D.V., 2016. Protein patterning by microcontact printing using pyramidal PDMS stamps. Biomedical microdevices 18(1), 9.

Fina, F., Goyanes, A., Gaisford, S., Basit, A.W., 2017. Selective laser sintering (SLS) 3D printing of medicines. International journal of pharmaceutics 529(1-2), 285-293.

Fiorini, G.S., Chiu, D.T., 2005. Disposable microfluidic devices: fabrication, function, and application. BioTechniques 38(3), 429-446.

Focke, M., Kosse, D., Müller, C., Reinecke, H., Zengerle, R., von Stetten, F., 2010. Lab-on-a-Foil: microfluidics on thin and flexible films. Lab on a Chip 10(11), 1365-1386.

Folch, A., 2016. Introduction to bioMEMS. CRC Press.

Fong, J., Xiao, Z., Takahata, K., 2015. Wireless implantable chip with integrated nitinol-based pump for radio-controlled local drug delivery. Lab on a Chip 15(4), 1050-1058.

Formanek, F., Takeyasu, N., Tanaka, T., Chiyoda, K., Ishikawa, A., Kawata, S., 2006. Selective electroless plating to fabricate complex three-dimensional metallic micro/nanostructures. Applied physics letters 88(8), 083110.

French, P., Sarro, P., 1998. Surface versus bulk micromachining: the contest for suitable applications. Journal of Micromechanics and microengineering 8(2), 45.

Göppert - Mayer, M., 1931. Über elementarakte mit zwei quantensprüngen. Annalen der Physik 401(3), 273-294.

Gaal, G., Mendes, M., de Almeida, T.P., Piazzetta, M.H., Gobbi, Â.L., Riul Jr, A., Rodrigues, V., 2017. Simplified fabrication of integrated microfluidic devices using fused deposition modeling 3D printing. Sensors and Actuators B: Chemical 242, 35-40.

Gibson, I., Rosen, D.W., Stucker, B., 2014. Additive manufacturing technologies. Springer.

Girardo, S., Cecchini, M., Beltram, F., Cingolani, R., Pisignano, D., 2008. Polydimethylsiloxane–LiNbO 3 surface acoustic wave micropump devices for fluid control into microchannels. Lab on a Chip 8(9), 1557-1563.

Gravesen, P., Branebjerg, J., Jensen, O.S., 1993. Microfluidics-a review. Journal of micromechanics and microengineering 3(4), 168.

Gritsenko, D., Lin, Y., Hovorka, V., Zhang, Z., Ahmadianyazdi, A., Xu, J., 2018. Vibrational modes prediction for water-air bubbles trapped in circular microcavities. Physics of Fluids 30(8), 082001.

Hammarström, B., Evander, M., Barbeau, H., Bruzelius, M., Larsson, J., Laurell, T., Nilsson, J., 2010. Non-contact acoustic cell trapping in disposable glass capillaries. Lab on a Chip 10(17), 2251-2257.

Han, C.-J., Chiang, H.-P., Cheng, Y.-C., 2018. Using micro-molding and stamping to fabricate conductive polydimethylsiloxane-based flexible high-sensitivity strain gauges. Sensors 18(2), 618.

Han, D.D., Zhang, Y.L., Ma, J.N., Liu, Y.Q., Han, B., Sun, H.B., 2016. Light - Mediated Manufacture and Manipulation of Actuators. Advanced Materials 28(38), 8328-8343.

Hashmi, A., Heiman, G., Yu, G., Lewis, M., Kwon, H.-J., Xu, J., 2013. Oscillating bubbles in teardrop cavities for microflow control. Microfluidics and nanofluidics 14(3-4), 591-596.

Hashmi, A., Xu, J., 2014. On the quantification of mixing in microfluidics. Journal of laboratory automation 19(5), 488-491.

He, Y., Wu, Y., Fu, J.z., Gao, Q., Qiu, J.j., 2016. Developments of 3D printing microfluidics and applications in chemistry and biology: a review. Electroanalysis 28(8), 1658-1678.

Hejazi, V., Moghadam, A.D., Rohatgi, P., Nosonovsky, M., 2014. Beyond Wenzel and Cassie–Baxter: second-order effects on the wetting of rough surfaces. Langmuir 30(31), 9423-9429.

Herr, A.E., Hatch, A.V., Throckmorton, D.J., Tran, H.M., Brennan, J.S., Giannobile, W.V., Singh, A.K., 2007. Microfluidic immunoassays as rapid saliva-based clinical diagnostics. Proceedings of the National Academy of Sciences

104(13), 5268-5273.

Hoppe, P.S., Schwarzfischer, M., Loeffler, D., Kokkaliaris, K.D., Hilsenbeck, O., Moritz, N., Endele, M., Filipczyk, A., Gambardella, A., Ahmed, N., 2016. Early myeloid lineage choice is not initiated by random PU. 1 to GATA1 protein ratios. Nature 535(7611), 299.

Hu, Z., Chen, X., 2018. Fabrication of polyethylene terephthalate microfluidic chip using CO2 laser system. International Polymer Processing 33(1), 106-109.

Huang, P.-H., Chan, C.Y., Li, P., Wang, Y., Nama, N., Bachman, H., Huang, T.J., 2018. A sharp-edge-based acoustofluidic chemical signal generator. Lab on a Chip 18(10), 1411-1421.

Huang, P.-H., Ian Lapsley, M., Ahmed, D., Chen, Y., Wang, L., Jun Huang, T., 2012. A single-layer, planar, optofluidic switch powered by acoustically driven, oscillating microbubbles. Applied physics letters 101(14), 141101.

Huang, P.-H., Nama, N., Mao, Z., Li, P., Rufo, J., Chen, Y., Xie, Y., Wei, C.-H., Wang, L., Huang, T.J., 2014. A reliable and programmable acoustofluidic pump powered by oscillating sharp-edge structures. Lab on a Chip 14(22), 4319-4323.

Huang, P.-H., Xie, Y., Ahmed, D., Rufo, J., Nama, N., Chen, Y., Chan, C.Y., Huang, T.J., 2013. An acoustofluidic micromixer based on oscillating sidewall sharp-edges. Lab on a Chip 13(19), 3847-3852.

Huang, Y., Paloczi, G.T., Yariv, A., Zhang, C., Dalton, L.R., 2004. Fabrication and replication of polymer integrated optical devices using electron-beam lithography and soft lithography. The Journal of Physical Chemistry B 108(25), 8606-8613.

Huh, D., Matthews, B.D., Mammoto, A., Montoya-Zavala, M., Hsin, H.Y., Ingber, D.E., 2010. Reconstituting organ-level lung functions on a chip. Science 328(5986), 1662-1668.

Hussein, H.J., Capp, S.P., George, W.K., 1994. Velocity measurements in a high-Reynolds-number, momentum-conserving, axisymmetric, turbulent jet. Journal of Fluid Mechanics 258, 31-75.

Hwang, Y., Paydar, O.H., Candler, R.N., 2015. 3D printed molds for non-planar PDMS microfluidic channels. Sensors and Actuators A: Physical 226, 137-142.

Jang, S., Lee, B., Jeong, H.-H., Jin, S.H., Jang, S., Kim, S.G., Jung, G.Y., Lee, C.-S., 2016. On-chip analysis, indexing and screening for chemical producing bacteria in a microfluidic static droplet array. Lab on a Chip 16(10), 1909-1916.

Jeon, N.L., Hu, J., Whitesides, G., Erhardt, M.K., Nuzzo, R.G., 1998. Fabrication of silicon MOSFETs using soft lithography. Advanced Materials 10(17), 1466-1469.

Jiang, L.J., Zhou, Y.S., Xiong, W., Gao, Y., Huang, X., Jiang, L., Baldacchini, T.,

Silvain, J.-F., Lu, Y.F., 2014. Two-photon polymerization: investigation of chemical and mechanical properties of resins using Raman microspectroscopy. Optics letters 39(10), 3034-3037.

Jin, H., Zhou, J., He, X., Wang, W., Guo, H., Dong, S., Wang, D., Xu, Y., Geng, J., Luo, J., 2013. Flexible surface acoustic wave resonators built on disposable plastic film for electronics and lab-on-a-chip applications. Scientific reports 3, 2140.

Jo, M.C., Liu, W., Gu, L., Dang, W., Qin, L., 2015. High-throughput analysis of yeast replicative aging using a microfluidic system. Proceedings of the National Academy of Sciences 112(30), 9364-9369.

Juodkazis, S., Mizeikis, V., Seet, K.K., Miwa, M., Misawa, H., 2005. Two-photon lithography of nanorods in SU-8 photoresist. Nanotechnology 16(6), 846.

Körner, C., 2016. Additive manufacturing of metallic components by selective electron beam melting—a review. International Materials Reviews 61(5), 361-377.

Kai, Y., 2004. Wafer warpage detection during bake process in photolithography.

Kaiser, W., Garrett, C., 1961. Two-photon excitation in Ca F 2: Eu 2+. Physical review letters 7(6), 229.

Kamei, K.-i., Mashimo, Y., Koyama, Y., Fockenberg, C., Nakashima, M., Nakajima, M., Li, J., Chen, Y., 2015. 3D printing of soft lithography mold for rapid production of polydimethylsiloxane-based microfluidic devices for cell stimulation with concentration gradients. Biomedical microdevices 17(2), 36.

Kanai, T., Tsuchiya, M., 2016. Microfluidic devices fabricated using stereolithography for preparation of monodisperse double emulsions. Chemical Engineering Journal 290, 400-404.

Kane, R.S., Takayama, S., Ostuni, E., Ingber, D.E., Whitesides, G.M., 1999. Patterning proteins and cells using soft lithography. The Biomaterials: Silver Jubilee Compendium, pp. 161-174. Elsevier.

Karlsen, J.T., Bruus, H., 2015. Forces acting on a small particle in an acoustical field in a thermoviscous fluid. Physical Review E 92(4), 043010.

Ke, Z., Yongping, B., 2005. Improve the gas barrier property of PET film with montmorillonite by in situ interlayer polymerization. Materials Letters 59(27), 3348-3351.

Khurana, V., Lindquist, S., 2010. Modelling neurodegeneration in Saccharomyces cerevisiae: why cook with baker's yeast? Nature Reviews Neuroscience 11(6), 436.

Kim, E., Xia, Y., Whitesides, G.M., 1995. Polymer microstructures formed by moulding in capillaries. Nature 376(6541), 581.

Kim, P., Kwon, K.W., Park, M.C., Lee, S.H., Kim, S.M., Suh, K.Y., 2008. Soft lithography for microfluidics: a review.

Kim, S., Qiu, F., Kim, S., Ghanbari, A., Moon, C., Zhang, L., Nelson, B.J., Choi, H., 2013. Fabrication and characterization of magnetic microrobots for three - dimensional cell culture and targeted transportation. Advanced Materials 25(41), 5863-5868.

King, E., Xia, Y., Zhao, X.M., Whitesides, G.M., 1997. Solvent - assisted microcontact molding: A convenient method for fabricating three - dimensional structures on surfaces of polymers. Advanced Materials 9(8), 651-654.

Koh, A., Kang, D., Xue, Y., Lee, S., Pielak, R.M., Kim, J., Hwang, T., Min, S., Banks, A., Bastien, P., 2016. A soft, wearable microfluidic device for the capture, storage, and colorimetric sensing of sweat. Science translational medicine 8(366), 366ra165-366ra165.

Kuang, Y., Biran, I., Walt, D.R., 2004. Simultaneously monitoring gene expression kinetics and genetic noise in single cells by optical well arrays. Analytical Chemistry 76(21), 6282-6286.

Kurihara, M., Heo, Y., Kuribayashi-Shigetomi, K., Takeuchi, S., 2012. 3D laser lithography combined with Parylene coating for the rapid fabrication of 3D microstructures. 2012 IEEE 25th International Conference on Micro Electro Mechanical Systems (MEMS), pp. 196-199. IEEE.

Kwon, H.-J., Yeo, J., Jang, J., Grigoropoulos, C., Yoo, J.-H., 2018. Single pass laser process for super-hydrophobic flexible surfaces with micro/nano hierarchical structures. Materials 11(7), 1226.

Kwon, Y., Patankar, N., Choi, J., Lee, J., 2009. Design of surface hierarchy for extreme hydrophobicity. Langmuir 25(11), 6129-6136.

Lawson, D.A., Bhakta, N.R., Kessenbrock, K., Prummel, K.D., Yu, Y., Takai, K., Zhou, A., Eyob, H., Balakrishnan, S., Wang, C.-Y., 2015. Single-cell analysis reveals a stem-cell program in human metastatic breast cancer cells. Nature 526(7571), 131.

Lee, C.-Y., Wang, W.-T., Liu, C.-C., Fu, L.-M., 2016. Passive mixers in microfluidic systems: A review. Chemical Engineering Journal 288, 146-160.

Lee, J.B., Choi, K.-H., Yoo, K., 2015. Innovative SU-8 lithography techniques and their applications. Micromachines 6(1), 1-18.

Lee, K.-S., Kim, R.H., Yang, D.-Y., Park, S.H., 2008. Advances in 3D nano/microfabrication using two-photon initiated polymerization. Progress in Polymer Science 33(6), 631-681.

Lemoff, A.V., Lee, A.P., 2000. An AC magnetohydrodynamic micropump. Sensors and Actuators B: Chemical 63(3), 178-185.

Li, H.-W., Kang, D.-J., Blamire, M., Huck, W.T., 2003. Focused ion beam fabrication of silicon print masters. Nanotechnology 14(2), 220.

Li, J., Liu, C., Qiao, H., Zhu, L., Chen, G., Dai, X., 2007. Hot embossing/bonding of a

poly (ethylene terephthalate)(PET) microfluidic chip. Journal of Micromechanics and Microengineering 18(1), 015008.

Li, Z., Pucher, N., Cicha, K., Torgersen, J., Ligon, S.C., Ajami, A., Husinsky, W., Rosspeintner, A., Vauthey, E., Naumov, S., 2013. A straightforward synthesis and structure–activity relationship of highly efficient initiators for two-photon polymerization. Macromolecules 46(2), 352-361.

Lin, C.-H., Lee, G.-B., Chang, B.-W., Chang, G.-L., 2002. A new fabrication process for ultra-thick microfluidic microstructures utilizing SU-8 photoresist. Journal of Micromechanics and Microengineering 12(5), 590.

Lin, L., Lin, X., Lin, L., Feng, Q., Kitamori, T., Lin, J.-M., Sun, J., 2017. Integrated Microfluidic Platform with Multiple Functions To Probe Tumor–Endothelial Cell Interaction. Analytical chemistry 89(18), 10037-10044.

Lin, P., Luo, X., Hsing, I.M., Yan, F., 2011. Organic electrochemical transistors integrated in flexible microfluidic systems and used for label - free DNA sensing. Advanced Materials 23(35), 4035-4040.

Lin, S.-C., Lu, J.-C., Sung, Y.-L., Lin, C.-T., Tung, Y.-C., 2013. A low sample volume particle separation device with electrokinetic pumping based on circular travelling-wave electroosmosis. Lab on a Chip 13(15), 3082-3089.

Lin, Y., Gao, C., Gao, Y., Wu, M., Yazdi, A.A., Xu, J., 2019a. Acoustofluidic micromixer on lab-on-a-foil devices. Sensors and Actuators B: Chemical 287, 312-319.

Lin, Y., Gao, C., Gritsenko, D., Zhou, R., Xu, J., 2018. Soft lithography based on photolithography and two-photon polymerization. Microfluidics and Nanofluidics 22(9), 97.

Lin, Y., Gao, Y., Wu, M., Zhou, R., Chung, D., Caraveo, G., Xu, J., 2019b. Acoustofluidic stick-and-play micropump built on foil for single-cell trapping. Lab on a Chip.

Lin, Y., Gritsenko, D., Feng, S., Teh, Y.C., Lu, X., Xu, J., 2016a. Detection of heavy metal by paper-based microfluidics. Biosensors and Bioelectronics 83, 256-266.

Lin, Y., Gritsenko, D., Liu, Q., Lu, X., Xu, J., 2016b. Recent advancements in functionalized paper-based electronics. ACS Applied Materials & Interfaces 8(32), 20501-20515.

Lin, Y., Xu, J., 2017. fluidic Based Sensing in Food Safety and Quality Analysis. Sensing Techniques for Food Safety and Quality Control, pp. 95-120.

Lin, Y., Xu, J., 2018. Microstructures Fabricated by Two - Photon Polymerization and Their Remote Manipulation Techniques: Toward 3D Printing of Micromachines. Advanced Optical Materials 6(8), 1701359.

Liu, B., He, Y., Fan, Y., Wang, X., 2006. Fabricating super - hydrophobic lotus - leaf - like surfaces through soft - lithographic imprinting. Macromolecular rapid

communications 27(21), 1859-1864.

Liu, R.H., Yang, J., Pindera, M.Z., Athavale, M., Grodzinski, P., 2002. Bubble-induced acoustic micromixing. Lab on a Chip 2(3), 151-157.

Liu, X., Gu, H., Wang, M., Du, X., Gao, B., Elbaz, A., Sun, L., Liao, J., Xiao, P., Gu, Z., 2018. 3D printing of bioinspired liquid superrepellent structures. Advanced Materials 30(22), 1800103.

Liu, Y., Das, A., Lin, Z., Cooper, I.B., Rohatgi, A., Wong, C., 2014. Hierarchical robust textured structures for large scale self-cleaning black silicon solar cells. Nano Energy 3, 127-133.

Liu, Y., Pharr, M., Salvatore, G.A., 2017. Lab-on-skin: a review of flexible and stretchable electronics for wearable health monitoring. ACS nano 11(10), 9614-9635.

Luong, D.X., Subramanian, A.K., Silva, G.A.L., Yoon, J., Cofer, S., Yang, K., Owuor, P.S., Wang, T., Wang, Z., Lou, J., 2018. Laminated Object Manufacturing of 3D - Printed Laser - Induced Graphene Foams. Advanced Materials 30(28), 1707416.

Ma, T., Sun, S., Li, B., Chu, J., 2019. Piezoelectric peristaltic micropump integrated on a microfluidic chip. Sensors and Actuators A: Physical 292, 90-96.

Malek, C.K., Robert, L., Salut, R., 2009. Femtosecond laser machining and lamination for large-area flexible organic microfluidic chips. The European Physical Journal-Applied Physics 46(1).

Mali, P., Sarkar, A., Lal, R., 2006. Facile fabrication of microfluidic systems using electron beam lithography. Lab on a Chip 6(2), 310-315.

Marino, A., Filippeschi, C., Mattoli, V., Mazzolai, B., Ciofani, G., 2015. Biomimicry at the nanoscale: current research and perspectives of two-photon polymerization. Nanoscale 7(7), 2841-2850.

Maruo, S., Nakamura, O., Kawata, S., 1997. Three-dimensional microfabrication with two-photon-absorbed photopolymerization. Optics letters 22(2), 132-134.

Mata, A., Fleischman, A.J., Roy, S., 2006. Fabrication of multi-layer SU-8 microstructures. Journal of micromechanics and microengineering 16(2), 276.

Mazutis, L., Gilbert, J., Ung, W.L., Weitz, D.A., Griffiths, A.D., Heyman, J.A., 2013. Single-cell analysis and sorting using droplet-based microfluidics. Nature protocols 8(5), 870.

Merkel, T., Bondar, V., Nagai, K., Freeman, B.D., Pinnau, I., 2000. Gas sorption, diffusion, and permeation in poly (dimethylsiloxane). Journal of Polymer Science Part B: Polymer Physics 38(3), 415-434.

Mitra, S.K., Chakraborty, S., 2016. Microfluidics and nanofluidics handbook: fabrication, implementation, and applications. CRC press.

Miyajima, H., Mehregany, M., 1995. High-aspect-ratio photolithography for MEMS applications. Journal of microelectromechanical systems 4(4), 220-229.

Morariu, M.D., Voicu, N.E., Schäffer, E., Lin, Z., Russell, T.P., Steiner, U., 2003. Hierarchical structure formation and pattern replication induced by an electric field. Nature materials 2(1), 48.

Muller, P.B., Barnkob, R., Jensen, M.J.H., Bruus, H., 2012. A numerical study of microparticle acoustophoresis driven by acoustic radiation forces and streaming-induced drag forces. Lab on a Chip 12(22), 4617-4627.

Nakashoji, Y., Tanaka, H., Tsukagoshi, K., Hashimoto, M., 2017. A poly (dimethylsiloxane) microfluidic sheet reversibly adhered on a glass plate for creation of emulsion droplets for droplet digital PCR. Electrophoresis 38(2), 296-304.

Nama, N., Huang, P.-H., Huang, T.J., Costanzo, F., 2014. Investigation of acoustic streaming patterns around oscillating sharp edges. Lab on a Chip 14(15), 2824-2836.

Narayan, S., Bae, K., Lehn, R., Yadav, S., Ott, M., Meckel, T., Stark, R.W., 2018. Low-pressure bonding of monolithic SU-8 microfluidic devices. Journal of Micromechanics and Microengineering 28(12), 125001.

Narimannezhad, A., Jennings, J., Weber, M.H., Lynn, K.G., 2013. Fabrication of high aspect ratio micro-Penning-Malmberg gold plated silicon trap arrays. arXiv preprint arXiv:1307.2335.

Ngo, T.D., Kashani, A., Imbalzano, G., Nguyen, K.T., Hui, D., 2018. Additive manufacturing (3D printing): A review of materials, methods, applications and challenges. Composites Part B: Engineering 143, 172-196.

Nie, J., Liang, Y., Zhang, Y., Le, S., Li, D., Zhang, S., 2013. One-step patterning of hollow microstructures in paper by laser cutting to create microfluidic analytical devices. Analyst 138(2), 671-676.

Niu, F., Wu, D., Ma, G., Zhang, B., 2015. Additive manufacturing of ceramic structures by laser engineered net shaping. Chinese Journal of Mechanical Engineering 28(6), 1117-1122.

Oskooei, A., Günther, A., 2015. Bubble pump: scalable strategy for in-plane liquid routing. Lab on a Chip 15(13), 2842-2853.

Ovsianikov, A., Chichkov, B.N., 2008. Two-Photon Polymerization–High Resolution 3D Laser Technology and Its Applications. Nanoelectronics and Photonics, pp. 427-446. Springer.

Ozcelik, A., Rufo, J., Guo, F., Gu, Y., Li, P., Lata, J., Huang, T.J., 2018. Acoustic tweezers for the life sciences. Nature methods, 1.

Pang, C., Lee, C., Suh, K.Y., 2013. Recent advances in flexible sensors for wearable and implantable devices. Journal of Applied Polymer Science 130(3), 1429-

1441.

Pang, M., Lin, J., Cheng, Z., Fu, J., Xing, R., Wang, S., 2003. Patterning and luminescent properties of nanocrystalline Y2O3: Eu3+ phosphor films by sol–gel soft lithography. Materials Science and Engineering: B 100(2), 124-131.

Park, J., Li, J., Han, A., 2010. Micro-macro hybrid soft-lithography master (MMHSM) fabrication for lab-on-a-chip applications. Biomedical microdevices 12(2), 345-351.

Park, S.H., Yang, D.Y., Lee, K.S., 2009. Two - photon stereolithography for realizing ultraprecise three - dimensional nano/microdevices. Laser & Photonics Reviews 3(1 - 2), 1-11.

Patel, M.V., Nanayakkara, I.A., Simon, M.G., Lee, A.P., 2014. Cavity-induced microstreaming for simultaneous on-chip pumping and size-based separation of cells and particles. Lab on a Chip 14(19), 3860-3872.

Patel, M.V., Tovar, A.R., Lee, A.P., 2012. Lateral cavity acoustic transducer as an on-chip cell/particle microfluidic switch. Lab on a Chip 12(1), 139-145.

Patel, M.V., Tovar, A.R., Tong, K.S., Lee, A.P., 2009. Lateral cavity acoustic transducer for particle sorting applications. The Proceedings of MicroTAS 2009.

Patko, D., Mártonfalvi, Z., Kovacs, B., Vonderviszt, F., Kellermayer, M., Horvath, R., 2014. Microfluidic channels laser-cut in thin double-sided tapes: Cost-effective biocompatible fluidics in minutes from design to final integration with optical biochips. Sensors and Actuators B: Chemical 196, 352-356.

Patra, D., Sengupta, S., Duan, W., Zhang, H., Pavlick, R., Sen, A., 2013. Intelligent, self-powered, drug delivery systems. Nanoscale 5(4), 1273-1283.

Pokroy, B., Kang, S.H., Mahadevan, L., Aizenberg, J., 2009. Self-organization of a mesoscale bristle into ordered, hierarchical helical assemblies. Science 323(5911), 237-240.

Qin, D., Xia, Y., Whitesides, G.M., 2010. Soft lithography for micro-and nanoscale patterning. Nature protocols 5(3), 491.

Queste, S., Salut, R., Clatot, S., Rauch, J.-Y., Malek, C.G.K., 2010. Manufacture of microfluidic glass chips by deep plasma etching, femtosecond laser ablation, and anodic bonding. Microsystem Technologies 16(8-9), 1485-1493.

Raimondi, M.T., Eaton, S.M., Nava, M.M., Laganà, M., Cerullo, G., Osellame, R., 2012. Two-photon laser polymerization: from fundamentals to biomedical application in tissue engineering and regenerative medicine. Journal of applied biomaterials & functional materials 10(1), 56-66.

Ramaratnam, K., Tsyalkovsky, V., Klep, V., Luzinov, I., 2007. Ultrahydrophobic textile surface via decorating fibers with monolayer of reactive nanoparticles and non-fluorinated polymer. Chemical Communications(43), 4510-4512.

Rambach, R.W., Linder, K., Heymann, M., Franke, T., 2017. Droplet trapping and fast

acoustic release in a multi-height device with steady-state flow. Lab on a Chip 17(20), 3422-3430.

Ren, K., Zhou, J., Wu, H., 2013. Materials for microfluidic chip fabrication. Accounts of chemical research 46(11), 2396-2406.

Rettig, J.R., Folch, A., 2005. Large-scale single-cell trapping and imaging using microwell arrays. Analytical chemistry 77(17), 5628-5634.

Rogers, J.A., Nuzzo, R.G., 2005. Recent progress in soft lithography. Materials today 8(2), 50-56.

Rumi, M., Barlow, S., Wang, J., Perry, J.W., Marder, S.R., 2008. Two-photon absorbing materials and two-photon-induced chemistry. Photoresponsive Polymers I, pp. 1-95. Springer.

Russel, M., Hasnain, S., Selvaganapathy, P., Ching, C., 2016. Effect of doping ferrocene in the working fluid of electrohydrodynamic (EHD) micropumps. Microfluidics and Nanofluidics 20(8), 112.

Santiago-Felipe, S., Tortajada-Genaro, L.A., Carrascosa, J., Puchades, R., Maquieira, Á., 2016. Real-time loop-mediated isothermal DNA amplification in compact disc micro-reactors. Biosensors and Bioelectronics 79, 300-306.

Saotome, Y., Iwazaki, H., 2001. Superplastic backward microextrusion of microparts for micro-electro-mechanical systems. Journal of Materials Processing Technology 119(1-3), 307-311.

Schizas, C., Melissinaki, V., Gaidukeviciute, A., Reinhardt, C., Ohrt, C., Dedoussis, V., Chichkov, B.N., Fotakis, C., Farsari, M., Karalekas, D., 2010. On the design and fabrication by two-photon polymerization of a readily assembled micro-valve. The International Journal of Advanced Manufacturing Technology 48(5-8), 435-441.

Schmid, L., Wixforth, A., Weitz, D.A., Franke, T., 2012. Novel surface acoustic wave (SAW)-driven closed PDMS flow chamber. Microfluidics and nanofluidics 12(1-4), 229-235.

Schneider, F., Draheim, J., Kamberger, R., Wallrabe, U., 2009. Process and material properties of polydimethylsiloxane (PDMS) for Optical MEMS. Sensors and Actuators A: Physical 151(2), 95-99.

Selimis, A., Farsari, M., 2017. Hybrid Materials for Multiphoton Polymerization. Multiphoton Lithography.

Settnes, M., Bruus, H., 2012. Forces acting on a small particle in an acoustical field in a viscous fluid. Physical Review E 85(1), 016327.

Shen, K., Chen, X., Guo, M., Cheng, J., 2005. A microchip-based PCR device using flexible printed circuit technology. Sensors and Actuators B: Chemical 105(2), 251-258.

Shibuichi, S., Onda, T., Satoh, N., Tsujii, K., 1996. Super water-repellent surfaces

resulting from fractal structure. The Journal of Physical Chemistry 100(50), 19512-19517.

Shin, Y.S., Cho, K., Lim, S.H., Chung, S., Park, S.-J., Chung, C., Han, D.-C., Chang, J.K., 2003. PDMS-based micro PCR chip with parylene coating. Journal of Micromechanics and Microengineering 13(5), 768.

Skylaki, S., Hilsenbeck, O., Schroeder, T., 2016. Challenges in long-term imaging and quantification of single-cell dynamics. Nature biotechnology 34(11), 1137.

Staudinger, U., Zyla, G., Krause, B., Janke, A., Fischer, D., Esen, C., Voit, B., Ostendorf, A., 2017. Development of electrically conductive microstructures based on polymer/CNT nanocomposites via two-photon polymerization. Microelectronic Engineering 179, 48-55.

Stavrakis, S., Holzner, G., Choo, J., DeMello, A., 2019. High-throughput microfluidic imaging flow cytometry. Current opinion in biotechnology 55, 36-43.

Steigert, J., Haeberle, S., Brenner, T., Müller, C., Steinert, C., Koltay, P., Gottschlich, N., Reinecke, H., Rühe, J., Zengerle, R., 2007. Rapid prototyping of microfluidic chips in COC. Journal of Micromechanics and Microengineering 17(2), 333.

Strandwitz, N.C., Khan, A., Boettcher, S.W., Mikhailovsky, A.A., Hawker, C.J., Nguyen, T.-Q., Stucky, G.D., 2008. One-and two-photon induced polymerization of methylmethacrylate using colloidal CdS semiconductor quantum dots. Journal of the American Chemical Society 130(26), 8280-8288.

Sugioka, K., Xu, J., Wu, D., Hanada, Y., Wang, Z., Cheng, Y., Midorikawa, K., 2014. Femtosecond laser 3D micromachining: a powerful tool for the fabrication of microfluidic, optofluidic, and electrofluidic devices based on glass. Lab on a Chip 14(18), 3447-3458.

Sun, G., Gao, T., Zhao, X., Zhang, H., 2010. Fabrication of micro/nano dual-scale structures by improved deep reactive ion etching. Journal of Micromechanics and Microengineering 20(7), 075028.

Sun, T., Feng, L., Gao, X., Jiang, L., 2005a. Bioinspired surfaces with special wettability. Accounts of chemical research 38(8), 644-652.

Sun, Y., Zhang, Z., Wong, C., 2005b. Photo-definable nanocomposite for wafer level packaging. Proceedings Electronic Components and Technology, 2005. ECTC'05., pp. 179-184. IEEE.

Synytska, A., Ionov, L., Grundke, K., Stamm, M., 2009. Wetting on Fractal Superhydrophobic Surfaces from "Core− Shell" Particles: A Comparison of Theory and Experiment. Langmuir 25(5), 3132-3136.

Tabeling, P., 2005. Introduction to microfluidics. OUP Oxford.

Taff, B.M., Voldman, J., 2005. A scalable addressable positive-dielectrophoretic cell-sorting array. Analytical chemistry 77(24), 7976-7983.

Tan, S.H., Nguyen, N.-T., Chua, Y.C., Kang, T.G., 2010. Oxygen plasma treatment for reducing hydrophobicity of a sealed polydimethylsiloxane microchannel. Biomicrofluidics 4(3), 032204.

Tan, S.J., Yobas, L., Lee, G.Y.H., Ong, C.N., Lim, C.T., 2009. Microdevice for the isolation and enumeration of cancer cells from blood. Biomedical microdevices 11(4), 883-892.

Tian, Y., Lu, D., Jiang, H., Lin, X., 2012. Preparation of a novel ferrofluidic photoresist for two-photon photopolymerization technique. Journal of Magnetism and Magnetic Materials 324(20), 3291-3294.

Tovar, A.R., Lee, A.P., 2009. Lateral cavity acoustic transducer. Lab on a Chip 9(1), 41-43.

Tovar, A.R., Patel, M.V., Lee, A.P., 2011. Lateral air cavities for microfluidic pumping with the use of acoustic energy. Microfluidics and Nanofluidics 10(6), 1269-1278.

Tricinci, O., Terencio, T., Mazzolai, B., Pugno, N.M., Greco, F., Mattoli, V., 2015. 3D micropatterned surface inspired by Salvinia molesta via direct laser lithography. ACS applied materials & interfaces 7(46), 25560-25567.

Truckenmüller, R., Giselbrecht, S., van Blitterswijk, C., Dambrowsky, N., Gottwald, E., Mappes, T., Rolletschek, A., Saile, V., Trautmann, C., Weibezahn, K.-F., 2008. Flexible fluidic microchips based on thermoformed and locally modified thin polymer films. Lab on a Chip 8(9), 1570-1579.

Van Phan, H., Coşkun, M.B., Şeşen, M., Pandraud, G., Neild, A., Alan, T., 2015. Vibrating membrane with discontinuities for rapid and efficient microfluidic mixing. Lab on a Chip 15(21), 4206-4216.

Vasileiou, T., Gerber, J., Prautzsch, J., Schutzius, T.M., Poulikakos, D., 2016. Superhydrophobicity enhancement through substrate flexibility. Proceedings of the National Academy of Sciences 113(47), 13307-13312.

Versura, P., Bavelloni, A., Blalock, W., Fresina, M., Campos, E.C., 2012. A rapid standardized quantitative microfluidic system approach for evaluating human tear proteins. Molecular vision 18, 2526.

Waheed, S., Cabot, J.M., Macdonald, N.P., Lewis, T., Guijt, R.M., Paull, B., Breadmore, M.C., 2016. 3D printed microfluidic devices: enablers and barriers. Lab on a Chip 16(11), 1993-2013.

Walczak, R., Adamski, K., 2015. Inkjet 3D printing of microfluidic structures—on the selection of the printer towards printing your own microfluidic chips. Journal of Micromechanics and Microengineering 25(8), 085013.

Waldner, J.-B., 2013. Nanocomputers and swarm intelligence. John Wiley & Sons.

Wang, L., Gong, Q., Zhan, S., Jiang, L., Zheng, Y., 2016a. Robust anti - icing performance of a flexible superhydrophobic surface. Advanced Materials

28(35), 7729-7735.

Wang, S., Chinnasamy, T., Lifson, M.A., Inci, F., Demirci, U., 2016b. Flexible substrate-based devices for point-of-care diagnostics. Trends in biotechnology 34(11), 909-921.

Wang, X., Cheng, C., Wang, S., Liu, S., 2009. Electroosmotic pumps and their applications in microfluidic systems. Microfluidics and Nanofluidics 6(2), 145-162.

Wang, X.Y., Ma, Y.T., Yan, G.Y., Huang, D., Feng, Z.H., 2014. High flow-rate piezoelectric micropump with two fixed ends polydimethylsiloxane valves and compressible spaces. Sensors and Actuators A: Physical 218, 94-104.

Wang, Y.-N., Fu, L.-M., 2018. Micropumps and biomedical applications–A review. Microelectronic Engineering 195, 121-138.

Wasay, A., Sameoto, D., 2015. Gecko gaskets for self-sealing and high-strength reversible bonding of microfluidics. Lab on a Chip 15(13), 2749-2753.

Weibel, D.B., Whitesides, G.M., 2006. Applications of microfluidics in chemical biology. Current opinion in chemical biology 10(6), 584-591.

Weiss, I., Marom, D.M., 2015. Direct 3D nano-printing on optical fiber tip. 2015 International Conference on Optical MEMS and Nanophotonics (OMN), pp. 1-2. IEEE.

Wheeler, A.R., Throndset, W.R., Whelan, R.J., Leach, A.M., Zare, R.N., Liao, Y.H., Farrell, K., Manger, I.D., Daridon, A., 2003. Microfluidic device for single-cell analysis. Analytical chemistry 75(14), 3581-3586.

Whitesides, G.M., 2006. The origins and the future of microfluidics. Nature 442(7101), 368.

Whitesides, G.M., Ostuni, E., Takayama, S., Jiang, X., Ingber, D.E., 2001. Soft lithography in biology and biochemistry. Annual review of biomedical engineering 3(1), 335-373.

Wong, K.V., Hernandez, A., 2012. A review of additive manufacturing. ISRN Mechanical Engineering 2012.

Wong, R.D.P., Posner, J.D., Santos, V.J., 2012. Flexible microfluidic normal force sensor skin for tactile feedback. Sensors and Actuators A: Physical 179, 62-69.

Wu, H., Lin, D., Pan, W., 2010a. High performance surface-enhanced Raman scattering substrate combining low dimensional and hierarchical nanostructures. Langmuir 26(10), 6865-6868.

Wu, J., Xia, J., Lei, W., Wang, B., 2010b. Superhydrophobic surface based on a coral-like hierarchical structure of ZnO. PLoS One 5(12), e14475.

Wu, J., Xia, J., Zhang, Y.-n., Lei, W., Wang, B.-p., 2010c. A simple method to fabricate

the different extents of superhydrophobic surfaces. Physica E: Low-dimensional Systems and Nanostructures 42(5), 1325-1328.

Wu, M., Huang, P.H., Zhang, R., Mao, Z., Chen, C., Kemeny, G., Li, P., Lee, A.V., Gyanchandani, R., Armstrong, A.J., 2018. Circulating Tumor Cell Phenotyping via High - Throughput Acoustic Separation. Small 14(32), 1801131.

Xia, H., Wang, J., Tian, Y., Chen, Q.D., Du, X.B., Zhang, Y.L., He, Y., Sun, H.B., 2010. Ferrofluids for fabrication of remotely controllable micro - nanomachines by two - photon polymerization. Advanced Materials 22(29), 3204-3207.

Xia, Y., Whitesides, G.M., 1998. Soft lithography. Annual review of materials science 28(1), 153-184.

Xing, J.-F., Zheng, M.-L., Duan, X.-M., 2015. Two-photon polymerization microfabrication of hydrogels: an advanced 3D printing technology for tissue engineering and drug delivery. Chemical Society Reviews 44(15), 5031-5039.

Xiu, Y., Liu, Y., Hess, D.W., Wong, C., 2010. Mechanically robust superhydrophobicity on hierarchically structured Si surfaces. Nanotechnology 21(15), 155705.

Xu, B.-B., Zhang, Y.-L., Xia, H., Dong, W.-F., Ding, H., Sun, H.-B., 2013. Fabrication and multifunction integration of microfluidic chips by femtosecond laser direct writing. Lab on a Chip 13(9), 1677-1690.

Xu, B., Du, W.-Q., Li, J.-W., Hu, Y.-L., Yang, L., Zhang, C.-C., Li, G.-Q., Lao, Z.-X., Ni, J.-C., Chu, J.-R., 2016. High efficiency integration of three-dimensional functional microdevices inside a microfluidic chip by using femtosecond laser multifoci parallel microfabrication. Scientific reports 6, 19989.

Xu, J., Attinger, D., 2007. Control and ultrasonic actuation of a gas–liquid interface in a microfluidic chip. Journal of Micromechanics and Microengineering 17(3), 609.

Xu, Q., Rioux, R.M., Dickey, M.D., Whitesides, G.M., 2008. Nanoskiving: a new method to produce arrays of nanostructures. Accounts of chemical research 41(12), 1566-1577.

Xu, Y., Wu, D., Sun, Y.H., Huang, Z.X., Jiang, X.D., Wei, X.F., Li, Z.H., Dong, B.Z., Wu, Z.H., 2005. Superhydrophobic antireflective silica films: fractal surfaces and laser-induced damage thresholds. Applied optics 44(4), 527-533.

Yang, C., Tartaglino, U., Persson, B., 2006. Influence of surface roughness on superhydrophobicity. Physical review letters 97(11), 116103.

Yang, D., Jhaveri, S.J., Ober, C.K., 2005. Three-dimensional microfabrication by two-photon lithography. MRS bulletin 30(12), 976-982.

Yang, P., Wirnsberger, G., Huang, H.C., Cordero, S.R., McGehee, M.D., Scott, B., Deng, T., Whitesides, G.M., Chmelka, B.F., Buratto, S.K., 2000. Mirrorless

lasing from mesostructured waveguides patterned by soft lithography. Science 287(5452), 465-467.

Yazdi, A.A., Popma, A., Wong, W., Nguyen, T., Pan, Y., Xu, J., 2016. 3D printing: an emerging tool for novel microfluidics and lab-on-a-chip applications. Microfluidics and Nanofluidics 20(3), 50.

Yeo, J.C., Yu, J., Koh, Z.M., Wang, Z., Lim, C.T., 2016. Wearable tactile sensor based on flexible microfluidics. Lab on a Chip 16(17), 3244-3250.

Yuen, P.K., Goral, V.N., 2010. Low-cost rapid prototyping of flexible microfluidic devices using a desktop digital craft cutter. Lab on a Chip 10(3), 384-387.

Zardetto, V., Brown, T.M., Reale, A., Di Carlo, A., 2011. Substrates for flexible electronics: A practical investigation on the electrical, film flexibility, optical, temperature, and solvent resistance properties. Journal of Polymer Science Part B: Polymer Physics 49(9), 638-648.

Zhang, Y.-L., Chen, Q.-D., Xia, H., Sun, H.-B., 2010. Designable 3D nanofabrication by femtosecond laser direct writing. Nano Today 5(5), 435-448.

Zhao, S., He, W., Ma, Z., Liu, P., Huang, P.-H., Bachman, H., Wang, L., Yang, S., Tian, Z., Wang, Z., 2019. On-chip stool liquefaction via acoustofluidics. Lab on a Chip 19(6), 941-947.

Zhou, R., Wang, C., 2016. Microfluidic separation of magnetic particles with soft magnetic microstructures. Microfluidics and Nanofluidics 20(3), 48.

Zhu, B., Jin, Y., Hu, X., Zheng, Q., Zhang, S., Wang, Q., Zhu, J., 2017. Poly (dimethylsiloxane) thin film as a stable interfacial layer for high - performance lithium - metal battery anodes. Advanced Materials 29(2), 1603755.

Vita

Yang Lin

842 W Taylor St, Chicago, IL 60607 | ylin212@uic.edu

https://doraylin25.wixsite.com/mysite | Google Scholar Profile: Yang Lin

EDUCATION

Doctor of Philosophy in Mechanical Engineering December 2019 (Expected)

University of Illinois at Chicago Chicago, USA

Thesis: Microfluidics with Nanoscale Additive Manufacturing: Devices and Applications

Advisor: Jie Xu

Master of Science in Mechatronic Engineering March 2015

Beijing Information Science and Technology University Beijing, China

Thesis: Fault Diagnosis and Evaluation of Turbine Bearing System Based on Sound Pressure and Vibration

Advisor: Jinhong Gao

Bachelor of Science in Mechanical Design Manufacturing and Automation July 2012

Beijing Information Science and Technology University Beijing, China

RESEARCH/TEACHING INTERESTS

Micro/Nanofluidics, Additive manufacturing, Micro/Nanofabrication, and Machine Learning;
Fluid Mechanics, Thermodynamics, Heat and Mass Transfer, Mechatronics, and Control theory;
BioMEMS, Biosensor, Microrobot, Acoustofluidics, Optofluidics, Organ on chip, and Lab on chip/paper/foil/tubing.

RESEARCH EXPERIENCE

University of Illinois at Chicago Fall 2015 to Present

Research Assistant, Microfluidics Laboratory Chicago, USA

- Investigated single-cell trapping on self-pumped lab-on-a-foil devices with 3D microstructures
- Invented efficient acoustofluidic lab-on-a-foil micromixers using microscale additive manufacturing
- Invented a fast way to construct high resolution 3D master moulds for soft lithography
- Created and characterized lung-on-a-chip devices using microscale additive manufacturing
- Characterized the separation force for resin replenishment enhancement in stereolithography
- Investigated and improved oxygen diffusion process in constrained surface stereolithography
- Developed and characterized superhydrophobic films with 3D printed microstructures
- Established and verified the theoretical model for the vibration modes of water-air bubbles
- Enhanced the performance of surface-based microfluidic sensors by acoustic bubbles
- Studied the separation of circulating tumor cells in microfluidic devices based on DEP and DLD
- Invented and characterized paper-based membrane-less microbial fuel cell
- Designed and organized microfluidic experiments for Fluid Mechanics course

Beijing Information Science and Technology University 2012 to 2015

Research Assistant Beijing, China

- Performed nonlinear dynamic analysis for biaxial rotor systems
- Studied nonlinear dynamics and established a fault diagnosis system for turbine rotor systems

TEACHING EXPERIENCE

University of Illinois at Chicago Fall 2015 to Present
Teaching Assistant, Department of Mechanical and Industrial Engineering Chicago, USA

- ME211 Fluid Mechanics Fall 2019
- ME341 Experimental Methods in Mechanical Engineering Spring 2019
- ME429 Internal Combustion Engines Fall 2018
- ME211 Fluid Mechanics Fall 2017
- ME347 Introduction to Computer-Aided Design Spring 2017
- ME347 Introduction to Computer-Aided Design Fall 2016
- ME211 Fluid Mechanics Spring 2016
- ME429 Internal Combustion Engines Fall 2015
- ME312 Dynamic System Control Fall 2015

PUBLICATIONS

(one book chapter and more than 10 journal papers, 8 first-authored; more than 220 citations at Google Scholar)

Thesis

[1] **Y. Lin**, Microfluidics with Nanoscale Additive Manufacturing: Devices and Applications, PhD Thesis

Book Chapter

[1] **Y. Lin** and J. Xu, *Paper-fluidic based sensing in food safety and quality analysis*, **Sensing Techniques for Food Safety and Quality Control**, Royal Society of Chemistry, 2017, 95-120

Peer-Reviewed Journal Articles

[12] **Y. Lin**, Y. Gao, M. Wu, R. Zhou, D. Chung, G. Piso, and J. Xu, *Acoustofluidic stick-and-play micropump built on foil for single-cell trapping*, **Lab on a Chip**, 2019 (Impact factor: 6.914)

[11] **Y. Lin**, C. Gao, Y. Gao, M. Wu, A.A. Yazdi, and J. Xu, *Acoustofluidic micromixer on Lab-on-a-Foil devices*, **Sensors & Actuators: B. Chemical**, 2019, 287, 312-319 (Impact factor: 6.393)

[10] **Y. Lin**, R. Zhou, and J. Xu, *Superhydrophobic surfaces based on fractal and hierarchical microstructures using two-photon polymerization: toward flexible superhydrophobic films*, **Advanced Materials Interfaces**, 2018, 1801126 (Impact factor: 4.834)

[9] **Y. Lin**, C. Gao, D. Gritsenko, R. Zhou, and J. Xu, *Soft lithography based on photolithography and two-photon polymerization*, **Microfluidics and Nanofluidics**, 2018, 22, 97 (Impact factor: 2.384)

[8] D. Gritsenko, **Y. Lin**, V. Hovorka, Z. Zhang, A. A. Yazdi, and J. Xu, *Vibrational modes analysis for water-air bubbles trapped on circular microcavities*, **Physics of Fluids**, 2018, 30, 082001 (Impact factor: 2.279)

[7] **Y. Lin** and J. Xu, *Microstructures Fabricated by Two-Photon Polymerization and Their Remote Manipulation Techniques: Towards 3D Printing of Micromachines*, **Advanced Optical Materials**, 2018, 6, 1701359 (Impact factor: 7.125)

[6] J. R. Choi, K. W. Yong, J. Y. Choi, A. Nilghaz, **Y. Lin**, J. Xu, and Xiaonan Lu, *Black Phosphorus and its Biomedical Applications*, **Theranostics**, 2018, 8(4), 1005-1026 (Impact factor: 8.063)

[5] D. Gritsenko, A. A. Yazdi, **Y. Lin**, V. Hovorka, Y. Pan, and J. Xu, *On characterization of separation force for resin replenishment enhancement in 3D printing*, **Additive Manufacturing**, 2017, 17, 151-156 (Impact factor: 7.173)

[4] A. De Vellis, D. Gritsenko, **Y. Lin**, Z. Wu, X. Zhang, Y. Pan, W. Xue and J. Xu, *Drastic sensing enhancement using acoustic bubbles for surface-based microfluidic sensors*, **Sensors and Actuators B**, 2017, 243, 298-302 (Impact factor: 6.393)

[3] **Y. Lin**, D. Gritsenko, Q. Liu, X. Lu and J. Xu, *Recent advancements in functionalized paper based electronics*, **ACS Applied Materials & Interfaces**, 2016, 8(32), 20501-20515 (Impact factor: 8.456)

[2] **Y. Lin**, D. Gritsenko, S. Feng, Y. C. Teh, X. Lu and J. Xu, *Detection of heavy metal by paper-based microfluidics*, **Biosensors and Bioelectronics**, 2016, 83, 256-266 (Impact factor: 9.518)

[1] **Y. Lin**, J. Gao, C. Ma, Z. Wang, X. Xu, *Research of Infrared Image Acquisition and Control System* (In Chinese), **Journal of Beijing Information Science and Technology University (natural science)**, 2014, 06: 56-59.

Peer-Reviewed Conference Articles

[2] C. Ma, **Y. Lin**, S. Wang, Z. Wang, L. Liu, *Nonlinear dynamic analysis on unity of loose support and rub-impact of double axis system with different velocities*. **Proceedings of the Fifth International Symposium on Test Automation & Instrumentation** (Vol.1), 2014: 5.

[1] **Y. Lin**, J. Gao, C. Ma, *Research and Application of Wireless Telemetry Image Acquisition and Control System* (In Chinese), **Computer Engineering and Applications**, 2014, 50 (S1): 226-229.

CONFERENCE PRESENTATIONS

[7] **Yang Lin**, Yuan Gao, Mengren Wu, Weiqi Zhao, and Jie Xu, *Acoustofluidic micropump on lab-on-a-foil devices*, ASME IMECE, 2019, Salt Lake City

[6] **Yang Lin**, Yuan Gao, Mengren Wu, and Jie Xu, *Acoustofluidic micromixer on lab-on-a-foil devices*, ASME IMECE, 2019, Salt Lake City

[5] **Yang Lin**, Can Gao, and Jie Xu, *Soft lithography based on photolithography and two-photon polymerization*, AIChE Midwest Regional Conference, 2019, Chicago

[4] **Yang Lin**, Can Gao, and Jie Xu, *Soft lithography based on photolithography and two-photon polymerization*, Lab-on-a-Chip and Microfluidics World Congress 2018, Coronado Island, San Diego

[3] Sébastien Méance, **Yang Lin**, Meghana Machireddy, Panfeng Fu, Vadim Gaponenko, Steven J. Ackerman, Viswanathan Natarajan and Jie Xu, *Fabrication of Extracellular Matrix Coated Membranes in Lung-on-Chips using Two-photon Polymerization*, 21st International Conference on Miniaturized Systems for Chemistry and Life Sciences (MicroTAS 2017), Savannah, Georgia, USA

[2] Dmitry Gritsenko, Andrea De Vellis, **Yang Lin** and Jie Xu, *Use of Acoustic Microstreaming for Drastic Sensing Enhancement*, AIChE Midwest Regional Conference, 2017, Chicago

[1] Andrea De Vellis, Dmitry Gritsenko, **Yang Lin**, Zhenping Wu, Xian Zhang, Yayue Pan, Wei Xue and Jie Xu, *Acoustic bubbles for microfluidic sensing enhancement*, Microfluidics Congress: USA, 2016, Philadelphia

FUNDING EXPERIENCE

- Assisted Dr. Xu in composing NSF proposal "Towards High-Throughput Label-Free Circulating Tumor Cell Separation using 3D Deterministic Dielectrophoresis (D-Cubed)" (funded) 2019
- Assisted Dr. Xu in composing proposal for NASA Early Career Faculty Award "PIPES: Piezoelectric Instrument for Precision Exploration" (funded) 2017

- Assisted Dr. Xu in composing NSF-BSF proposal "Complex liquid droplet structures as new optical and optomechanical materials" (funded) 2017
- Received research grant from Sigma Xi Grants-in-Aid program "Paper-based green bio-battery for portable electrics" (Sole PI) 2016

SERVICES AND AFFILIATIONS

Reviewer for Journals

- Scientific Reports
- Advanced Materials Technologies
- Journal of Electronic Packaging
- Engineering
- Biomicrofluidics
- Review of Scientific Instruments
- Journal of Applied Physics
- Research

Reviewer for Conferences

- ASME ICNMM2018
- ASME Turbo Expo 2019

Professional Memberships

- Sigma Xi - The Scientific Research Society
- American Society of Mechanical Engineers (ASME)

HONORS, AWARDS AND ACCOMPLISHMENTS

- Research featured: *Advances in 3D Printed Micromachines by UIC Researchers* 2019
- Inducted, full member of Sigma Xi - The Scientific Research Society 2018
- Supervised senior design team and won the 1st place Globe Award in the College of Engineering EXPO-Senior Design Competition 2017
- Academic Scholarship, Beijing Information Science and Technology University 2015
- Outstanding student fellowship, Beijing Information Science and Technology University 2008-2012
- National Motivational Scholarship, China 2010
- 2nd Prize in the University's Mechanical Innovation Design Competition 2010
- Various prizes in National Composition, Mathematics, Physics, and Chemistry Olympiad, China 2002-2008

SKILLS/LANGUAGES

Proficient in microfabrication (e.g., additive manufacturing, lithography, machining, etching, and deposition), operation of biomedical equipment (e.g., autoclave, centrifuge, incubator, spectrophotometer, and electrophoresis system), engineering software (SolidWorks, AutoCAD, COMSOL, ANSYS and ImageJ), programming software (e.g., Python, C, C++ and LabVIEW), microscopy (e.g., SEM, TEM, AFM and Raman microscopy), and languages (English and Chinese).